For Reference

NOT TO BE TAKEN FROM THIS ROOM

Ex libris
universitatis
albertaensis

QUAECUMQUE VERA

THE UNIVERSITY OF ALBERTA

INTERACTION OF Hg $6(^3P_0)$ and $6(^3P_1)$ WITH PARAFFINS

BY

© JOHN MICHAEL CAMPBELL

A THESIS

SUBMITTED TO THE FACULTY OF GRADUATE STUDIES AND RESEARCH

IN PARTIAL FULFILMENT OF THE REQUIREMENTS FOR THE

DEGREE OF DOCTOR OF PHILOSOPHY

DEPARTMENT OF CHEMISTRY

UNIVERSITY OF ALBERTA

EDMONTON, ALBERTA

SPRING, 1972

Thesis
1972
14D

UNIVERSITY OF ALBERTA

FACULTY OF GRADUATE STUDIES AND RESEARCH

The undersigned certify that they have read, and recommend to the Faculty of Graduate Studies and Research for acceptance, a thesis entitled

INTERACTION OF Hg $6(^3P_0)$ AND $6(^3P_1)$ WITH PARAFFINS

submitted by John Michael Campbell in partial fulfilment of the requirements for the degree of Doctor of Philosophy.

ABSTRACT

The primary processes occurring in the mercury photosensitization of propane and propane-nitrogen mixtures have been studied in detail.

By following the rates of production of the three isomeric hexanes produced from recombination of the *n*-propyl and isopropyl radicals formed in the initial process, and employing a detailed kinetic scheme, it has been shown that both Hg $6(^3P_0)$(Hg°) and Hg $6(^3P_1)$(Hg*) atoms decompose propane via C-H bond cleavage. The initial rates of *n*-propyl (*n*) and isopropyl (*i*) radical formation are found to vary with temperature between 0° and 200°C. For the Hg° reaction, the relative Arrhenius parameters are found to be $A_n^\circ/A_i^\circ = 0.78$ and $\Delta E_n^\circ - \Delta E_i^\circ = 1.90$ kcal/mole and for Hg*, $A_n^*/A_i^* = 0.89$ and $\Delta E_n^* - \Delta E_i^* = 1.25$ kcal/mole.

Using various nitrogen-propane mixtures, the decomposition quantum yield of propane by Hg* atoms was found to decrease while that of Hg° atoms to increase with increasing temperature.

The mercury photosensitized decomposition of hydrogen has been used to accurately determine the relative Arrhenius parameters of H-atom reaction with the primary and secondary positions of propane between 45° and 180°C and the values are $A_n/A_i = 1.35$ and $\Delta E_n - \Delta E_i = 2.01$ kcal/mole.

Band fluorescence spectra from the mercury photosensitization of CO, H_2O, NH_3, C_2H_5OH, SF_6, the rare gases, the fluorinated methanes and paraffins have been photographed. The observed

emission bands have been atributed to transitions between the van der Waals molecules formed between the excited Hg atom and the substrate, and the ground state mercury plus the substrate. To a first approximation, the trends observed throughout a homologous series can be explained in terms of changes in the polarizabilities of the two colliding species. Simple Lennard-Jones force constant calculations of the excited and ground state complexes have been carried out for comparison with experiment.

By treating the decomposition of paraffins by excited metal atoms analogous to abstraction reaction, the potential energies of activation have been computed using a modified bond-energy-bond-order method. These calculations predict the experimentally observed trends in the relative activation energies for the reactions of Hg* and Hg° atoms with propane.

A detailed mechanism has been described for the interaction of excited mercury atoms with paraffins in terms of a systematic potential energy diagram. This adequately explains the various trends observed in the mercury photosensitization of paraffins such as the changes in the quenching cross section with structure and deuterium substitution, the relative reactivity of the Hg* and Hg° atoms, band fluorescence and the effects of temperature on the quantum yields of decomposition and spin-orbit relaxation.

ACKNOWLEDGEMENTS

The author wishes to express his sincere gratitude to Dr. H. E. Gunning and Dr. O. P. Strausz for their guidance and assistance throughout the course of this investigation.

Special thanks go to Dr. H. S. Sandhu for his helpful advice and criticism during the preparation of this thesis.

Thanks go to Dr. E. M. Lown and Dr. E. J. Jakubowski for reading the manuscript.

The author would like to thank Dr. E. J. Jakubowski, Dr. R. E. Berkley, Dr. S. Penzes, Dr. T. Pollock, Mr. P. J. Young and Mr. S. De Paoli of the photochemistry group for their advice and criticism.

The diligent efforts of Mrs. R. Tarnowski in the typing of this thesis is appreciated.

The author would like to express his gratitude to his wife, Alice, whose devotion and unceasing co-operation have made this work possible.

The financial assistance provided by the University of Alberta and the National Research Council of Canada during the course of this work is gratefully acknowledged.

TABLE OF CONTENTS

Page

ABSTRACT.. i

ACKNOWLEDGEMENTS.. iii

LIST OF TABLES.. vii

LIST OF FIGURES... x

CHAPTER I. INTRODUCTION... 1

1. Mercury as a Photosensitizer....................... 3

2. Quenching of Excited Mercury Atoms.............. 7

a. Determination of Hg* Quenching Cross Sections 8

b. Production and Detection of Hg° Atoms........ 12

c. Removal of Hg° Atoms........................ 15

d. Excited Mercury-Substrate Complex Formation.. 19

3. Interaction of Hg* and Hg° Atoms with Various Substrates.................................. 24

a. Ground State Mercury and Nitrogen........... 25

b. Nitrogen and Oxygen Containing Compounds..... 27

c. Rare Gases.................................. 29

d. Hydrogen.................................... 32

e. Paraffins................................... 33

4. Radical Reactions Occurring in the Sensitization of C_3H_8.................................... 43

a. H-Atom Reactions............................ 43

b. The Reaction $n\text{-}C_3H_7 + C_3H_8 \rightleftarrows i\text{-}C_3H_7 + C_3H_8$.................................... 44

TABLE OF CONTENTS

Page

c. Measured Total Rate and Local Rate of Reaction.................................... 45

5. Objectives of the Present Work.................. 46

CHAPTER II. EXPERIMENTAL

1. Materials and Apparatus.......................... 48

a. Materials.................................... 48

b. Analytical System............................ 52

c. Filter Solution.............................. 52

2. Static Cell...................................... 55

3. Circulating Flow Cell............................ 55

a. Mercury Lamps................................ 56

b. Actinometry.................................. 56

c. Operating Procedure.......................... 57

4. Emission Flow System............................ 57

a. Emission Cell................................ 57

b. Exciting Lamp................................ 58

c. Spectrograph and Photographic Plates......... 58

d. Operating Procedure.......................... 58

CHAPTER III. THE REACTIONS OF H-ATOMS WITH PROPANE........... 59

CHAPTER IV. MERCURY $6(^3P_1)$ SENSITIZED DECOMPOSITION OF PROPANE 66

TABLE OF CONTENTS

Page

CHAPTER V. REACTIONS OF $Hg6(^3P_0)$ ATOMS WITH PROPANE......... 78

1. Results.. 78

a. Calculation of the Decomposition Quantum Yields of Propane by Hg* and Hg° Atoms....... 84

b. Calculation of the Ratio k_{32}/k_{31}............ 88

2. Discussion.................................... 95

CHAPTER VI. EMISSION FROM EXCITED MERCURY-SUBSTRATE COMPLEXES 101

1. Results.. 101

2. Discussion.................................... 126

CHAPTER VII. SUMMARY AND CONCLUSION........................ 137

BIBLIOGRAPHY.. 148

APPENDIX A.. 157

APPENDIX B.. 160

APPENDIX C.. 168

APPENDIX D.. 172

LIST OF TABLES

TABLE Page

I Some Optical Characteristics of the Lower Excited States of the Mercury Atom.. 5

II Quantum Yields of Hg° Formation from the Hg* Level by Various Compounds.. 16

III Calculated and Experimental Emission Lifetimes (τ_o in sec) of the Hg° Atom.. 17

IV Summary of Quenching Cross Sections of Mercury Atoms in the $^3P_1$ and $^3P_0$ States.. 20

V Rates of Various Reactions Occurring in the Mercury Photosensitization of Ammonia at Room Temperature...... 30

VI Quantum Yields of Mercury Hydride Formation in the Sensitization of Various Isotopic Hydrogens and Acetylene at Room Temperature in the Presence of Ar or N_2.. 34

VII Experimental and Calculated Values of Quenching Cross Sections of Hg* Atoms with Some Deuterated Alkanes..... 36

VIII Summary of Radical Yields from the Mercury Photosensitization of Alkanes.. 39

IX Source and Purity of Materials Used.................... 50

X Operating Conditions of GLC Columns and Retention Times of Various Compounds.. 54

XI Mercury Photosensitization of Hydrogen in the Presence of Propane.. 61

XII Mercury Photosensitization of Propane................ 69

LIST OF TABLES

TABLE Page

XIII Mercury Photosensitization of Propane-Ethylene Mixtures 74

XIV Mercury Photosensitization of Propane-Nitrogen Mixtures 79

XV Quenching Cross Sections and Rate Constants Used in the Calculation of k_{32}/k_{31}.................................. 86

XVI Calculation of Φ^* at 63° and 200° from the Data Shown in Figure 8 for Points Greater than F = 0.2........... 89

XVII Summary of Results from Figures 9 and 10.............. 91

XVIII Computed Quantities Employing Various Values of Input Rate Constants.. 99

XIX Separation of Emission Band Maxima from the 2536.5Å ($39,424\ cm^{-1}$) Resonance Line.......................... 105

XX Calculated Values of Lennard-Jones Force Constants of Mercury-Rare Gas Pairs................................ 130

XXI Physical Parameters of Some Fluorinated Compounds...... 134

XXII Disproportionation to Combination Ratios of Radicals... 159

XXIII Lennard-Jones Force Constants Calculated for the Collision of Ground State Mercury with Different Molecules.. 170

XXIV Lennard-Jones Force Constants Calculated for Collision of Excited Mercury Atoms with Different Molecules...... 171

XXV Lennard-Jones Force Constants for Different Collision Pairs... 175

XXVI Calculated Potential Energies of Activation for Excited Mercury-Paraffin Systems Using Attractive Term Only.... 176

LIST OF TABLES

TABLE Page

XXVII Calculated Potential Energies of Activation for Excited Cadmium- and Zinc-Paraffin Systems Using Attractive Term Only.. 177

LIST OF FIGURES

FIGURE Page

1 Lower excited states of the mercury atom............. 4

2 High vacuum and gas handling system.................. 49

3 Gas purification line and circulating flow system..... 51

4 Gas chromatography line.............................. 53

5 Arrhenius plot of the k_{13}/k_{12} ratio for the H-atom abstraction from propane by H-atoms, from Table XI.... 64

6 A plot of $2R_{(n)}/R_{(n+i)}$ against $[C_3H_8][R^{\frac{1}{2}}_{DMB}/R_{(n+i)}(R_{MP}/R_{DMB} - 2K^{-1}_{14})$ from the mercury photosensitization of propane at 200°C from Table XII.................. 70

7 Arrhenius plot of the k_{27}/k_{26} ratio for the Hg* sensitized decomposition of propane................. 76

8 Variation of the quantum yield equation [49] with F, from the mercury sensitized decomposition of propane.. 87

9 Plots of $2R_{(n)}/R_{(n+i)} - k_{12}/(k_{12}+k_{13}) + \delta Q_3$ against β at 27°, 124° and 166°C............................. 92

10 Plots of $2R_{(n)}/R_{(n+i)} - k_{13}/(k_{12}+k_{13}) + \delta Q_3$ against β at 63° and 200°C.................................. 93

11 Arrhenius plot of the k_{32}/k_{31} ratio for the Hg° sensitized decomposition of propane including the error limits from Table XVII........................ 94

12 Microdensitometer trace of the emission spectra from the mercury resonance lamp used in the fluorescence studies with 1 sec exposure time. Maximum pen deflection of 2.1 optical density units (O.D.)....... 106

LIST OF FIGURES

FIGURE Page

13 Detail of the mercury resonance line from the photolysis lamp, 1 sec.................................. 107

14 Fluorescence spectra: 728 torr N_2, 2 hours.......... 107

15 Fluorescence spectra: 600 torr N_2, 5 hours.......... 108

16 Fluorescence spectra: 400 torr NH_3, 1 min............ 108

17 Fluorescence spectra: 14 torr H_2O, 12 min.......... 109

18 Fluorescence spectra: 40 torr C_2H_5OH, 30 min........ 109

19 Fluorescence spectra: 420 torr CO, 4 hours.......... 110

20 Fluorescence spectra: 430 torr He, 4.5 hours........ 110

21 Fluorescence spectra: 440 torr Ne, 1.5 hours........ 111

22 Fluorescence spectra: 600 torr Ar, 20 min............ 111

23 Fluorescence spectra: 750 torr Kr, 10 min............ 112

24 Fluorescence spectra: 860 torr Xe, 30 min............ 112

25 Fluorescence spectra: 750 torr Kr, 10 min............ 113

26 Fluorescence spectra: 830 torr Xe, 10 min............ 113

27 Fluorescence spectra from excited mercury-substrate complexes: a, 60 torr N_2, 5 hours; b, 400 torr C_2H_6, 15 min; c, 600 torr C_3H_8, 3 hours; d, 510 torr $C(CH_3)_4$, 1.2 hours; e, 600 torr Ar, 20 min; f, 750 torr Kr, 10 min; g, 830 torr Xe, 10 min........................ 114

28 Fluorescence spectra: 500 torr CH_4, 60 min.......... 115

29 Fluorescence spectra: 400 torr C_2H_6, 15 min.......... 116

30 Fluorescence spectra: 600 torr C_3H_8, 3 hours......... 116

31 Fluorescence spectra: 500 torr CH_4, 60 min.......... 117

LIST OF FIGURES

FIGURE Page

32 Fluorescence spectra: 400 torr C_2H_6, 15 min.......... 117

33 Fluorescence spectra: 600 torr C_3H_8, 3 hours......... 118

34 Fluorescence spectra: a, 8 torr *i*-C_4H_{10}, 180 min..... 118

b, 645 torr *i*-C_4H_{10}, 46 min.... 118

35 Fluorescence spectra: 8 torr $C(CH_3)_4$, 120 min........ 119

36 Fluorescence spectra: 510 torr $C(CH_3)_4$, 1.2 hours.... 119

37 Fluorescence spectra: 400 torr *c*-C_3H_8, 1.5 hours..... 120

38 Fluorescence spectra: 720 torr *c*-C_4H_8, 1.5 hours..... 120

39 Fluorescence spectra: 210 torr *c*-C_5H_{10}, 55 min....... 121

40 Fluorescence spectra: 70 torr *c*-C_6H_{12}, 180 min...... 121

41 Fluorescence spectra: 330 torr CH_3F, 14.5 min........ 122

42 Fluorescence spectra: 310 torr CH_2F_2, 15 min......... 122

43 Fluorescence spectra: 280 torr CHF_3, 15 min.......... 123

44 Fluorescence spectra: 614 torr CF_4, 30 min........... 123

45 Fluorescence spectra: 190 torr SF_6, 60 min........... 124

46 Fluorescence spectra: 330 torr CH_3F, 14.5 min........ 124

47 Fluorescence spectra: 310 torr CH_2F_2, 15 min......... 125

48 Fluorescence spectra: 280 torr CHF_3, 15 min.......... 125

49 Schematic potential energy diagram for the optical transitions between the van der Waals molecules (Hg*-X) and (Hg-X) ground state...................... 132

50 Schematic potential surfaces representing emission from a high vibrational level and the accompanying emission probability, assuming the oscillator strength of the transition does not change with r.................... 135

CHAPTER I

INTRODUCTION

Electronic energy transfer between two species is of fundamental interest in chemical kinetics. In photochemistry, the absorption of electromagnetic radiation from about 1000 to 10,000Å is one source of electronically excited species. The energies of quanta in this wavelength region, about 23 to 230 kcal per mole, are comparable with the strengths of chemical bonds. Thus, absorption of light can lead to definite chemical effects: for example, an oxygen molecule absorbing light between 2450Å and 1950Å forms an electronically excited species which rapidly dissociates to oxygen atoms.

$$O_2(^3\Sigma_g^-) + h\nu \longrightarrow O_2(^3\Sigma_u^+) \longrightarrow 2O(^3P)$$

Usually, several paths exist for the dissipation of electronic energy residing in the absorbing species and are generally grouped into photochemical processes, such as isomerization or decomposition of the substrate, and photophysical processes, such as fluorescence and phosphorescence. Direct photolysis, the absorption of light by a substance, is restricted to compounds which absorb. On the other hand, chemical changes can be induced by energy transfer from a different absorbing species. This photosensitization technique is of general applicability since it is not restricted to any particular phase or sensitizer. The simplest photosensitization reactions are those occurring in the vapor phase involving atoms and

simple molecules. Atom sensitizers, mercury in particular, have been extensively studied over the past half century both as a convenient source of excitation energy (1) and as a means of elucidating the mechanism of energy transfer (1,2,3).

The atom photosensitization process can be divided into three consecutive steps:

i. absorption of light by the atom,
ii. transfer of energy to the substrate, and
iii. the physical and chemical changes occurring in the substrate caused by the transfer of energy.

Step i can be well established from the spectroscopy of the atom. Steps ii and iii, however, must be inferred from information about both the physical and chemical properties of the donor and acceptor as well as effects produced through this interaction.

1. Mercury as a Photosensitizer

Mercury has all the requirements of a good sensitizing agent, namely a) a chemically inert ground state with a good vapor pressure, b) absorption of light of discrete wavelengths, c) a large absorption coefficient, and d) a long excited state lifetime.

Promotion of one of the $6s^2$ electrons in the mercury atom ground state (designated as $6(^1S_0)$ and hereafter referred to as Hg) to the 6p level results in a singlet or triplet term depending on the spin orientation (Figure 1). The singlet level is designated as $Hg6(^1P_1)$(Hg'), and the triplet level is further split by spin-orbit interaction into three states; $Hg6(^3P_2)$, $Hg6(^3P_1)$(Hg*), and $Hg6(^3P_0)$(Hg°). Some characteristics of these levels are listed in Table I. Oscillator strengths of optical transitions from these levels are a manifestation of the selection rules governing the process. Because of heavy atom effects, only the total angular momentum quantum number J is well defined. Thus the transitions $Hg° \longrightarrow Hg$ ($\underline{J} = 0 \rightarrow \underline{J} = 0$) and $Hg(^3P_2) \longrightarrow Hg$ ($\underline{J} = 2 \longrightarrow \underline{J} = 0$) have very low oscillator strengths and a long emission lifetime. On the other hand absorption of the resonance lines 2537Å ($Hg \longrightarrow Hg^*$) and 1849Å ($Hg \longrightarrow Hg'$) readily occur and photosensitization is usually initiated from one of these two states.

Absorption of monochromatic light by a homogeneous system is described by the Beer-Lambert Law:

$$I/I_o = 10^{-\varepsilon Cl}$$

where I_o is the intensity of light incident on the absorbing species

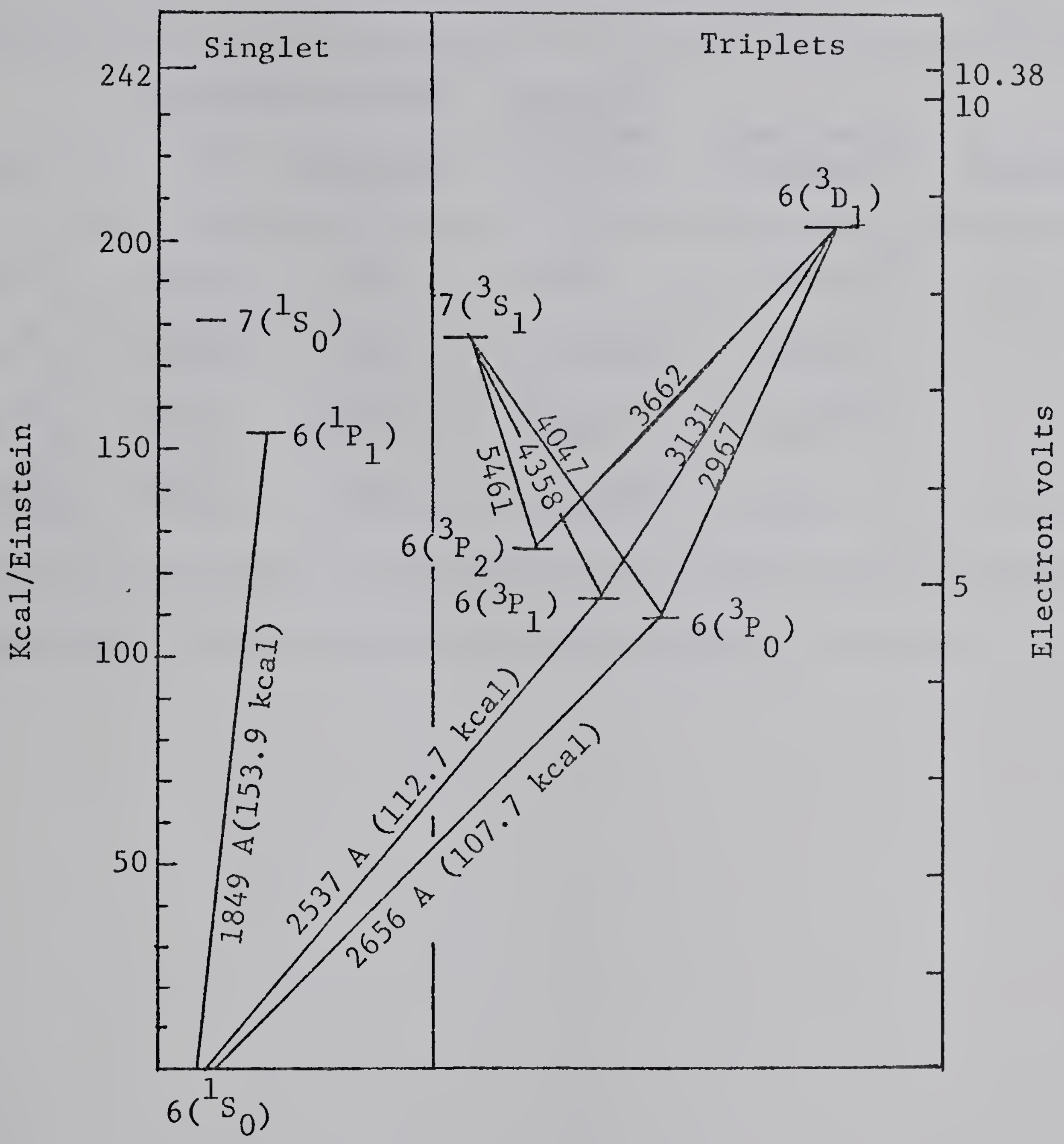
Singlet
Triplets
Kcal/Einstein
242
200
150
100
50
Electron volts
10.38
10
5
7($^1S_0$)
6($^1P_1$)
7($^3S_1$)
6($^3D_1$)
6($^3P_2$)
6($^3P_1$)
6($^3P_0$)
6($^1S_0$)
1849 A(153.9 kcal)
2537 A (112.7 kcal)
2656 A (107.7 kcal)
5461
4358
4047
3662
3131
2967

FIGURE 1: Lower excited states of the mercury atom.

TABLE I

Some Optical Characteristics of the Lower Excited States of the Mercury Atom

Level	Excitation Energy Å	kcal/mole	Emission Lifetime τ_o (sec)	Oscillator Strength	Reference
$Hg6(^3P_0)$	2656	107.7	2.0[a]	5.3×10^{-10}	4
$Hg6(^3P_1)$	2536.5	112.7	1.14×10^{-7}	2.5×10^{-2}	5
$Hg6(^3P_2)$	2271	125.9	$>4.7\times10^{-5}$	$<8.3\times10^{-5}$	6
$Hg6(^1P_1)$	1849	154.6	1.31×10^{-9}	1.18	7

[a] See Table III for lifetimes of the individual isotopes.

of concentration C, I is the intensity transmitted through a path length 1, and the constant ε is the extinction coefficient of the absorber. A large value of εCl is required in photosensitization studies to obtain measurable amounts of absorption. Too large a value can cause additional complications, however. Mercury at a vapor pressure of 2 microns in the presence of a quencher absorbs over 90% of the 2537Å resonance line in less than 2 cm of path length resulting in a large gradient in the concentration of excited atoms near the cell window (1). The associated phenomenon of multiple absorption-emission processes or "imprisonment" of the radiation also tends to increase the apparent lifetime of the excited state and must be accounted for when calculating rates based on the emission lifetime (5).

2. Quenching of Excited Mercury Atoms

When a cell containing mercury vapor and another gas (A) is irradiated with 2537Å light the electronic energy of the excited mercury atom can be dissipated in a variety of ways. A general reaction scheme for this system is given below.

$$\mathrm{Hg} + h\nu(2537\text{Å}) \longrightarrow \mathrm{Hg}^* \qquad [\mathrm{I}]$$

$$\mathrm{Hg}^* \longrightarrow \mathrm{Hg} + h\nu(2537\text{Å}) \qquad [-\mathrm{I}]$$

$$\mathrm{Hg}^* + \mathrm{A} \longrightarrow (\mathrm{HgA})^* \qquad [1]$$

$$(\mathrm{HgA})^* \longrightarrow \mathrm{Hg} + \mathrm{A}'(\text{Products}) \qquad [2]$$

$$\longrightarrow \mathrm{Hg}^{\circ} + \mathrm{A} \qquad [3]$$

$$\longrightarrow \mathrm{Hg} + \mathrm{A} + h\nu' \qquad [4]$$

$$\mathrm{Hg}^{\circ} \longrightarrow \mathrm{Hg} + h\nu(2656\text{Å}) \qquad [5]$$

$$\xrightarrow{\text{wall}} \mathrm{Hg} \qquad [6]$$

$$\mathrm{Hg}^{\circ} + \mathrm{A} \rightleftarrows (\mathrm{HgA})^{\circ} \qquad [7]$$

$$(\mathrm{HgA})^{\circ} \longrightarrow \mathrm{Hg} + \mathrm{A}'(\text{Products}) \qquad [8]$$

$$\longrightarrow \mathrm{Hg} + \mathrm{A} + h\nu'' \qquad [9]$$

$$\mathrm{Hg}^{\circ} + \mathrm{H_g} + \mathrm{A} \longrightarrow \mathrm{Hg_2}^* + \mathrm{A} \qquad [10]$$

Since, in the vapor phase, the transfer of energy is usually the result of a bimolecular collision of the excited atom and the substrate, the reactivity of excited mercury atoms is commonly expressed in terms of the quenching cross section (σ^2) related to the collision rate constant k_q

$$Z = k_q[A] = \sigma^2 (8\pi RT \frac{M_{Hg}+M_A}{M_{Hg}M_A})^{\frac{1}{2}} [A]$$

where Z is the bimolecular collision frequency, M_A is the atomic weight of compound A in a concentration [A], T is the temperature in degrees Kelvin, and R is Boltzmann's constant.

a. Determination of Hg* Quenching Cross Sections

Two methods of determining quenching cross sections of Hg* atoms have been developed and are discussed in detail in the literature (1,2). Only the general features are described here.

i. Physical Method

The quenching of excited Hg* atoms can be related to the emission rate by the following reactions

$$Hg + h\nu(2537\text{Å}) \longrightarrow Hg^*$$

$$Hg^* \longrightarrow Hg + h\nu(2537\text{Å})$$

$$Hg^* + A \xrightarrow{k_q} Hg + A'$$

where products of the last reaction are not specified. Steady-state treatment of these reactions leads to the Stern-Volmer formula

$$[I/I_o - 1] = \tau k_q[A]$$

where I and I_o are the fluorescence intensities measured at right angles to the incident beam with and without the quencher gas at a concentration [A] and τ is the observed lifetime of excited mercury. The slope of a plot of $[I/I_o - 1]$ against [A] is given by τk_q from which the quenching cross section can be determined if τ is known. Since k_q is given by

$$k_q = k_1(k_2 + k_3 + k_4)/(k_{-1} + k_2 + k_3 + k_4)$$

in the detailed reaction scheme, this method leads to a total rate of quenching independent of the products.

The major drawback of applying this technique is the problem of properly taking into account the imprisonment correction ($=\tau/\tau_o$) to the natural lifetime τ_o. Yarwood, Strausz and Gunning (8) showed that the quenching cross section values obtained by four different calculations of the imprisonment lifetime listed earlier (1,2) vary by constant factors:

$$\sigma^2_{I} = 1.23\sigma^2_{II} = 1.23\sigma^2_{III} = 1.75\sigma^2_{IV}$$

where I denotes values based on Holstein's solution (9) of the Boltzmann-type integrodifferential transport equation including the line shape as well as the cell geometry.

II denotes values obtained by Zemansky (10) using Samson's "equivalent opacity" (11)

III denotes values obtained by Biberman (12) using a numerical solution to the integrodifferential equation, and

IV denotes values obtained by the original Zemansky (13) treatment of the imprisonment as coherent scattering.

More recently, a slightly larger value of 48.2Å^2 has been found for ethylene using an experimental imprisonment correction (14). This, combined with a more accurate determination of the natural lifetime of the Hg* atom ($\tau_o = 1.145\text{x}10^{-7}$ sec) (7) leads to an additional 10% increase in the quenching cross sections. Thus:

$$\sigma_V^2 = 1.10\sigma_I^2 = 1.35\sigma_{II}^2 = 1.35\sigma_{III}^2 = 1.92\sigma_{IV}^2$$

where σ_V^2 is the preferred set of quenching cross sections.

The problem of imprisonment has been reviewed and examined in detail by Michael and Yeh (5) using Lyman-α photometry over a range of mercury pressures to evaluate the quenching cross section of H_2. A value of $10.8\mathring{A}^2$ for H_2 at low mercury opacity was found, in agreement with recent determinations (8,14,15,16). Waddel and Hurst (17) further extended the Holstein theory of imprisonment of resonance radiation to very high mercury concentrations ([Hg] > 10^{16} atoms/cc). The spin-orbit relaxation process

$$Hg^* + Hg \longrightarrow Hg^\circ + Hg + \text{kinetic energy}$$

was required in the mechanism ($0.03\mathring{A}^2 < \sigma^2 < 0.1\mathring{A}^2$) to explain the abnormal values of the experimental lifetime observed.

Regardless of the absolute value of the quenching cross section, the ratio of any two values determined by a particular method are independent of the imprisonment correction used. From the slope of the Stern-Volmer equation for two compounds 1 and 2, the ratio becomes

$$\frac{S_1}{S_2} = \frac{\tau k_{q,1}}{\tau k_{q,2}} = \frac{\sigma_1^2}{\sigma_2^2}\left(\frac{M_{Hg}+M_1}{M_{Hg}+M_2} \times \frac{M_2}{M_1}\right)^{\frac{1}{2}}$$

which is independent of τ. Thus an accurate comparison of quenching cross sections can be made without knowing their absolute values accurately.

ii. Chemical Method

This technique, developed by Cvetanović (2), is based on competitive quenching between N_2O and another compound A.

$$Hg^* + N_2O \xrightarrow{k_{N_2O}} Hg + N_2 + O$$

$$Hg^* + A \xrightarrow{k_d} Hg + \text{Products}$$

$$\xrightarrow{k_s} Hg^\circ + A$$

The quantum yield of nitrogen in the complete quenching region is given by

$$\Phi_{N_2}^{-1} = \alpha + \beta[A]/[N_2O]$$

where β/α is related to the relative quenching cross sections

$$\frac{\sigma_A^2}{\sigma_{N_2O}^2} = \frac{\beta}{\alpha}\left(\frac{1 + M_{Hg}/M_{N_2O}}{1 + M_{Hg}/M_A}\right)^{\frac{1}{2}}$$

and $\beta/\alpha = (k_d + k_s)/k_{N_2O}$ assuming that the products of the above reactions do not further affect the production of nitrogen.

The chemical quenching method has been used by Bellas, Rousseau, Strausz and Gunning (18) to determine the σ^2 values of a large number of compounds, and in some cases, significant discrepancies appeared between the physical and chemical measurements. It was noted that alcohols and ethers had lower, and ethyl mercaptan much higher, chemical quenching cross sections than those determined by the physical method. It was suggested (18,19) that Hg° atoms were formed and could participate further in the chemical quenching of N_2O by the reaction

$$Hg° + N_2O \longrightarrow Hg + N_2 + O$$

leading to a low chemical σ^2. The chemical method of determining quenching cross sections has further been criticized (20) since σ^2 values of some compounds appeared to be dependent on the light intensity.

b. Production and Detection of Hg° Atoms

In addition to deactivation of Hg* atoms directly to the ground state (reaction [2])

$$Hg^* + A \longrightarrow (HgA)^* \qquad [1]$$

$$(HgA)^* \longrightarrow Hg + A'(\text{Products}) \qquad [2]$$

several compounds have been found to promote the spin-orbit relaxation to the Hg° level.

$$(HgA)^* \longrightarrow Hg° + A \qquad [3]$$

Since Hg° atoms thus produced may react rapidly with the parent compound, there has been considerable confusion as to which molecules form Hg° atoms and what is their quantum yield of formation.

It has been known for some time that, when mercury vapor at sufficiently high pressures is irradiated with the 2537Å resonance line, two intense, broad emission bands centered at λ_{max} ∿4850Å and λ_{max} ∿3350Å appear (21). It was further shown (22) that the Hg° atom is the precursor of both these bands. Concurrent absorption of the 4047Å line in this system produced emission of the 4047Å, 4358Å and 5461Å lines (23), directly indicating the presence of Hg° atoms (Figure 1). At low mercury pressures the bands are

absent because the spin-orbit relaxation process becomes very slow. Addition of nitrogen restores the 4850Å and 3350Å bands however (24) and enhances the emission of 2656Å line (25,26). Pool (27) has used the absorption of the 4047Å line to show that the quenching reaction probably involves vibrationally excited nitrogen:

$$\mathrm{Hg}^* + \mathrm{N}_2(v=0) \longrightarrow \mathrm{Hg}^\circ + \mathrm{N}_2(v=1) - 1.6\ \mathrm{kcal/mole}$$

It was also noted that nitrogen does not quench the Hg° atom appreciably to the ground state. This technique was improved by Kimbel and LeRoy (28) and later by others (24) to study the reactions of Hg° atoms in nitrogen. It was further modified (29,30,24) to measure emission of the 5461Å and 4358Å lines at right angles to the exciting beam by the following sequence:

$$6(^3P_0) \xrightarrow[\text{abs.}]{4047\mathring{A}} 7(^3S_1) \begin{array}{l} \xrightarrow{5461\mathring{A}} 6(^3P_2) \\ \xrightarrow[\text{emission}]{4358\mathring{A}} 6(^3P_1) \end{array}$$

A different method of detecting Hg° atoms, based on its ability to eject electrons from a metal surface, has been described (31) and used to study Hg° reactions in nitrogen (24). Employing this method, Darwent and Hurtubise (32) found that C_2H_4, C_2H_6, H_2 and N_2, but not O_2 or CO_2, promoted the spin-orbit relaxation of the Hg* atoms. The sensitization of N_2 and CO was studied in detail (33) and it was concluded that they were equally efficient in producing Hg° atoms despite the large difference in quenching cross sections ($\sigma^2_{CO}/\sigma^2_{N_2} = 21$). This was supplemented with a quantum mechanical treatment of the process

$$\mathrm{Hg^* + XY(v=0) \longrightarrow Hg^\circ + XY(v=1)}$$

carried out by Bykhovskii and Nikitin (34). This treatment indicated that the most probable result would be vibrationally excited XY, particularly when the donor to acceptor energy discrepancy was small.

Callear and Norrish (35-37) and later Callear and Williams (38) described a flash photolysis method of studying the reactions of $\mathrm{Hg^\circ}$ atoms. Nitrogen (P = 780 torr) was used to pressure-broaden the 2537Å resonance line and to convert the Hg* atoms to the $\mathrm{Hg^\circ}$ level and kinetic absorption spectroscopy of the 4047Å and 2967Å lines was then related to the $\mathrm{Hg^\circ}$ atom concentration. The presence of $\mathrm{Hg^\circ}$ atoms was detected when N_2, CO, H_2O or D_2O were added to a flashed mixture of argon and mercury but not when NO, H_2, O_2, N_2O, CH_4, C_2H_6, C_3H_8, C_2H_4, NH_3 or BF_3 were present. Callear (39) suggested that the electron ejection technique used earlier (32) was not specific to $\mathrm{Hg^\circ}$ atoms and that any electronically excited species could produce the same effect.

Using a more sensitive technique based on steady-state absorption of 4047Å light, Penzes, Yarwood, Strausz and Gunning (40) detected $\mathrm{Hg^\circ}$ atoms in eight deuterated paraffins and light neopentane. It was shown that the discrepancies between the physical and chemical quenching cross sections observed in many cases could be due to the participation of $\mathrm{Hg^\circ}$ atoms in the system.

The flash technique was later modified by using a microwave pulse generator (41,42,43) or a large number of closely spaced electrodes in the flash lamp (44,45,46) to produce a monochromatic flash of 2537Å light. This set-up resulted in very high concentrations

of excited mercury atoms and allowed careful study of the Hg* and Hg° reactions. The early work of Callear and Williams (38) was shown to be in error due to the effect of excited N_2 $A^3\Sigma_u^+$ (45) and the quantum yields of Hg° formation with several compounds were determined (Table II) (44).

Vikis, Torrie and LeRoy (47) determined the quantum yield of Hg° formation by several molecules using the technique of enhanced decomposition of C_2H_4 by Hg° atoms (51) under partial quenching conditions (Table II).

c. Removal of Hg° Atoms

i. Emission of the Forbidden 2656Å Line

Emission from the Hg° level to the ground state is forbidden by optical selection rules. The observation that the Hg° atom undergoes spontaneous emission to the ground state was explained by a small amount of coupling with the nuclear magnetic moment. Since mercury is a mixture of 7 stable isotopes, two of which have odd nuclei with magnetic moments different from zero, it was proposed (22), and found (52), that emission was taking place only from the two odd isotopes 199 and 201 (Table III).

While studying the 4047Å absorption and 2656Å emission at up to 140 torr nitrogen, Kimbel and LeRoy (28) proposed that the 2656Å emission was a combination of both spontaneous and pressure-induced emission. By substituting a 4047Å lamp containing only mercury of atomic weight 198 it was concluded that "either the transition probability of emission of the forbidden line is essentially independent of nuclear spin or the exchange reaction

TABLE II

Quantum Yields of Hg° Formation from the Hg* Level by Various Compounds

Compound	Quantum Yield (Φ')[a]			
N_2	$0.9<\Phi'<1.0$ (43)	1.0[b] (44)	1.0[b] (47)	>0.92 (48)
O_2	0	<0.1		
N_2O	0	<0.1		
NO	0	<0.1		0.20
CO	0.12	0.85	$\sim$1	0.76
CO_2	0.02	$\sim$0.02	<0.01	
NH_3	0.06	0.62	0.8	0.7 (49)
ND_3			$\sim$1.0	1.0
H_2O		0.38	$\sim$1.0	0.19 (50)
D_2O			$\sim$1.0	0.49
H_2	0	<0.03		
CH_4	0.1	0.15		
C_2H_6	0.3	0.80		
C_3H_8	0.11	0.38		
n-C_4H_{10}	0.11			
$C(CH_3)_4$			0.57	
c-C_3H_6			0.68	
C_2H_4		<0.1		

[a] References in parenthesis.

[b] Φ' assumed equal to 1.0 for nitrogen.

TABLE III

Calculated and Experimental Emission Lifetimes (τ_o in sec) of the Hg° Atom

Hg Isotope	Experimental	Calculated	
199	1.7 (4)	1.5 (4)	1.43 (8)
201	2.6	2.22	2.08

$$Hg^{\circ}_{even} + Hg_{odd} \longrightarrow Hg_{even} + Hg^{\circ}_{odd}$$

is extremely fast". Recently it has been shown that the absorption of the 4047Å line does not follow Beer's law (48) and their second conclusion is probably correct.

ii. Excitation to Higher States by Collision and Absorption

Bigeon (53) has shown Hg° atoms produced in a mixture of Hg and N_2 (total pressure of 2 torr) irradiated by a mercury resonance lamp are destroyed primarily by collisions with metastable nitrogen molecules excited in the (v=1) level, in agreement with earlier proposals (27,54). Other routes of Hg° destruction were shown to be absorption of 4047Å and 2967Å radiation present in the spectrum of the lamp, and collision with ground state mercury atoms, in the ratio of about 10:3:7.

It is interesting to note that nitrogen (v=1) molecules arise from two sources: a) collisional excitation between two (v=0) molecules or collision of a (v=0) molecule with the wall and b) spin-orbit relaxation of Hg* atoms. The equilibrium concentration of nitrogen (v=1) molecules is very low since the first vibrational level is some 6.6 kcal/mole above the zero level. Process a) leads to the activation of about 1 out of 10^5 molecules at room temperature but process b) can lead to high concentrations of excited nitrogen dependent on the intensity. The relaxation of nitrogen (v=1) is very slow at room temperature despite the large exothermicity, and only becomes significant at higher temperatures (55,56). Consequently nitrogen (v=1) must be considered in pure mercury-nitrogen systems irradiated with 2537Å resonance light.

iii. Quenching of Hg° Atoms

In order to understand the reactivity of excited mercury atoms with various compounds, the rates of both Hg* and Hg° atoms must be separated and compared. These are listed in Table IV. The first comparison of the quenching rates was done by Callear and Williams (38) who found that the rate of deactivation of Hg° atoms is much lower than that of Hg* atoms in every case. Table IV also includes the quenching rates determined by Vikis and Moser (57) using the ethylene technique and electron emission from silver metal, and the rates determined by the decrease in 4047Å absorption (58) and 3350Å and 4850Å emission (59). The trends in the reactivity of Hg° atoms are similar to those established by the Hg* atoms but the rates are lower. However, there is a considerable difference in the absolute values of σ^2 determined by the different workers.

d. Excited Mercury-Substrate Complex Formation

The intervention of complex formation between an excited species and a ground state molecule has been proposed in several systems. In solution, eximers and exiplexes (from the combination of an excited molecule with a similar, and different ground state molecule respectively) have been observed in many aromatic hydrocarbon systems (61). The eximer usually emits at longer wavelengths than the monomer and can have a significant binding energy. In the vapor phase, structureless emission and absorption bands associated with particular spectral lines of the alkali metals in the presence of rare gases and paraffins have been attributed to excited complexes (62,63).

TABLE IV

Summary of Quenching Cross Sections of Mercury Atoms in the $^3P_1$ and $^3P_0$ States[a]

Compound	$Hg(^3P_1)$, σ^{2*}(Å^2)[e]		$Hg(^3P_0)$, $\sigma^{2\circ}$(Å^2)[e]					
	Physical Method	Chemical Method						
			Inorganic Compounds					
H_2	11.6 (1)[d]		0.018 (38)	0.96 (44)	0.12 (57)[c]			1.6 (50b)
D_2	16.1				0.12			
N_2	0.37		9×10^{-6}					
O_2	26.9		0.093	12.1				18.0
NO	47.7	44.6 (1)[d]	0.34	1.63				13.0
CO	7.86		0.028	0.65				2.4
N_2O	28.6	24.3	0.51	8.54		0.42 (59)	0.43 (58)	4.4
CO_2	4.78		0.0014	0.034				
NH_3	5.67		0.0033	0.019				0.02
ND_3	2.11							

TABLE IV (cont'd)

Summary of Quenching Cross Sections of Mercury Atoms in the $^3P_1$ and $^3P_0$ States[a]

Compound	$Hg(^3P_1)$, σ^{2*} ($\mathring{A}^2$)[e]		$Hg(^3P_0)$, $\sigma^{2\circ}$ ($\mathring{A}^2$)[e]					
	Physical Method	Chemical Method						
H_2O	1.93 (1)[d]		0.0066 (38)					
D_2O	0.89		0.0048					
Hg			7.6					
			Hydrocarbons					
CH_4	0.115		0.007	2.9×10^{-4} (44)				
C_2H_6	0.216	0.189 (1)[d]	0.011	0.0058	0.001 (57)[c]	0.087 (59)	0.07 (58)	0.03 (50b)
C_3H_8	3.1	2.3	0.16	0.034	0.0097	0.29	0.50	
$CH_3CD_2CH_3$	1.09[b]	0.324			7.7×10^{-4}		0.069	
C_3D_8	0.902[b]	0.176					0.037	
n-C_4H_{10}	7.7	6.88			0.017			
i-C_4H_{10}	9.45	9.32			0.054			
$C(CH_3)_4$	2.84				0.0011			

TABLE IV (cont'd)

Summary of Quenching Cross Sections of Mercury Atoms in the $^3P_1$ and $^3P_0$ States[a]

	Hg($^3P_1$), σ^{2*} ($\mathring{A}^2$)[e]				
Compound	Physical Method	Chemical Method			Hg($^3P_0$), $\sigma^{2°}$ ($\mathring{A}^2$)[e]
c-C_3H_6	2.16 (1)[d]				4.5×10^{-4} (57)[c]
C_2H_4	48.6	41.8 (1)[d]	0.6 (38)	26.4 (44)	2.5[c]
C_2D_4	47.3[b]				2.3

[a] References in parenthesis.

[b] From reference (60).

[c] Note that the $\sigma^{2°}$ values obtained by Vikis and Moser (57) are relative to that of ethylene, which was determined to be 2.5 A^2.

[d] Corrected to σ_V^{2*} from section I-2-a.

[e] The symbols σ^{2*}, $\sigma^{2°}$ and σ^2 refer to the quenching cross section respectively for excited mercury atoms in the Hg* level, Hg° level, and where the excited state is not specified.

Mercury also forms a variety of complexes. The 4850Å and 3360Å emission bands originate from the mercury eximer molecule (22). Complexes have been observed with rare gases (64,65), water (25,26), ammonia (26), methane (66), and more recently kinetic studies have been carried out on the complexes of mercury with paraffins (67), rare gases (68,69), ammonia (44,49,70-73), water (50), alcohols (74), and amines (75). It is thus essential to include intermediate complex formation in the mechanism of deactivation of Hg^* and Hg° atoms.

3. Interaction of Hg* and Hg° Atoms with Various Substrates

From a comparison of the Hg* quenching cross sections of various classes of compounds with the reactivity of oxygen and sulfur atoms, it has been shown (76) that the excited mercury atom behaves as an electrophilic reagent. The initial interaction between Hg* atoms and substrate molecules was proposed to involve the following configurations:

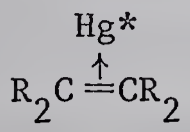

$R_2C\overset{\overset{Hg^*}{\uparrow}}{=}CR_2$ (olefins)

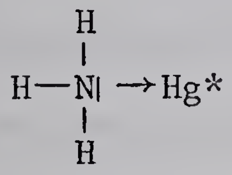

$H-\overset{H}{\underset{H}{N}}|\rightarrow Hg^*$ (NH_3, PH_3, AsH_3 and their alkyl derivatives)

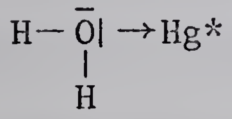

$H-\underset{H}{\bar{O}}|\rightarrow Hg^*$ (H_2O, H_2S, and their alkyl derivatives)

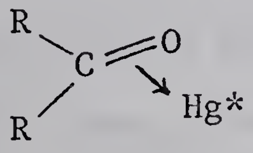

(carbonyl compounds)

$R-\underline{\overline{X}}|\rightarrow Hg^*$ (alkyl halides with the exception of fluorides)

and

$R-H\rightarrow Hg^*$ (paraffins).

The total σ^2 is primarily determined by the most reactive site in the molecule. Since the alkyl groups and fluorine atoms have low electron donating power, they are only important in the quenching of paraffins and fluorine substituted paraffins. For this reason, a comparison of Hg* and Hg° reactivities and their relationship to the electronic energy transfer process can more easily be made by

discussing the various classes of quenchers.

a. Ground State Mercury and Nitrogen

The broad emission bands centered at 4850Å and 3350Å have been observed in pure mercury at a high pressure and mercury-nitrogen mixtures irradiated with the 2537Å resonance line. Mrozowski (22) has assigned these to the $A(^3 0_u^-) \rightarrow X(^1\Sigma_g^+)$ and $A(^3 1_u) \rightarrow X(^1\Sigma_g^+)$ transitions of the diatomic mercury eximer molecule, respectively. The $A(^3 0_u^-)$ state, which correlates with Hg° + Hg at large separation, collapses together with the $A(^3 1_u)$ state from Hg* + Hg, into a $(^3\Sigma_u^+)$ state at small internuclear distances. This combination of states allows the spin-orbit relaxation of the Hg* atom by Hg ground state. The relaxation energy is consequently taken up by translational modes of the two species. Later, McCoubrey (77) on the basis of his observation of a common persistence time for these emissions in a pure mercury system, postulated that both bands arise from the $A(^3 0_u^-)$ state, the first by a pressure-induced and the second by a spontaneous transition to the ground state. The eximer molecules were also shown to form in a third order reaction involving a metastable Hg° atom and two ground state mercury atoms,

$$Hg^\circ + 2Hg \longrightarrow Hg_2^* + Hg$$

and that the intensity ratio of the two continua is pressure dependent, the 4850Å band emission being enhanced by pressure.

By observing the 2537Å decay time of mercury in nitrogen between 52 and 252°C, Matland (78) found the $\sigma_{N_2}^2$ increased by a factor of two. This was explained by assuming only those colliding molecules

with energy above 1.6 kcal/mole were effective and the quenching cross section given by

$$\sigma^2_{N_2} = f\sigma^2_T$$

where the constant σ^2_T, the quenching cross section for those molecules with sufficient energy to react, is 1.7Å^2, and f is the fraction of molecules with energy greater than ε (79)

$$f = (1 + \varepsilon/RT)\exp(-\varepsilon/RT)$$

where R is Boltzmann's constant and T the absolute temperature.

Berberet and Clark (24) studied the reactions occurring in the mercury and nitrogen system using absorption of the 4047Å line, 4850Å emission continuum, and ion formation to detect Hg° atoms. From the dependence of these measurements on intensity and nitrogen pressure it was concluded that Hg° is formed by nitrogen quenching of Hg* and destroyed by a termolecular collision with nitrogen and a ground state mercury atom.

$$Hg^\circ + Hg + N_2 \longrightarrow Hg_2^* + N_2$$

On the other hand, using the flash technique, Callear and Williams (38) found the deactivation of Hg° atoms to be first order in nitrogen and Hg concentration by the reactions

$$Hg^\circ + N_2 \longrightarrow Hg + N_2 \qquad k = 8.7 \times 10^7 \text{ cc mole}^{-1}\text{sec}^{-1}$$

$$Hg^\circ + Hg \longrightarrow 2Hg \qquad k = 3.4 \times 10^{13} \text{ cc mole}^{-1}\text{sec}^{-1}$$

The reactions of Hg° atoms in pure nitrogen were further studied by LeRoy and coworkers under steady state conditions (pressure less than 8 torr) using the 4047Å absorption technique (80) and measurement of

the 3350Å and 4850Å emission bands (81). A third order reaction with nitrogen as a chaperone was required which was assumed to be made up of a series of second order reactions to agree with Callear and Williams' results at higher pressures:

$$\mathrm{Hg}^{\circ} + \mathrm{Hg} \longrightarrow \mathrm{Hg}_2^{*+}$$

$$\mathrm{Hg}_2^{*+} + \mathrm{N}_2 \longrightarrow \mathrm{Hg}_2^{*} + \mathrm{N}_2$$

$$\longrightarrow 2\mathrm{Hg} + \mathrm{N}_2$$

$$\mathrm{Hg}_2^{*} \longrightarrow 2\mathrm{Hg} + h\nu(3350\text{Å})$$

$$\mathrm{Hg}_2^{*} + \mathrm{N}_2 \longrightarrow \mathrm{Hg}_2^{\circ} + \mathrm{N}_2$$

$$\mathrm{Hg}_2^{\circ} \longrightarrow 2\mathrm{Hg} + h\nu(4850\text{Å})$$

where Hg_2^{*}, Hg_2^{*+} and Hg_2° are the stabilized and nascent $A(^31_u)$ and $A(^30_u^-)$ states of the mercury molecule. These conclusions have been questioned in the light of recent studies which have shown that the 4047Å and 4358Å absorption lines do not obey the Beer-Lambert law above 1 torr total pressure (48).

From the emission of the 3350Å and 4850Å bands (up to 27 torr nitrogen) Penzes, Gunning and Strausz (82) found a third order reaction rate of 1.1×10^{18} cc moles^{-2} sec^{-1} for nitrogen as a chaperone, in good agreement with the value of 3.6×10^{17} found by McCoubrey (77) for mercury as a chaperone.

b. Nitrogen and Oxygen Containing Compounds

The presence of nonbonding electrons in the molecule has significant effects on the quenching reactions (76). Electronic to vibrational energy transfer has been observed in reactions of Hg^* and Hg°

atoms from the infrared emissions of CO ($v \leq 9$) (83) and NO ($v \leq 17$) (84). The reactivity of the Hg° atoms was estimated to be an order of magnitude lower than that of Hg* atoms towards CO and NO.

Addition of a small amount of CO had been shown to enhance the rate of sensitized decomposition of ethylene (85) and H_2 (86) (the "carbon monoxide effect"). London, Vikis and LeRoy (51) later made a detailed search for the presence of a long lived Hg*CO complex. Although no conclusive evidence was found it was proposed that formation of Hg° atoms in excess of that found by Scheer and Fine (33) (about 5%) could explain the effect. This was later confirmed by the observation (44,48) of a large quantum yield of Hg° formation by CO (see Table II).

Phillips and coworkers have recently studied the kinetics of emission from excited mercury complexes with NH_3, and ND_3 (49,70-72), H_2O and D_2O (50), alcohols (74), and amines (75). Modified rotating sector and phase shift methods were used to study the dependence of the rate of emission from the complex on the pressure of the substrate, third body, and mercury. The Hg* atoms are rapidly quenched to the Hg° level with quantum yields of about 0.7 and 1.0 for NH_3 and ND_3 respectively. The slow step in the reaction was the formation of a complex between Hg° and NH_3. This was followed by rapid emission from the complex of a broad band centered at about 3460Å (3500Å for ND_3) with no fine structure (±1Å). By assuming that the probability of emission is greatest near the equilibrium internuclear distance, it was shown (71) that the shift in the peak wavelength with pressure leads to a dissociation energy of about 5.0 kcal/mole.

These reactions of excited mercury-ammonia complexes were also studied by Callear and coworkers (44,73), using the resonance flash technique to study the quenching rate of Hg° atoms by various compounds (see Table IV). They showed that the $(HgNH_3)°$ complex was formed both in a bimolecular and termolecular collision with ammonia. Rate constant values obtained for these association reactions and spontaneous emission are summarized in Table V. The difference in emission rates of $(HgNH_3)°$ and $(HgND_3)°$ was attributed to the dependence of spontaneous emission on the internal energy of the complex.

The results obtained by Phillips and coworkers on H_2O and D_2O (50) and alcohols (74) were similar to those in the NH_3 system with the exception that no termolecular reaction was observed. The $(HgH_2O)°$ band had a peak intensity at about 2860Å while the band maxima of the D_2O and alcohol emissions appeared progressively further to longer wavelengths (up to about 3030Å). The measured rate of Hg° deactivation by different alcohols are listed in Table IV.

c. Rare Gases

Interactions of excited mercury atoms with rare gases are of interest because the quenching reaction is restricted to photophysical processes. Oldenberg (64,65) observed fluorescence bands on both sides of the mercury resonance line in the presence of rare gases. Helium and neon showed one band on the short wavelength side of the 2537Å line, while Ar, Kr and Xe gave two diffuse bands. Argon and krypton also gave discrete bands on the long wavelength side of the resonance line. Preston (87) also found emission

TABLE V

Rates of Various Reactions Occurring in the Mercury Photosensitization of Ammonia at Room Temperature

Reaction	Rate Constant[a]		Units
$(HgNH_3)° \longrightarrow Hg + NH_3 + h\nu$	5.5×10^{5} (73)	5.38×10^{5} (72)	sec^{-1}
$(HgND_3)° \longrightarrow Hg + ND_3 + h\nu$	5.4×10^{5}		sec^{-1}
$Hg° + NH_3 \longrightarrow Hg + NH_3 + h\nu$	1.87×10^{11}	1.93×10^{11}	$cc\ mole^{-1} sec^{-1}$
$Hg° + ND_3 \longrightarrow Hg + ND_3 + h\nu$	1.47×10^{11}	1.2×10^{11} (49)	$cc\ mole^{-1} sec^{-1}$
$Hg° + NH_3 + N_2 \longrightarrow (HgNH_3)° + N_2$	7.54×10^{16}		$cc^{2} mole^{-2} sec^{-1}$
$Hg° + ND_3 + N_2 \longrightarrow (HgND_3)° + N_2$	1.7×10^{17}		$cc^{2} mole^{-2} sec^{-1}$
$Hg° + 2NH_3 \longrightarrow (HgNH_3)° + NH_3$	7.5×10^{17}	8.3×10^{17} (72)	$cc^{2} mole^{-2} sec^{-1}$
$Hg° + 2ND_3 \longrightarrow (HgND_3) + ND_3$	2.24×10^{18}		$cc^{2} mole^{-2} sec^{-1}$

[a] References in parenthesis.

bands associated with 13 lines of the mercury discharge spectra with He and Ar, with 12 lines of cadmium, and with 6 lines of tellurium. Jablonski (88) proposed that quenching by the rare gases was due to crossing of the repulsive potential curves representing the excited mercury atom-ground state noble gas atom, and ground state mercury-ground state noble gas atom system. Olsen (89) found that the depolarization of the resonance line was "negligible" for He and Kr but quenching cross sections for He and Ar were found to be 0.325Å^2 and 0.222Å^2 respectively.

Various proposals have been put forward to explain the origin of this band fluorescence. Kuhn (90) suggested that the bands originated from transitions between repulsive branches of the ground and excited states. Jefimenko (91) showed that the presence of auxiliary minima or maxima in the excited potential energy curve could adequately explain these satellite bands. On the other hand Leycuras (92) suggested that local perturbations of the optical electron oscillations during the collision were responsible for emission of light other than the resonance line. Fiutak and Frackoweak (93) pointed out that the electronic correlation and potential energy relations of the Hg-Ar van der Waals molecule would lead to slightly bonding states for the ground state of mercury as well as the $(Ar+Hg)^{\circ}$ and $(Ar+Hg)^{*}$ states. The band structure was later assigned to transitions between quantized levels of these van der Waals molecules (94). These band structures have been extensively studied in absorption at high densities (62,63) in discharges of many different metals with rare gases (95-97), and in

liquids and solids (98,99), a review of which is beyond the scope of this introduction.

Gunning, Penzes, Sandhu and Strausz (68) have shown that quenching of Hg* atoms by the noble gas atoms leads to small but not negligible quenching cross sections ($0.1\mathring{A}^2<\sigma^2<0.9\mathring{A}^2$). Simple Lennard-Jones potential curves of the van der Waals molecules indicate that within reasonable limits, crossing to the ground state proposed by Jablonski (88) is of little importance and that quenching occurs exclusively by radiative dissipation.

Phillips and coworkers (69) have obtained an emission spectrum from the excited Hg-Xe complex which showed a broad structureless band with a peak at 2750Å extending from the 2537Å resonance line to about 3000Å, and was attributed to a complex between Hg° atoms and Xe. Rates of reaction of Hg° atoms with Xe and Hg were also obtained.

d. Hydrogen

Yang and coworkers (16,100) noted the large value of the ratio of the rates $\sigma^{2*}/\sigma^{2\circ}$ with H_2 ($\sim 3.3\times 10^3$) compared to $\sigma^{2*}/\sigma^{2\circ}$ ~ 10 for hydrocarbons (38). Light's phase space theory (101) was applied to the quenching reaction with hydrogen and the quantum yield of formation of H, HgH, and undissociated H_2 was calculated to be 0.52, 0.16, and 0.58 respectively. The recent experimental demonstration (102) that the quantum yield of hydrogen decomposition is unity, however, contradicts these conclusions.

Callear and coworkers (42,43,46) using the monochromatic flash technique, have found that the yield of HgH is large in the

quenching of hydrogen but could not be detected at all in hydrocarbons (with the exception of C_2H_2, Table VI). From the Hg* decomposition of HD molecules it was proposed that the Hg* (and probably the Hg°) atom reacts with hydrogen by direct insertion between the H-atoms to form an electronically excited (H-Hg-H)* intermediate which subsequently "predissociates" by crossing to a second state of H-Hg-H which, in turn, correlates with, and dissociates to the ground state of H + HgH.

e. Paraffins

Darwent (103) noted that the quenching diameter σ [i.e. $(\sigma^2)^{\frac{1}{2}}$] of paraffins is approximately a linear function of the carbon number within a homologous series and that the specific increments in σ for methyl, methylene, and methine groups are 0.15-0.30, 1.0, and 1.3Å respectively. This was consistent with the trend in the electron-donating power of these groups and lead Rousseau, Strausz and Gunning (76) to postulate a direct interaction between the Hg* and C-H bond on the paraffin.

i. Isotope Effect on σ^2

Evidence for this direct interaction has been inferred from effects of substitution of deuterium for hydrogen (k_H/k_D effect). Gunning and coworkers (76,104-106) have studied the effect of deuterium substitution on the σ^2 values of various hydrocarbons by the chemical method, and have shown that the large k_H/k_D effect observed in the paraffins was probably due to a primary kinetic isotope effect, that is, the Hg* interacts directly with the H-atom

TABLE VI

Quantum Yields of Mercury Hydride Formation in the Sensitization of Various Isotopic Hydrogens and Acetylene at Room Temperature in the Presence of Ar or N_2

Reaction	Quantum Yield	Reference
$Hg^* + H_2 \longrightarrow HgH + H$	0.8 ± 0.1	43
$Hg^* + D_2 \longrightarrow HgD + D$	0.96 ± 0.1	46
$Hg^* + HD \longrightarrow HgH + D$	0.14 ± 0.02	46
$\longrightarrow HgD + H$	0.80 ± 0.1	46
$Hg^\circ + H_2 \longrightarrow HgH + H$	0.93 ± 0.1	43
$Hg^\circ + D_2 \longrightarrow HgD + D$	0.65 ± 0.2	43
$Hg^* + C_2H_2 \longrightarrow HgH + C_2H$	0.18 ± 0.07	43

of the C-H bond. The much lower k_H/k_D effect found for H_2O, NH_3, PH_3 and C_3H_6 was attributed to a secondary kinetic isotope effect. Furthermore (18,76) the observed isotope effects could be calculated using absolute reaction rate theory (107) assuming a linear transition state, C···H···Hg in the rate determining step. Table VII contains the observed and calculated quenching cross sections using this model. Agreement is reasonable when account is taken of the difference in the stretching and bending frequencies between the C-H and C-D bonds.

Yang (16) pointed out that, according to this transition state mechanism, the isotope effect arises mainly from differences in the heights of the potential barriers that must be surmounted with thermal energy. This difference (ΔE) originating from the zero point energies of the C-H and C-D bonds, contributes a factor $\exp(\Delta E/RT)$ to the k_H/k_D ratio. Thus the isotope effect on the σ^2 should be temperature dependent. Yang has studied the effect of temperature on the quenching cross sections of C_3H_8 and $CH_3CD_2CH_3$, by both the physical and chemical methods. The chemical quenching cross sections of the two compounds were found to be identical at 30 and 150°C. Although the physical σ^2 values for each compound decreased by a factor of about 4 going from 25 to 202°C the ratio $(\sigma^2)_H/(\sigma^2)_D$ varied only slightly. This decrease was attributed to a temperature effect on the imprisonment of the resonance radiation (108) with the actual temperature dependence given by the ratio $(\sigma^2)_H/(\sigma^2)_D$.

Penzes, Strausz and Gunning (67) have observed fluorescence in both light and deuterated paraffins as well as in several other compounds, in the reverse order of quenching reactivity $CH_4 > C_2H_6 >$

TABLE VII

Experimental and Calculated Values of Quenching Cross Sections of Hg* Atoms with Some Deuterated Alkanes[a]

Compound	Quenching Cross Section (Å^2)			Minimum Quenching on the CH_2 or CH Group (%)
	Exp.	Calc.[b]	Calc.[c]	
$CH_3CH_2CH_3$	1.2	-	-	87
$CH_3CD_2CH_3$	0.17	0.23	0.15	64
$CD_3CH_2CD_3$	1.0	1.02	0.99	96
$CD_3CD_2CD_3$	0.09	0.16	0.08	87
$(CH_3)_3CH$	4.8	-	-	91
$(CH_3)_3CD$	0.44	0.83	0.52	71
$(CD_3)_3CH$	-	4.3	4.2	-
$(CD_3)_3CD$	-	0.59	0.30	-

[a] Taken directly from reference 76.

[b] Values calculated taking into account the difference in stretching frequencies between C-H and C-D bonds.

[c] Values calculated taking into account the difference in the stretching and bending frequencies between the C-H and C-D bonds.

C_3H_8. Since no deactivation effect was apparent up to 500 torr of propane, an upper limit of 10^{-9} sec was estimated for the emission lifetime.

The absence of temperature dependence of the isotope effect can not be reconciled with the calculation based on the zero point energy difference and a more sophisticated approach to the problem of energy transfer was proposed (16,109). Methane has a lower than unit quantum yield of decomposition (110). This fact, combined with the observations that excited mercury forms a complex with the quencher (67) can be used to construct the potential surface leading to a linear complex between Hg* and a paraffin quencher. The Hg* + RH system forms a weakly bonded complex with a binding energy partially dependent on the polarizabilities of Hg* and RH. Further along the reaction path there is a potential barrier whose height is dependent on the R-H bond strength. These two effects could qualitatively explain the temperature independence of the isotope effect and the emission from the complex. It does not, however, provide an explanation for the observed isotope effect or the formation of Hg° atoms.

ii. Decomposition of Paraffins

The mercury sensitized decomposition of paraffins has been the subject of much experimental work in the past. Although the general features of the reactions have been known for some time, details of the reaction mechanism have only recently begun to appear.

Since the excitation energy of Hg* (112 kcal/mole) is sufficient to break any of the bonds in paraffins (80-88 kcal/mole for C-C and 91-108 kcal/mole for the C-H bonds) one might expect

a distribution of products associated with each bond rupture. Early work (111) indicated that the only primary step was carbon-hydrogen bond rupture. Carbon-carbon bond cleavage was conspicuously absent below about 220°C, above which thermal decomposition of the radicals becomes significant. If more than one type of C-H bond is present, products associated with all possible C-H bond ruptures are observed. In propane both primary and secondary C-H bonds are broken (111,112).

$$\mathrm{Hg}^* + C_3H_8 \longrightarrow n\text{-}C_3H_7 + H + \mathrm{Hg}; \qquad \Delta H = -13.6 \text{ kcal/mole}$$

$$\longrightarrow i\text{-}C_3H_7 + H + \mathrm{Hg}; \qquad \Delta H = -19.3 \text{ kcal/mole}$$

Holroyd and Klein (113) and Chesick (114) have studied the decomposition of propane, employing ethylene-C^{14} as a hydrogen radical trap

$$\dot{H} + C_2H_4 \longrightarrow C_2H_5$$

and internal scavenger of propyl radicals

$$C_2H_5 + n\text{- or } i\text{-}C_3H_7 \longrightarrow n\text{-pentane or isopentane}$$

$$\longrightarrow C_2H_4 + C_3H_8 \text{ or } C_2H_6 + C_3H_6$$

The relative yields of the pentanes and hexanes were related to the formation of propyl radicals in the initial step. Jakubowski, Kebarle, Strausz and Gunning (115) used the mass spectrometric technique (116) with methyl radicals as a propyl radical trap. The results of these studies are tabulated in Table VIII and in every case the initial *n*- to isopropyl ratio is about 1:9. However, since these studies did not take into account reaction [3]

$$\mathrm{Hg}^* + A \longrightarrow (\mathrm{HgA})^* \qquad [2]$$

$$(\mathrm{HgA})^* \longrightarrow \mathrm{Hg}^\circ + A \qquad [3]$$

TABLE VIII

Summary of Radical Yields from the Mercury Photosensitization of Alkanes

Sensitizer	Compound	Temp.	1°/2°/3°[a]	Reference
Hg($^3P_1$)	C_3H_8	25°	1/ 10/ -	113
		30°	1/9.9/ -	114
		54°	1/9.1/ -	115
	$CD_3CH_2CD_3$	54°	1/>30/ -	115
	$CH_3CD_2CH_3$	54°	1/0.6/ -	115
	C_3D_8	54°	1/7.0/ -	115
	$CH(CH_3)_3$	25°	1/ - /32.4	113
Hg($^1P_1$)	C_3H_8	25°	1/1.0/ -	117
	$CH(CH_3)_3$	0°	1/ - /1.4	117

[a] Ratios of primary, secondary and tertiary hydrogen atom rupture not corrected for the number of similar H-atoms.

this 1:9 ratio may not be representative of only the Hg* reaction. Holroyd and Klein further found that (per H-atom) a tertiary hydrogen is about 350 times, and secondary hydrogen about 65 times more reactive than a primary hydrogen atom toward Hg* sensitized decomposition. Thus both the quenching cross section data (Table VII) and decomposition data (Table VIII) indicate that the quenching of excited mercury atoms occurs directly in the C-H bond and leads to cleavage from the initial site of quenching. The reactivity of the H-atom sites increases in the order 1° < 2° < 3°.

Holroyd and Pierce (117) have studied the Hg' sensitization of a number of paraffins. Again, only C-H bond cleavage is observed, but the reactivity of the hydrogen atom sites is markedly different. Per H-atom, the tertiary is about 12 times, and the secondary only about 3 times more reactive than the primary hydrogen atom toward sensitized decomposition (Table VIII). It was suggested that the difference in reactivity between the Hg' and Hg* states was due to the greater exothermicity of the Hg' reactions ($\Delta H = -55.6$ kcal/mole for the *n*-propyl and $\Delta H = -61.2$ kcal/mole for the isopropyl product). Thus a type of linear transition state model discussed above is indicated for the step leading to decomposition of the initially formed complex.

This model would predict the 1°:2°:3° yield ratio to vary with temperature in contradiction to Yang's arguments (16,109). However all experiments in Table VIII were done near room temperature. Takumuku and Back (118) have studied the effect of temperature on the Hg* sensitized decomposition of a mixture of light and deuterated

propane and NH_3. Although the system was very complex, and involved Hg° as well as Hg* atoms, it was concluded that the temperature and competitive quenching effect could be explained by assuming that the first, and perhaps the following reactions have a positive temperature coefficient:

$$NH_3 + (Hg^* \text{ or } Hg^\circ) \longrightarrow Hg + NH_2 + H$$

$$(RHHg)^* \longrightarrow R + H + Hg$$

$$Hg^\circ + RH \longrightarrow R + H + Hg$$

Vikis and Moser (119) have discussed the decomposition of the (R-HHg)* bond in the excited complex along the lines of Yang's theories (15). The interaction of Hg°, Hg* and Hg' atoms with alkanes was proposed to form a relatively long lived (RHHg)* complex on a potential surface which decomposes by C-H bond rupture or back to initial substrates. The energy content of the complex was dependent on which excited mercury state was initially present and the depth of the potential surface. The complex surface was assumed to correlate with a $Hg^+ - H^- - R$ ionic surface. Unimolecular decomposition rate constants were calculated using the Rice-Ramsperger-Kassel-Marcus (RRKM) theory restricted to this upper surface. Their results can be summarized as follows:

1. The experimentally determined trends in the rates of Hg* and Hg° quenching with various paraffins are predicted by theory but the absolute magnitudes of the calculated and experimental $\sigma^{2*}/\sigma^{2\circ}$ ratios are as much as a factor of 50 lower than the observed values.

2. Predicted isotope effects on the σ^2 values agree well with those observed, where available.
3. Fair agreement is found between the relative amounts of quenching of the Hg* and Hg' atoms by primary, secondary, and tertiary C-H rupture.
4. Lifetimes of the $C(CH_3)_4$, CH_4 and perhaps c-C_3H_6 complexes with mercury were predicted to be several orders of magnitude longer than those of other hydrocarbons.

However, since application of the RRKM theory to sensitization reactions requires the limiting assumptions on the shape of the potential surface and positions of crossover to decomposition, the conclusions must be regarded as only approximate.

Another approach to the study of the sensitization of paraffins can be used. If the mercury atom is considered as a species which abstracts a hydrogen, we may apply the simple Bond-Energy-Bond-Order (BEBO) method developed by Johnston (120). This treatment can also yield relative activation energies for abstraction of the various H-atoms in paraffins.

4. Radical Reactions Occurring in the Sensitization of C_3H_8

a. H-Atom Reactions

The H-atom abstraction reactions by hydrogen atoms from numerous paraffin molecules have been studied and Arrhenius parameters determined (121). In relatively few cases, however, was the site of attack specified. The Arrhenius parameters reported for the propane reaction $\log k = 12.7 - 7400/2.3\ RT$ (cc mole^{-1} sec^{-1}) (122), determined by γ-radiolysis of the C_3H_8-C_3H_6 mixture, refers to the composite sum of the two concurrent reactions:

$$H + C_3H_8 \longrightarrow i\text{-}C_3H_7 + H_2 \qquad [12]$$

$$\longrightarrow n\text{-}C_3H_7 + H_2 \qquad [13]$$

The ratio k_{13}/k_{12} has not been determined directly. An estimate of the ratio can be made if it is assumed that the reactivity of the primary C-H bonds in propane is the same as that of the C-H bonds in ethane. Using the known rate constants for ethane $10^{12.5}\exp(-9000/RT)$ cc mole^{-1} sec^{-1} and

$$H + C_2H_6 \longrightarrow C_2H_5 + H_2 \qquad [11]$$

for propane $10^{12.7}\exp(-7400/RT)$ cc mole^{-1}sec^{-1} (122,123), one obtains

$$k_{13}/(k_{12}+k_{13}) \approx 0.62\ \exp(-1600/RT)$$

which leads to a value of k_{13}/k_{12} of about $0.8\ \exp(-1700/RT)$ between 30 and 200°C.

Since the mercury photosensitization of propane produces H-atoms which can subsequently react with propane, giving both *n*- and isopropyl radicals, the ratio k_{13}/k_{12} must be known accurately.

The Hg* photosensitization of H_2 produces H-atoms with near unit efficiency (102) and therefore the H_2-C_3H_8 system is ideally suited for the study of competitive reactions of H-atoms with propane. The same analysis technique and temperature study as used for pure propane photosensitization can also be used.

Reid and LeRoy (124) have studied the reaction of C_2H_5 radicals with H_2 in a similar system. Mercury photosensitization of H_2 in the presence of ethylene was used to produce the C_2H_5 radicals which then were allowed to react with H_2.

$$C_2H_5 + H_2 \xrightarrow{k_a} C_2H_6 + H$$

The rate for this reaction was found to be:

$$\log k_a = 12.7 - 13.7\text{x}10^3/2.3RT \quad (\text{cc mole}^{-1}\ \text{sec}^{-1})$$

after proper precautions were taken to minimize secondary reactions. Beer's law for the absorption of 2537Å radiation was shown to hold for $(Hg)L < 2.4 \times 10^{-3}$ torr cm in the expression $I_t/I_0 = \exp[-\varepsilon(Hg)L]$. The value of ε was found to be $2.7\text{x}10^{-14}$ cm^2 atom^{-1} in the presence of 92 torr H_2, independent of temperature. This corresponds to a cell path of 6 cm and mercury at its equilibrium vapor pressure at 10°C.

b. The Reaction n-C_3H_7 + $C_3H_8 \rightleftarrows$ i-C_3H_7 + C_3H_8

Berkley, Woodall, Strausz and Gunning (125) have studied the abstraction of an H-atom from propane by n-propyl radicals:

$$n\text{-}C_3H_7 + C_3H_8 \rightleftarrows i\text{-}C_3H_7 + C_3H_8 \qquad [14]$$

The rate constant, relative to recombination of n-C_3H_7 radicals (k_r)

was found to be

$$\text{Log } k_{14}/k_r^{\frac{1}{2}} = 2.6 - \frac{7.91\text{x}10^3}{2.3RT} \qquad (\text{cc mole}^{-1}\ \text{sec}^{-1})^{\frac{1}{2}}$$

At room temperature this reaction is negligibly slow but at higher temperatures it must be taken into account.

c. Measured Total Rate and Local Rate of Reaction

In order to obtain expressions for the observed rates of product formation rather than the local rates given by a simple steady state treatment, the following relations have been derived (126,127). Let us assume that the local rate of formation of compound A in a small volume increment, where the absorption of light is uniform across the increment, is given by:

$$\left(\frac{d[A]}{dt}\right)_{\text{local}} = \gamma I_a^n$$

where γ is a function which includes all reactant concentrations and temperature dependent terms, and I_a is the absorbed intensity. The ratio of the measured rate of production of A to that of the local rate which is representative of the steady state treatment is given by:

$$\delta = \frac{(d[A]/dt)_{\text{measured}}}{(d[A]/dt)_{\text{local}}} = \frac{(\varepsilon cL)^{n-1}(1-e^{-\varepsilon cLn})}{n(1-e^{-\varepsilon cL})^n}$$

where ε is the absorption coefficient, c the concentration of the absorber, and L the path length. When $n = \frac{1}{2}$ this becomes

$$\delta = \frac{2(1-e^{-\varepsilon[\text{Hg}]L/2})}{\{\varepsilon[\text{Hg}]L(1-e^{-\ [\text{Hg}]L})\}^{\frac{1}{2}}}$$

This expression for δ is based on Beer's law and consequently is not exact for mercury pressures greater than $4\text{x}10^{-4}$ torr but still can be used as a good approximation to the required correction.

5. Objectives of the Present Work

Several general observations can be made from the foregoing discussion of mercury photosensitization. The initial step in the sensitization process in most cases is formation of a van der Waals complex molecule:

$$Hg^* + A \longrightarrow (HgA)^* \qquad [1]$$

However, the nature of this complex has not been well established. The complex can then decay by several different modes other than reversal to Hg* and A; decomposition of the substrate molecule,

$$(HgA)^* \longrightarrow Hg + A'(\text{Products}) \qquad [2]$$

spin-orbit relaxation,

$$(HgA)^* \longrightarrow Hg^\circ + A \qquad [3]$$

or direct emission of the complex,

$$(HgA)^* \longrightarrow Hg + A + h\nu'. \qquad [4]$$

The Hg° atoms react in a similar manner; formation of the complex,

$$Hg^\circ + A \longrightarrow (HgA)^\circ \qquad [7]$$

decomposition to give products,

$$(HgA)^\circ \longrightarrow Hg + A'(\text{Products}) \qquad [8]$$

emission of the complex,

$$(HgA)^\circ \longrightarrow Hg + H + h\nu'' \qquad [9]$$

or formation of the mercury eximer molecule,

$$Hg^\circ + Hg + A \longrightarrow Hg_2^* + A. \qquad [10]$$

The relative importance of each mode of reaction will depend not only on the accessibility of a particular reaction surface, but also on the competitive rates of processes into other channels. For example, spin-orbit relaxation is significant in both ethane and ammonia (Table II). However, decomposition quantum yield of ethane is near unity (109) but the decomposition of ammonia is very low and emission from the $(NH_3Hg)^\circ$ complex predominates (72).

The present work attempts to clarify the participation of this excited mercury-substrate complex in the reaction and to distinguish between the various theories proposed to explain the quenching reaction. Although the sensitization of paraffins has been extensively studied, the reaction mechanism is far from clear and in some cases experiments appear to give contradictory results. Since propane has two different H-atom abstraction sites, gives band fluorescence, and promotes spin-orbit relaxation to the Hg° level, it has been chosen as a model system in which to test the various theoretical proposals. The following questions are considered:

1. What is the effect of temperature on the product yields of photosensitized decomposition of paraffins?

2. Will this effect be different for the Hg° and Hg^* reactions and how does this relate to the quenching cross section studies?

3. Can the nature of the complex be inferred from the spectral distribution of the emission from the mercury-substrate complex?

CHAPTER II

EXPERIMENTAL

1. Materials and Apparatus

A conventional high-vacuum system evacuated to 10^{-6} torr of mercury by a two-stage mercury diffusion pump was used (Figure 2). The cell and analysis section were kept grease-free using Delmar mercury float valves and helium-tested Hoke valves. A mercury manometer, McLeod Gauge and Pirani gauge tubes (Consolidated Vacuum Corporation) were used to measure the pressure.

a. Materials

The materials used, their source and purity are given in Table IX. Those condensable at -196°C were degassed by trap to trap distillation. To eliminate all traces of unsaturated impurities, propane was first bubbled through 60 cm of a concentrated H_2SO_4 solution containing added P_2O_5, then through 120 cm of a saturated basic $KMnO_4$ solution, passed through a Drierite-Ascarite drying column, and finally distilled at -139°C and collected at -161°C (Figure 3). It was stored in a 5 liter bulb and degassed again before transference into the cell.

Hydrogen and nitrogen were both purified in an apparatus, Figure 2, which consisted of a 20 mm glass tube filled with copper turnings heated to about 275°C, followed by a trap filled with a molecular sieve material kept either at -196°C or -78°C. Oxygen impurity in the hydrogen stream is converted to water at the copper surface and trapped in the molecular sieve. Oxygen impurity in

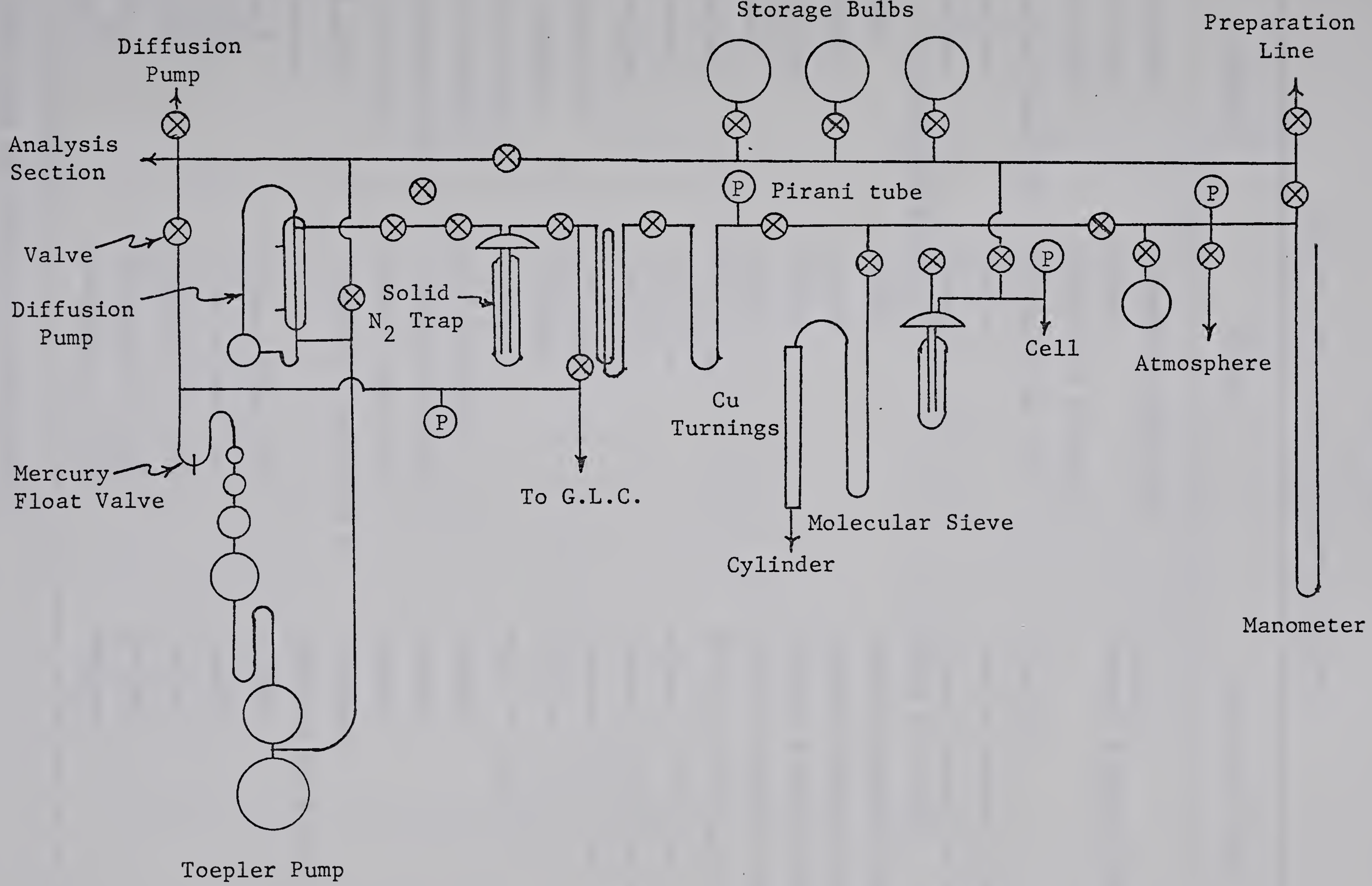
Storage Bulbs
Preparation Line
Diffusion Pump
Analysis Section
Pirani tube
P
Valve
Diffusion Pump
Solid N_2 Trap
Cell
Atmosphere
Cu Turnings
Mercury Float Valve
To G.L.C.
Molecular Sieve
Cylinder
Manometer
Toepler Pump

FIGURE 2: High vacuum and gas handling system.

TABLE IX

Source and Purity of Materials Used

Compound	Source	Grade and Purity
Hydrogen	Canadian Liquid Air	a
Nitrogen	Airco	Assayed Reagent Grade
Nitrogen	Linde Air Products	a
Carbon monoxide	Matheson Co. Inc.	Research
Helium	Airco	Assayed Reagent Grade
Helium (for chromatography)	Canadian Liquid Air	Passed through molecular sieve at -196°C
Neon	Airco	Assayed Reagent Grade
Argon	Airco	Assayed Reagent Grade
Krypton	Airco	Assayed Reagent Grade
Xenon	Airco	Assayed Reagent Grade
Methane	Phillips	Research 99.9 mole %
Ethane	Phillips	Research 99.91 mole %
Propane	Phillips	Research 99.99+ mole %; a
Neopentane	Phillips	Research 99.97 mole %
Isobutane	Phillips	Pure 99. mole %
Cyclopropane	Phillips	Pure 99. mole %
Cyclobutane	Frinton Labs	Reagent
Cyclopentane	Aldrich Chem. Co.	Reagent
Cyclohexane	Fisher Chem. Co.	Reagent
Ammonia	Canadian Liquid Air Co.	Anhydrous
Ethanol		Absolute 99.9 mole %
CH_3F	Pierce Chem. Co.	Reagent
CH_2F_2	Pierce Chem. Co.	Reagent
CHF_3	Matheson Co. Inc.	Reagent
CF_4	Matheson Co. Inc.	Reagent
SF_6	Matheson Co. Inc.	Reagent

[a] See text for purification and purity.

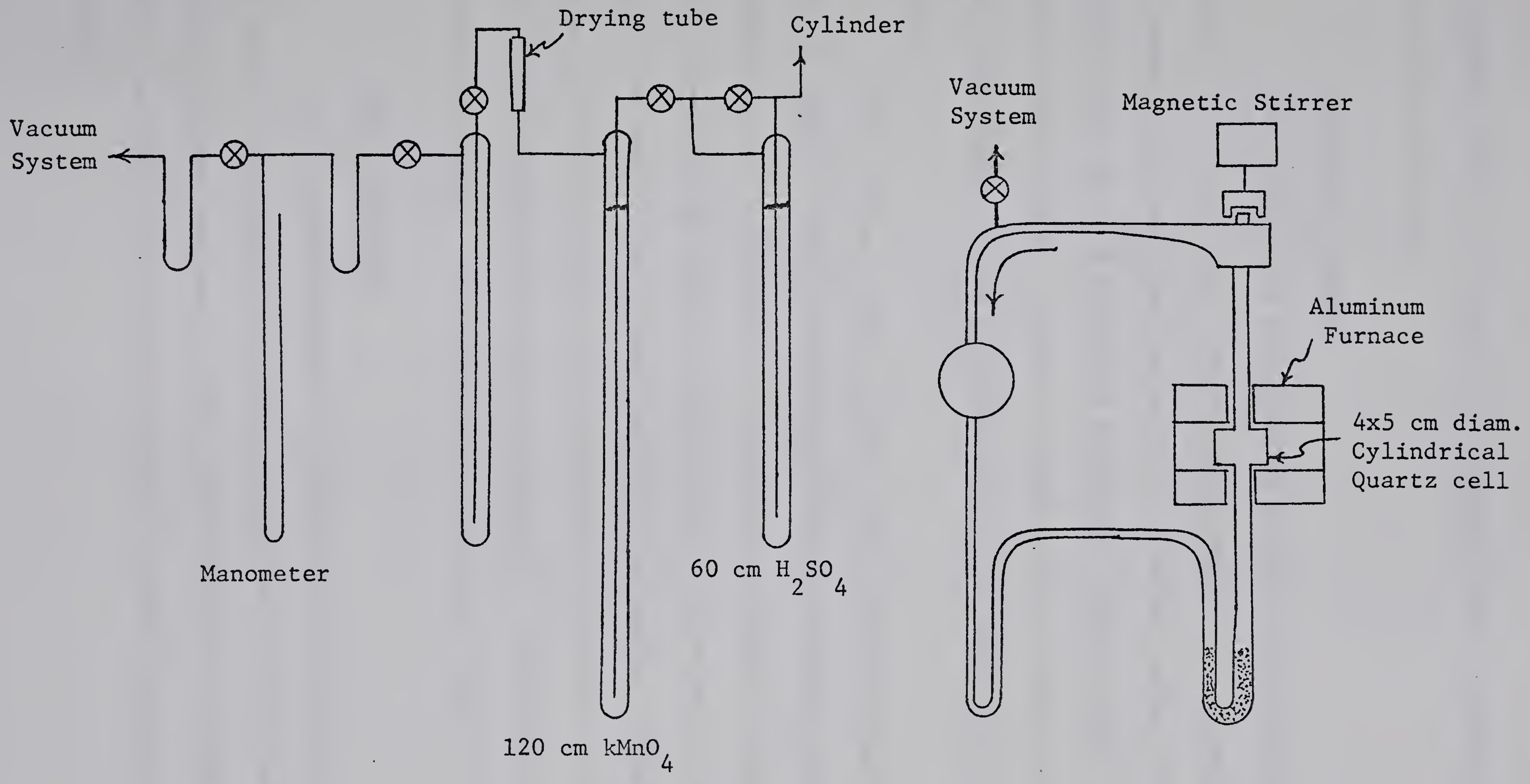
Vacuum System
Manometer
Drying tube
Cylinder
120 cm $kMnO_4$
60 cm H_2SO_4
Vacuum System
Magnetic Stirrer
Aluminum Furnace
4x5 cm diam. Cylindrical Quartz cell

FIGURE 3: Gas purification line and circulating flow system.

the nitrogen stream is converted to copper oxide, and water is trapped by the molecular sieve.

b. Analytical System

Low temperature distillation and gas chromatography (Figures 2, 4) were used to separate and measure the products. The gas chromatograph was constructed from a thermal conductivity cell (Gow-Mac model TR II B with W-II filaments, 300°F), power supply (Gow-Mac 9999-C, 250 ma), Sargent recorder (1.0 mv range), and 6 mm od glass coil columns filled with the appropriate packing and liquid phases.

The helium carrier gas was first passed through a molecular sieve at -196°C. The flow was controlled by an Edwards needle valve and measured by a calibrated oil manometer and bubble flowmeter. The injection system was made of three-way Hoke valves and a 4-way stopcock to isolate the column from the flow system. Gases were trapped at -196°C in glass coils filled with glass wool, attached by 4-way stopcocks downstream from the detector. The columns used and the retention times of the compounds studied are listed in Table X.

c. Filter Solution

A 1:1 aqueous mixture of concentrated $NiSO_4$-$CoSO_4$ solution and "uv dye" 2,7-dimethyl-3,6-diazacyclohepta-1,6-diene perchlorate (157) 200 mg/liter was used. This combination had a transmission of about 1% at 4047Å and about 3% at 2967Å and 4358Å compared to that at 2537Å.

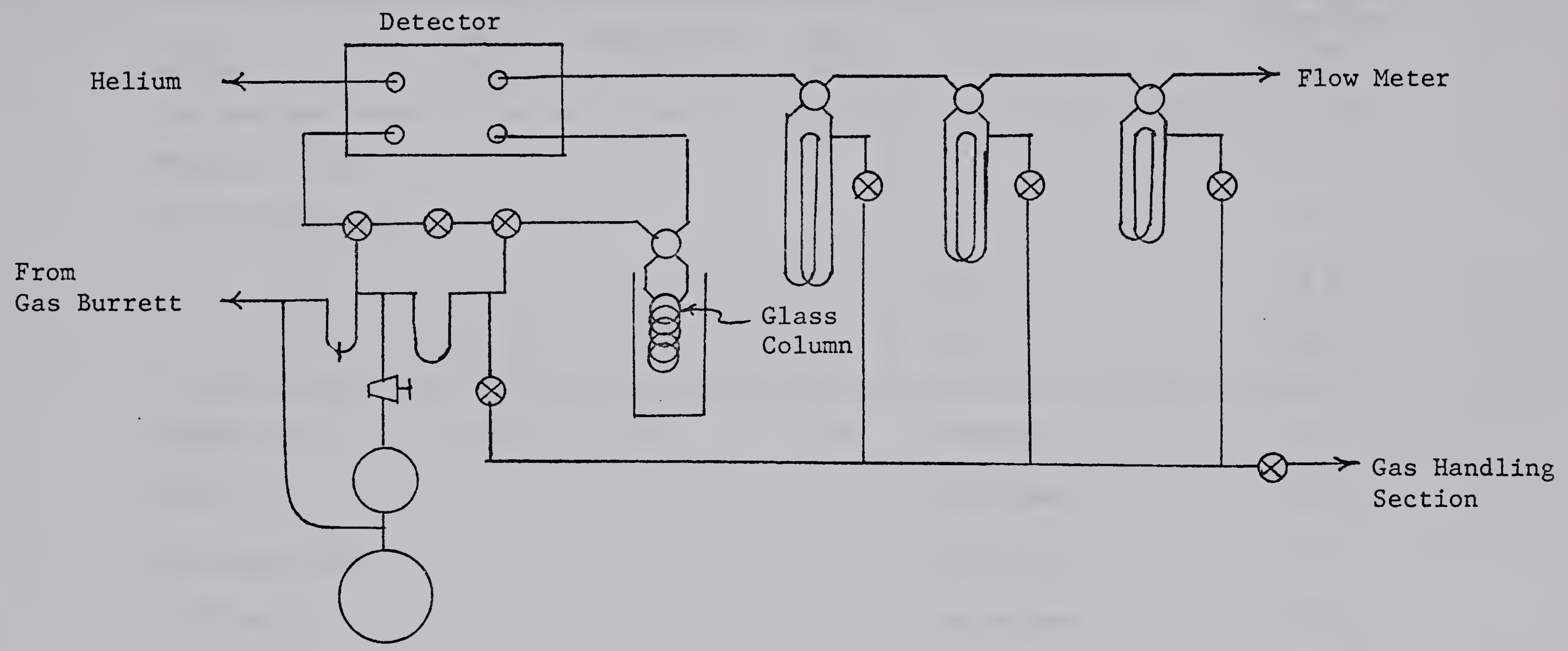
Detector
Helium
Flow Meter
From
Gas Burrett
Glass
Column
Gas Handling
Section

FIGURE 4: Gas chromatography line.

TABLE X

Operating Conditions of GLC Columns and Retention Times of Various Compounds

Column	Length ft	Temperature °C	Flow cc/min	Compounds	Retention Time min.
Molecular Sieve	10	0	45	H_2	2.4
(13X) 60/80 mesh				O_2	6.5
				N_2	8.2
				CH_4	13.6
Isoquinoline	20	27	80	Propane	3.4
(40%) on				Isobutane	4.2
Chromosorb WAW				*n*-Butane	5.5
60/80 mesh				Isopentane	8.65
				n-Pentane	11.9
				2,3-Dimethylbutane	19.2
				2-Methylpentane	21.0
				n-Hexane	33.4

2. Static Cell

Low temperature experiments with ethylene-propane mixtures were carried out in a 50 x 99 mm cylindrical quartz cell, and some hydrogen-propane mixtures in a 50 x 300 mm cylindrical quartz cell.

3. Circulating Flow Cell

In order to control the mercury concentration, two types of flow systems were used for all other experiments. One was designed to study the products and the other to study the emission occurring in the sensitization reaction.

A simple circulating system shown in Figure 3, was used to maintain low conversions while allowing a measurable buildup of products. The 50 x 40 mm cylindrical quartz cell, illuminated from the end, was enclosed in an aluminum block furnace with Hot-Watt pencil heaters. The tube leading to the cell was preheated about 5°C higher than the furnace to insure temperature equilibration of the gas. The temperature was controlled by Silicon Control Rectifiers with thermocouple detectors. Some experiments between 20° and 80°C were performed with a water bath instead of the aluminum block furnace. In all experiments the temperature was measured to ±1°C by a calibrated thermocouple-potentiometer detector.

The gas was circulated by a magnetically operated stirrer constructed of metal vanes and shaft, teflon bearings, and a glass-encased magnet. This pump was operated at about 1800 rpm to establish a rapid flow of gas through the cell (∿5 cc/sec). The mercury concentration was controlled by flowing the gas mixture through a

trap containing a drop of mercury, then through another trap filled with 1/8" glass helices before entering the cell. These two traps were kept at 0°C by an ice bath unless otherwise specified. The total volume of the system was controlled by the size of a ballast volume.

a. Mercury Lamps

In most experiments, photolyses were done by a Hanovia low pressure mercury resonance lamp #87a-45. A few runs with added H_2 were performed with a high intensity, low pressure quartz spiral mercury lamp powered by a 5000 V, 120 ma luminous tube transformer and had a 2537Å line intensity about 30 times greater than that of the Hanovia lamp. A Vycor 7910 filter was placed in front of the lamps to eliminate wavelengths below 2300Å.

b. Actinometry

Two actinometers were used to determine the 2537Å light intensity before each quantum yield experiment. a) The Hg* sensitization of propane at 800 torr and 25°C has been shown to have a quantum yield of hydrogen production of 0.58 after it has been pre-irradiated to establish an equilibrium concentration of propylene (128). b) The Hg* sensitized decomposition of N_2O at 400 torr with 1% butene added has a nitrogen quantum yield of 1.0 below 120°C.(2,124). To insure complete absorption, all the quantum yield experiments were done with the saturator at room temperature.

c. Operating Procedure

Propane was admitted to the reaction cell and frozen into the first loop. If required, hydrogen or nitrogen could then be added to obtain the desired total pressure. The gases were circulated for about 20 min with the saturator at -78°C and then 1 hr at 0°C before each run. The photolysis time was normally in the range of 5 to 20 minutes depending upon the intensity.

After irradiation, circulation was continued for about 15 minutes with both traps at -196°C in order to trap the condensable products. The added gas was then carefully pumped off through another trap kept at -196°C. In the case of pure propane, noncondensables (found to be hydrogen only) were measured in a gas burette. The remaining condensable products were distilled at -139°C and the fraction not volatile at this temperature (pentanes and hexanes) was transferred to the gas chromatograph injection loop for analysis.

4. Emission Flow System

This system was essentially the same as described earlier by Penzes, Strausz and Gunning (67).

a. Emission Cell

The cell consisted of a 10 x 140 mm "spectrosil" tube with plane 1/8" thick LiF windows. The outlet and inlet tubes were sealed close to the windows to ensure complete circulation of the gas. In some experiments this was replaced by a 200 mm double wall "spectrosil" cell which allowed a filter solution of 6 mm radial path length to surround the reaction cell. Closely spaced, blackend

brass plates collimated the exciting beam.

b. Exciting Lamp

A Hanovia low pressure mercury lamp similar to that used in the circulating system placed parallel to the emission cell was used. A stream of nitrogen cooled the lamp slightly and prevented ozone formation within the cell enclosure.

c. Spectrograph and Photographic Plates

The light emerging from the end of the cell was focused onto the entrance slit (normally 20 μm) of a Hilger-Watts medium quartz spectrograph. Kodak 130a-0 photographic plates with a linear response from 2400Å to 5000Å were used throughout. The plates were developed in Kodak D-19 developer for 3.5 minutes (25°C) and microdensitometry carried out on a Joyce, Loebl automatic recording MK IIIC instrument. The photographic plates were preexposed for 15 seconds to weak white light before the experiment to insure that the optical density of the plate was linear with log intensity.

d. Operating Procedure

A ballast pressure was first established by a low temperature bath. The flow and pressure of the gas in the cell was then controlled by two Edwards needle valves and measured on a Matheson R-2-15-AAA rotometer. The mercury saturator was maintained at 20°C. Exposure times varied from 30 seconds to 5 hours depending on the intensity.

CHAPTER III

THE REACTIONS OF H-ATOMS WITH PROPANE

The mercury photosensitized decomposition of hydrogen was used to study the reactions of H-atoms with propane as a function of temperature. The rate of reaction can be easily controlled by the intensity since, under the present conditions, the quantum yield of H_2 decomposition is unity (102), independent of temperature and pressure.

Various mixtures of hydrogen and propane at a total pressure of about 1100 torr were photolyzed at 2537Å between 37° and 177°C. The mercury vapor pressure was maintained in equilibrium with a drop of mercury at 0.7°C in the static system and 0.0°C in the flow system. The only products observed were *n*-hexane, 2-methylpentane, and 2,3-dimethylbutane. Propylene formed in the disproportionation reactions could not be separated from the propane present in the system.

The important reactions occurring in the Hg* sensitization of hydrogen in the presence of small amounts of propane are:

$$\mathrm{Hg^* + H_2 \longrightarrow H + HgH\ (Hg + H)} \qquad [15]$$

$$\mathrm{H + C_3H_8 \rightleftarrows \mathit{i}\text{-}C_3H_7(\mathit{i}\text{-}Pr) + H_2} \qquad [12]$$

$$\mathrm{\rightleftarrows \mathit{n}\text{-}C_3H_7(\mathit{n}\text{-}Pr) + H_2} \qquad [13]$$

$$\mathrm{\mathit{n}\text{-}Pr + C_3H_8 \rightleftarrows \mathit{i}\text{-}Pr + C_3H_8} \qquad [14]$$

$$\mathrm{2\mathit{n}\text{-}Pr \longrightarrow \mathit{n}\text{-}Hexane\ (Hx)} \qquad [16]$$

$$\mathrm{\longrightarrow C_3H_8 + C_3H_6} \qquad [17]$$

$$n\text{-Pr} + i\text{-Pr} \longrightarrow \text{2-methylpentane (MP)} \qquad [18]$$

$$\longrightarrow C_3H_8 + C_3H_6 \qquad [19]$$

$$2i\text{-Pr} \longrightarrow \text{2,3-dimethylbutane (DMB)} \qquad [20]$$

$$\longrightarrow C_3H_8 + C_3H_6 \qquad [21]$$

A steady-state treatment of this reaction scheme gives the following expression for the fractional rate of production of *n*-propyl radicals in terms of the total propyl radicals produced (see Appendix B for derivation):

$$R_{(n)}/R_{(n+i)} = Q_1 - Q_2 - Q_3/2 \qquad [22]$$

where

$$Q_1 = \frac{k_{13}[H][C_3H_8]}{(k_{12}+k_{13})[H][C_3H_8] - \{k_{-12}[i\text{-Pr}] + k_{-13}[n\text{-Pr}]\}[H_2]}$$

$$Q_2 = \frac{k_{-13}[H_2][n\text{-Pr}]}{R_{(n+i)}}$$

$$Q_3 = \frac{2[C_3H_8]\{k_{14}[n\text{-Pr}] - k_{-14}[i\text{-Pr}]\}}{R_{(n+i)}}$$

The terms $R_{(n)}$ and $R_{(n+i)}$ denote the local rates of production of *n*-propyl and total propyl radicals, and are proportional to the local absorbed intensity. The ratio $R_{(n)}/R_{(n+i)}$ has been calculated for each experiment assuming reactions [16] to [21] are the only ones producing hexane products and the disproportionation to recombination ratios from Terry and Futrell (130, Table XXII in Appendix A). These results are summarized for both the static and flow systems in Table XI. The quantities Q_2 and Q_3 make only small

TABLE XI

Mercury Photosensitization of Hydrogen in the Presence of Propane

Temp °C	Time min	H_2 torr	C_3H_8 torr	DMB μmoles	$\frac{R_{(n)}}{R_{(n+i)}}$	δQ_1	$\delta(Q_2+Q_3/2)$	$\frac{R_{24}}{R_{12+13}}$	$\frac{k_{13}}{k_{12}}$
					Static System				
45	5.0	745	267	0.398	.0505	0.0003	0.0003	0.027	0.0536
45	3.0	745	267	0.239	.0536	0.0004	0.0004	0.017	0.0571
93	4.0	833	307	0.310	.0826	0.0079	0.0054	0.007	0.0964
144	4.0	981	347	0.365	.0870	0.0635	0.0353	0.004	0.1381
116	4.0	921	326	0.345	.0851	0.0230	0.0139	0.005	0.1096
70	4.0	806	288	0.357	.0669	0.0019	0.0015	0.014	0.0733
116	4.0	945	232	0.358	.0915	0.0248	0.0140	0.008	0.1176
					Flow System				
177	4.0	909	152	1.81	.1001	0.0374	0.0183	0.014	0.1337
86	2.5	907	151	1.40	.0660	0.0007	0.0004	0.039	0.0711
70	2.8	901	150	1.80	.0591	0.0003	0.0002	0.067	0.0630
37	2.5	902	151	1.49	.0502	0.0	0.0	0.110	0.0529
140	2.8	902	150	2.70	.0923	0.0069	0.0035	0.033	0.1059

contributions to the rate equation and can be calculated in the following way. Since

$$R_{Hx} = k_{16}[n\text{-Pr}]^2 \quad \text{and} \quad R_{DMB} = k_{20}[i\text{-Pr}]^2$$

therefore, $Q_2 = \dfrac{k_{-13}[H_2]}{R_{(n+i)}}\left(\dfrac{R_{Hx}}{k_{16}}\right)^{\frac{1}{2}}$

and $$Q_3 = \frac{2R_{DMB}^{\frac{1}{2}}}{R_{(n+i)}}\left(\frac{R_{MP}}{2R_{DMB}} - K_{14}^{-1}\right)\frac{k_{14}}{k_{20}^{\frac{1}{2}}}[C_3H_8]$$

where $K_{14} = k_{14}/k_{-14}$. Rearrangement of equation [22] gives

$$\frac{k_{12}}{k_{13}} = [R_{(n)}/R_{(n+i)} + Q_2 + Q_3/2]^{-1} + Q_1' - 1 \qquad [23]$$

where $$Q_1' = \frac{[H_2]\{k_{-13}[n\text{-Pr}] + k_{-12}[i\text{-Pr}]\}}{k_{13}[H][C_3H_8]}$$

Substituting expressions for the concentrations of *n*-propyl and isopropyl and assuming $k_{13}[H][C_3H_8] = R_{(n)}$, Q_1' becomes

$$Q_1' = \frac{(k_{-13}R_{MP}/R_{DMB} + k_{-12})[H_2](R_{DMB}/k_{20})^{\frac{1}{2}}}{R_{(n+i)}}$$

It should be noted that equation [23] is in terms of local rates, whereas evaluation of Q_1', Q_2 and Q_3 all require measured rates. Written in terms of measured rates, equation [23] contains the factor δ

$$\delta = \frac{2\{1-\exp(-\varepsilon[Hg]L/2)\}}{\{\varepsilon[Hg]L[1-\exp(-\varepsilon[Hg])]\}^{\frac{1}{2}}}$$

which takes into account the effect of nonlinear absorption of the incident light.

$$\frac{k_{12}}{k_{13}} = [R_{(n)}/R_{(n+i)} + \delta(Q_2 + Q_3)]^{-1} + \delta Q_1' - 1$$

The following rate constants were employed in calculating k_{12}/k_{13}:

$K_{14} = \exp(3.6\text{x}10^3/RT - 0.51)$ (125),

$\frac{k_{14}}{k_{20}^{\frac{1}{2}}} = 6.76 \exp(-8.25\text{x}10^3/RT)\ (\text{cc mole}^{-1}\text{sec}^{-1})^{\frac{1}{2}}$ (125),

k_{-13} has been estimated from the analogous reaction with ethyl radicals as $\log k_{-13} = 12.57 - 13.73\text{x}10^3/2.3RT$ (cc mole^{-1}sec^{-1}) (124),

k_{-12} has been estimated from k_{-13} assuming the same frequency factor and increasing the activation energy by the difference in the heats of formation of the propyl radicals, $\Delta H_f = 2.9$ kcal/mole (112). Thus, $\log k_{-12} = 12.57 - 16.6\text{x}10^3/2.3RT$ (cc mole^{-1}sec^{-1}). Although this may be far from accurate it is adequate for these calculations.

The calculations of these quantities for the static and flow systems are given in Table XI. The ratio $R_{(n)}/R_{(n+i)}$ primarily determines the k_{13}/k_{12} value. Figure 5 displays an Arrhenius plot of k_{13}/k_{12} and a least mean square treatment of the data, weighing the flow system points as twice the others, gives

$$\log \frac{k_{13}}{k_{12}} = 0.13\pm0.09 - \frac{2010\pm190}{2.3RT}$$

for 90% confidence limit. Thus $k_{13}/k_{12} = 1.38 \exp(-2.0\text{x}10^3/RT)$ in good agreement with the ratio estimated from the individual rate

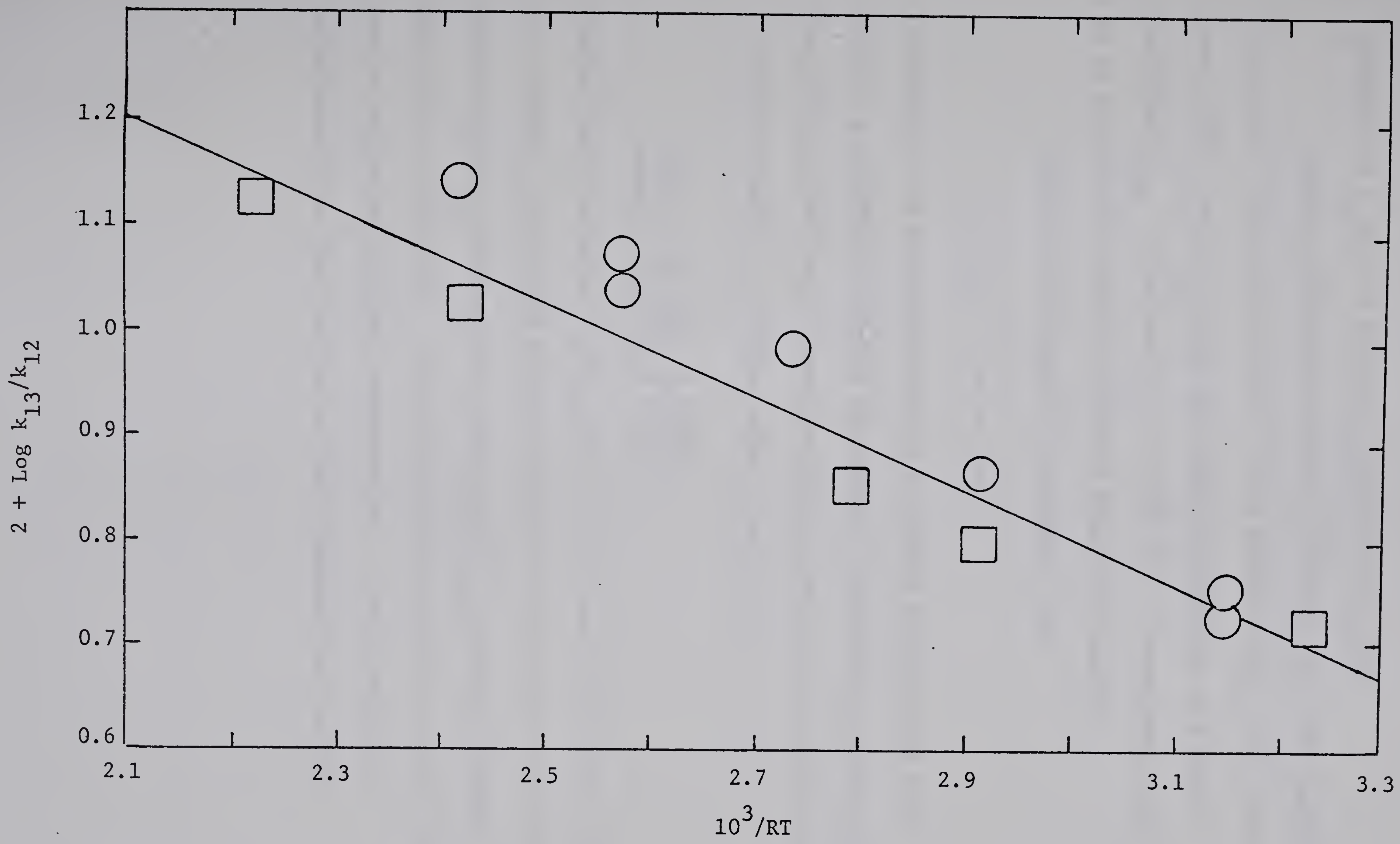

FIGURE 5: Arrhenius plot of the k_{13}/k_{12} ratio for the H-atom abstraction from propane by H-atoms, from Table XI.

constants of $k_n/k_i = 0.8 \exp(-1.7\text{x}10^3/RT)$ (122,123).

Mercury photosensitization of propane has been neglected in the above treatment because, at the maximum $[C_3H_8]/[H_2]$ ratio used (0.36), only 8% of the Hg* atoms are quenched by propane assuming $\sigma^2_{C_3H_8} = 2.9\text{Å}^2$ and $\sigma^2_{H_2} = 10.8\text{Å}^2$ (8). Consequently less than 4% of the propyl radicals originate from this reaction.

Addition of H-atoms to propylene (129)

$$H + C_3H_6 \longrightarrow n\text{- or } i\text{-Pr} \qquad [24]$$

produced in the disproportionation of propyl radicals has been kept to a minimum by keeping the percent conversion of propane low. The ratio of the rate of reaction [24] to the rate of H-atom abstraction from propane by hydrogen atoms is given by

$$\frac{R_{24}}{R_{12+13}} = \left(\frac{k_{24}}{k_{12}+k_{13}}\right)\frac{[C_3H_6]}{[C_3H_8]}$$

Taking Yang's value of $k_{24}/(k_{12}+k_{13}) = 0.715 \exp(4.8\text{x}10^3/RT)$ (123) and assuming the average propylene concentration to be half of the total propylene produced, the ratio R_{24}/R_{12+13} can be estimated for each run (Table XI). Since this ratio is small, reaction [24] can be neglected at higher temperatures. It may contribute significantly to the kinetics at lower temperatures, however.

CHAPTER IV

MERCURY 6($^3P_1$) SENSITIZED DECOMPOSITION OF PROPANE

RESULTS AND DISCUSSION

In order to determine the effect of temperature on the initial yields of *n*- and isopropyl radicals, the mercury photosensitized decomposition of propane has been carried out between 0° and 200°C. The yield ratio can be determined from the observed rates of production of *n*-propyl and isopropyl radicals provided all other reactions producing propyl radicals in the system are taken quantitatively into account, or alternately can be suppressed, and the only reactions removing propyl radicals from the system are radical-radical recombination and disproportionation. The important steps in the mercury photosensitization of propane at moderate pressures (P > 100 torr) are as follows:

$$\mathrm{Hg} + h\nu(2537\,\mathring{A}) \rightleftarrows \mathrm{Hg}^* \tag*{[I]}$$

$$\mathrm{Hg}^* + C_3H_8 \longrightarrow (\mathrm{Hg}C_3H_8)^* \tag*{[25]}$$

$$(\mathrm{Hg}C_3H_8)^* \longrightarrow i\text{-Pr} + \mathrm{H} + \mathrm{Hg} \tag*{[26]}$$

$$\longrightarrow n\text{-Pr} + \mathrm{H} + \mathrm{Hg} \tag*{[27]}$$

$$\longrightarrow C_3H_8 + \mathrm{Hg}^\circ \tag*{[28]}$$

$$\longrightarrow C_3H_8 + \mathrm{Hg} + h\nu' \tag*{[29]}$$

$$\mathrm{Hg}^\circ + C_3H_8 \longrightarrow (\mathrm{Hg}C_3H_8)^\circ \tag*{[30]}$$

$$(\mathrm{Hg}C_3H_8)^\circ \longrightarrow i\text{-Pr} + \mathrm{H} + \mathrm{Hg} \tag*{[31]}$$

$$\longrightarrow \textit{n}\text{-Pr} + \mathrm{H} + \mathrm{Hg} \qquad [32]$$

$$\longrightarrow \mathrm{C_3H_8} + \mathrm{Hg} + h\nu'' \qquad [33]$$

$$\textit{n}\text{-Pr} + \mathrm{C_3H_8} \rightleftarrows \textit{i}\text{-Pr} + \mathrm{C_3H_8} \qquad [14]$$

$$\mathrm{H} + \mathrm{C_3H_8} \longrightarrow \textit{i}\text{-Pr} + \mathrm{H_2} \qquad [12]$$

$$\longrightarrow \textit{n}\text{-Pr} + \mathrm{H_2} \qquad [13]$$

$$2\textit{n}\text{-Pr} \longrightarrow \textit{n}\text{-Hexane (Hx)} \qquad [16]$$

$$\longrightarrow \mathrm{C_3H_6} + \mathrm{C_3H_6} \qquad [17]$$

$$\textit{n}\text{-Pr} + \textit{i}\text{-Pr} \longrightarrow \text{2-methylpentane (MP)} \qquad [18]$$

$$\longrightarrow \mathrm{C_3H_8} + \mathrm{C_3H_6} \qquad [19]$$

$$2\textit{i}\text{-Pr} \longrightarrow \text{2,3-dimethylbutane (DMB)} \qquad [20]$$

$$\longrightarrow \mathrm{C_3H_8} + \mathrm{C_3H_6} \qquad [21]$$

The quantum yield of propane decomposition by Hg* atoms is given by

$$\Phi^* = (k_{26}+k_{27})/(k_{26}+k_{27}+k_{28}+k_{29}),$$

the quantum yield of spin-orbit relaxation of Hg* atoms to the Hg° level by propane is

$$\Phi' = k_{28}/(k_{26}+k_{27}+k_{28}+k_{29}),$$

and the quantum yield of propane decomposition by Hg° atoms is

$$\Phi^\circ = (k_{31}+k_{32})/(k_{31}+k_{32}+k_{33}).$$

A steady-state treatment of these reactions gives the following expression (Appendix B):

$$\frac{2R_{(n)}}{R_{(n+i)}} = Q_4 + k_{13}/(k_{12}+k_{13}) - \delta Q_3 \qquad [43]$$

where $Q_4 = \dfrac{k_{27}[(HgC_3H_8)^*] + k_{32}[(HgC_3H_8)^\circ]}{(k_{26}+k_{27})[(HgC_3H_8)^*] + (k_{31}+k_{32})[(HgC_3H_8)^\circ]}$

and $Q_3 = \dfrac{R_{DMB}^{\frac{1}{2}}}{R_{(n+i)}}\left(\dfrac{R_{MP}}{R_{DMB}} - 2K_{14}^{-1}\right)\dfrac{k_{14}}{k_{20}^{\frac{1}{2}}}[C_3H_8]$

The term δ is the correction factor which must be applied when the observed rates of product formation are used rather than local rates given by the steady state treatment, because of the very large absorption coefficient of mercury (1,124). Since $R_{DMB}^{\frac{1}{2}}/R_{(n+i)}$ is proportional to $I^{-\frac{1}{2}}$, Q_3 is the only term in equation [43] dependent on intensity and δ is given by

$$\delta = \frac{2\{1-\exp(-\varepsilon[Hg]L/2)\}}{\{\varepsilon[Hg](1-\exp(-\varepsilon[Hg]L))\}}$$

where ε is the extinction coefficient of mercury and L is the optical path length. The rates of *n*-propyl radicals $[R_{(n)}]$ and total propyl radicals $[R_{(n+i)}]$ produced in the system are calculated from the hexane products as described in Appendix A.

In order to verify this kinetic treatment, a series of experiments was performed at 202°C by varying the light intensity and propane pressure (Table XII). The ratio $2R_{(n)}/R_{(n+i)}$ from Table XII is plotted in Figure 6 against $\delta[C_3H_8](R_{DMB}^{\frac{1}{2}}/R_{(n+i)})(R_{MP}/R_{DMB}-2K_{14}^{-1})$. The slope $(k_{14}/k_{20}^{\frac{1}{2}})$ is -0.132 in good agreement with the value -0.130 $(\text{cc mole}^{-1}\ \text{sec}^{-1})^{\frac{1}{2}}$ calculated from the data of Berkley, Woodall, Strausz and Gunning (125). Therefore the value of $k_{14}/k_{20}^{\frac{1}{2}}$ obtained

TABLE XII

Mercury Photosensitization of Propane

Temp °C	Time min	C_3H_8 torr	DMB μmoles	$\frac{2R_{(n)}}{R_{(n+i)}}$	δQ_3	β	χ^a	$\frac{k_{27}}{k_{26}}$
203	16	101	0.324	0.276	0.015	0.63	0.112	0.230
203	20	202	0.516	0.261	0.025	0.63	0.186	0.218
201	70	254	1.012	0.237	0.036	0.63	0.282	0.193
201	17	94	0.333	0.282	0.014	0.63	0.110	0.246
200	180	203	0.350	0.214	0.068	0.63	0.546	0.217
202	70	205	0.224	0.235	0.062	0.63	0.478	0.249
164	60	184	0.853	0.253	0.016	0.64		0.238
139	50	178	1.62	0.241	0.006	0.65		0.225
115	40	179	0.899	0.210	0.004	0.66		0.183
96	40	180	0.790	0.196	0.002	0.69		0.175
57	50	184	0.822	0.163	0.001	0.76		0.143
190	40	184	0.561	0.267	0.026	0.63		0.256
37	35	184	0.483	0.143	0.001	0.82		0.121
152	35	184	0.708	0.225	0.007	0.64		0.174

[a] $\chi = \delta[C_3H_8](R^{\frac{1}{2}}_{DMB}/R_{(n+i)})(R_{MP}/R_{DMB}-2K^{-1}_{14})$

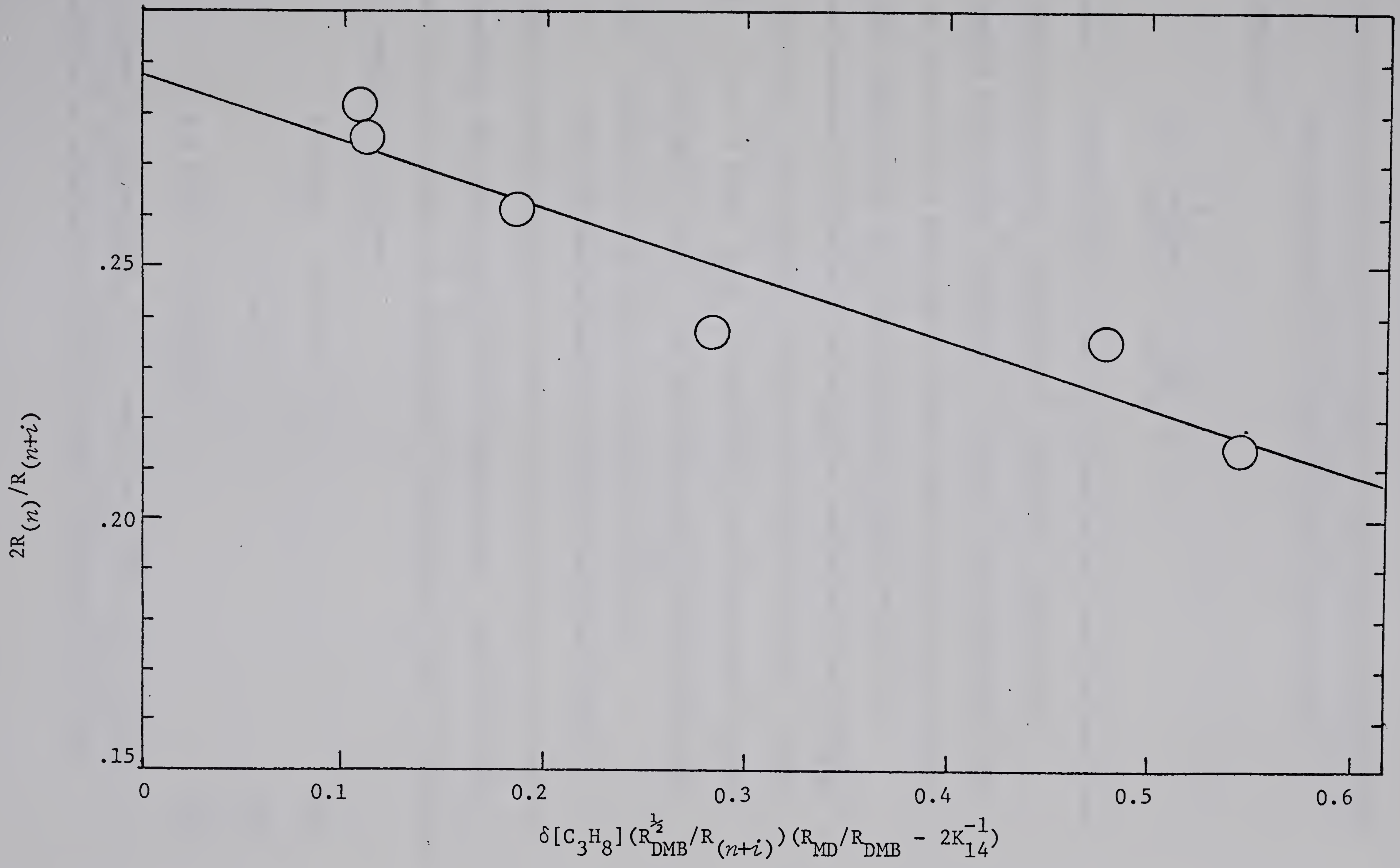

FIGURE 6: A plot of $2R_{(n)}/R_{(n+i)}$ against $\delta[C_3H_8][R^{1/2}_{DMB}/R_{(n+i)})(R_{MP}/R_{DMB} - 2K^{-1}_{14})$ from the mercury photosensitization of propane at 200°C from Table XII.

from reference (125) has been adopted in the following computations.

The expression Q_4 can be separated into two terms (Appendix B):

$$Q_4 = \frac{k_{27}}{k_{26}+k_{27}}\,\beta + \frac{k_{32}}{k_{31}+k_{32}}\,(1 - \beta)$$

where $\beta = \Phi^*/(\Phi^* + \Phi^\circ\Phi')$. Thus Q_4 is made up of contributions from both the Hg* and Hg° decomposition reactions. Since Φ', the quantum yield of Hg° formation, is 0.38 at room temperature (44), the value of β is near unity and the ratio $k_{27}/(k_{26}+k_{27})$ is the major component of Q_4. The quantitites $k_{32}/(k_{31}+k_{32})$ and Φ° are evaluated in Chapter V assuming that emission of the $(HgC_3H_8)^*$ complex is small compared to the other reactions (67,69) so that $\Phi^* = 1 - \Phi' = 0.62$. Also, calculations have been carried out for Q_3, $k_{13}/(k_{12}+k_{13})$, and β, and the ratio k_{27}/k_{26} derived from each run. A summary of the results is given in Table XII.

The ethylene scavenging technique described earlier (113,114) which suppresses reactions [12] and [13] has been used to determine the ratio k_{27}/k_{26} at low temperatures. Since the ratio of the rate constant for abstraction from propane to that of addition to ethylene by H-atoms

$$H + C_3H_8 \longrightarrow i\text{-Pr} + H_2 \qquad [12]$$

$$\longrightarrow n\text{-Pr} + H_2 \qquad [13]$$

$$H + C_2H_4 \longrightarrow C_2H_5(Et) \qquad [34]$$

is given by $(k_{12}+k_{13})/k_{34} = 1.1\exp(-4.4\times10^3/RT)$ (123), H-atom addition to ethylene is favored at lower temperatures and only

very small concentrations of ethylene are required to suppress the abstraction reactions [12] and [13]. Larger amounts of ethylene needed above room temperature can, however, interfere with the initial sensitization reaction by direct quenching of the excited mercury atoms,

$$Hg^* + C_2H_4 \longrightarrow Hg + C_2H_4^* \longrightarrow C_2H_4$$

resulting in an overall reduction in the decomposition rate. The primary yield of *n*- and isopropyl radicals is not affected however, since the excited ethylene does not lead directly to the production of propyl radicals or pentane products (131).

At room temperature and below, the reaction

$$n\text{-Pr} + C_3H_8 \rightleftarrows i\text{-Pr} + C_3H_8 \qquad [14]$$

can be neglected in the present system. At low temperatures, addition of a few percent ethylene leads to the production of ethyl radicals which can combine with the propyl radicals present in the system as follows:

$$\text{Et} + n\text{-Pr} \longrightarrow n\text{-pentane} \qquad [35]$$

$$\longrightarrow C_2H_4 + C_3H_8 \text{ or } C_2H_6 + C_3H_6 \qquad [36]$$

$$\text{Et} + i\text{-Pr} \longrightarrow \text{isopentane} \qquad [37]$$

$$\longrightarrow C_2H_4 + C_3H_8 \text{ or } C_2H_6 + C_3H_6 \qquad [38]$$

$$2\text{Et} \longrightarrow n\text{-butane} \qquad [39]$$

$$\longrightarrow C_2H_4 + C_2H_6 \qquad [40]$$

The rates of *n*-propyl and total propyl radical products are calculated

from the pentane and hexane products (Appendix A) and are summarized in Table XIII. The maximum percentage of the H-atoms reacting with propane and the percent of the Hg* atoms quenched by ethylene are also included in this table. The amount of propyl radical addition to ethylene

$$n\text{-Pr or } i\text{-Pr} + C_2H_4 \longrightarrow C_5H_{11} \qquad [41]$$

can be estimated from the total propyl radical production

$$2i\text{-Pr} \longrightarrow \text{2,3-dimethylbutane} \qquad [20]$$

$$\frac{R_{41}}{R_{20}} = \frac{k_{41}[C_2H_4]}{k_{20}[i\text{-Pr}]} = \frac{k_{41}[C_2H_4]}{k_{20}(R_{20}/k_{20})^{\frac{1}{2}}}$$

by taking log $k_{41} = 11.22 - 6.93\text{x}10^3/2.3RT$ (132) and $k_{20} = 10^{13.8}$ cc mole^{-1} sec^{-1} (133). The ratio R_{41}/R_{20} is 0.006 for the run at 29°C and therefore it is reasonable to neglect the addition of propyl radicals to the ethylene in the kinetic treatment.

A steady-state treatment of reactions [16] - [21] and [25] - [40] gives

$$\frac{R_{(n)}}{R_{(n+i)}} = \frac{k_{27}[(HgC_3H_8)^*] + f^\circ k_{32}[(HgC_3H_8)^\circ]}{(k_{26}+k_{27})[(HgC_3H_8)^*] + f^\circ(k_{31}+k_{32})](HgC_3H_8)^\circ]}$$

where f° is the fraction of Hg* atoms which leads to decomposition of propane _via_ the Hg° level. An expression for f° can be estimated from the competitive quenching of Hg° atoms by ethylene and propane

$$Hg^\circ + C_2H_4 \longrightarrow Hg + C_2H_4^* \longrightarrow C_2H_4 \qquad [42]$$

$$Hg^\circ + C_3H_8 \longrightarrow (HgC_3H_8)^\circ \qquad [30]$$

TABLE XIII

Mercury Photosensitization of Propane-Ethylene Mixtures

Temp °C	Time min	C_3H_8 torr	$\frac{C_2H_4}{C_3H_8}$ %	*i*-P µmoles	DMB µmoles	$\frac{R_{(n)}}{R_{(n+i)}}$	$\frac{R_{12+13}}{R_{34}}$	χ^a	f° x10^2	$\frac{k_{27}}{k_{26}}$
0	15	494	1.03	0.134	0.0878	0.0797	0.031	14	0.4	0.0869
0	40	399	0.69	0.334	0.209	0.0793	0.046	11	0.6	0.0865
0	30	401	1.97	0.320	0.189	0.0845	0.017	22	0.2	0.0925
29	30	299	1.55	0.593	0.320	0.0918	0.044	19	0.7	0.1016
28	40	301	2.81	0.557	0.292	0.0914	0.025	25	0.4	0.1009

[a] Per cent Hg* quenched by ethylene.

and is given by

$$f^\circ = \Phi'\Phi^\circ/(1 + k_{42}[C_2H_4]/k_{30}[C_3H_8])$$

The value of f° for each experiment (Table XIII) has been calculated assuming $k_{42}/k_{30} = 954.$ (44), $\Phi' = 0.38$ (44), and the evaluation of Φ° described in Chapter V. Since f° is small, the expression for $R_{(n)}/R_{(n+i)}$ can be approximated by the equation

$$\frac{R_{(n)}}{R_{(n+i)}} = \frac{k_{27}}{k_{26}+k_{27}}(1 - f^\circ) + \frac{k_{32}}{k_{31}+k_{32}} f^\circ$$

The ratio of $k_{32}/(k_{31}+k_{32})$ is known (Chapter V) and the ratio $k_{27}/(k_{26}+k_{27})$ has been calculated from the observed $R_{(n)}/R_{(n+i)}$ ratio for each run. These computations are summarized in Table XIII.

An Arrhenius plot of k_{27}/k_{26} from Tables XII and XIII is shown in Figure 7. A least mean square calculation of the experimental points in Figure 7 gives

$$\log k_{27}/k_{26} = -0.05 \pm 0.04 - \frac{1251 \pm 76}{2.3RT}$$

where the error limits are one standard deviation. For comparison, the results of Holroyd and Klein (113), Chesick (114) and Jakubowski, Kebarle, Strausz and Gunning (115) are also plotted in Figure 7. Since these studies did not take into account the effect of spin-orbit relaxation by propane

$$(HgC_3H_8)^* \longrightarrow Hg^\circ + C_3H_8 \qquad [28]$$

their values are expected to represent a combination of both the Hg* and Hg° decomposition of propane, leading to a k_{27}/k_{26} ratio lower than that found in the present study. The ethylene scavenging

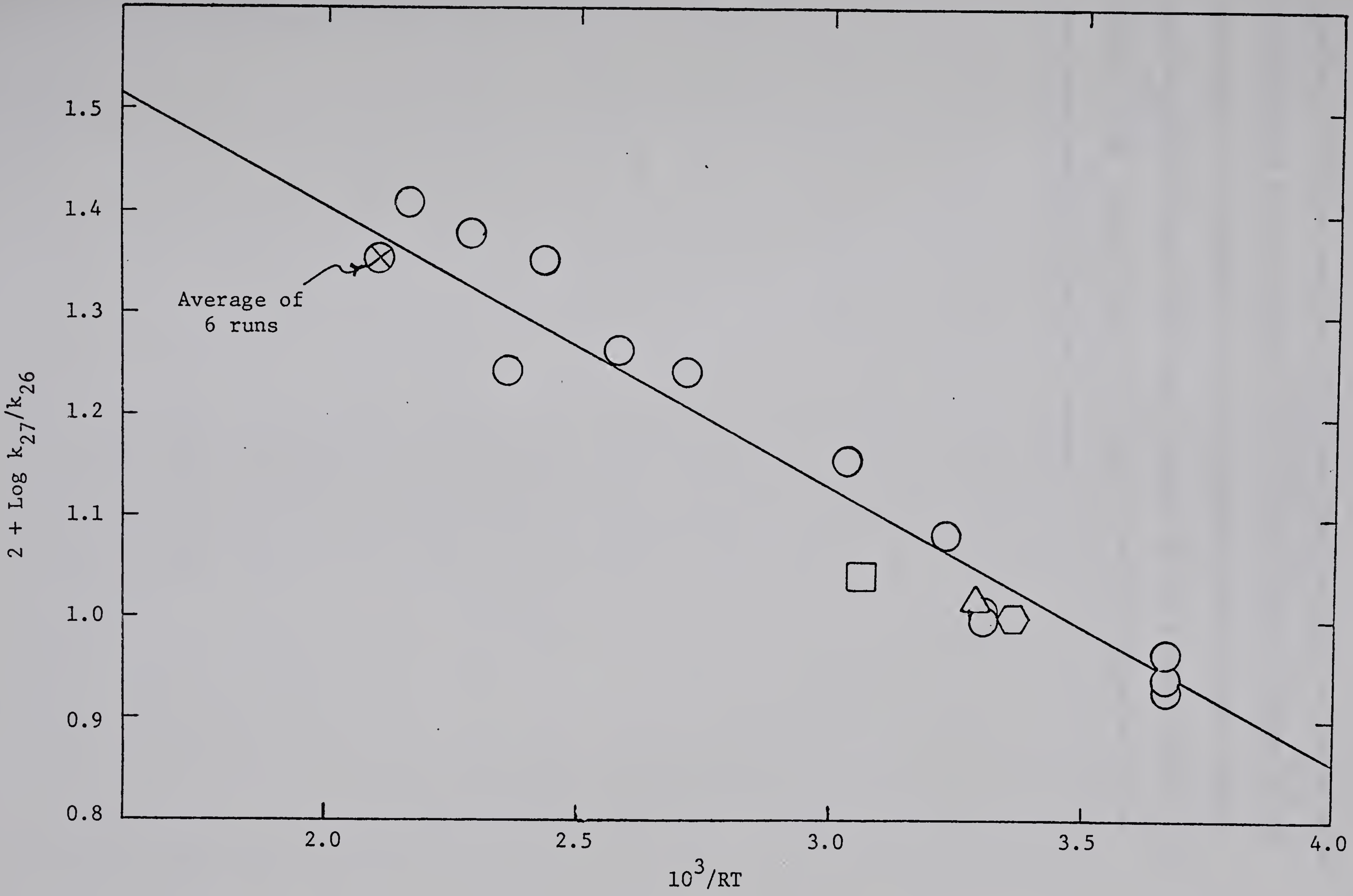

FIGURE 7: Arrhenius plot of the k_{27}/k_{26} ratio for the Hg* sensitized decomposition of propane: ○, this work (Tables XII and XIII); ⬡, reference (113); △, reference (114); □, reference (115).

studies of Holroyd and Klein (113) and Chesick (114) are not affected significantly by the presence of Hg° atoms, however, because of the quenching by the ethylene as in the present system. These results are in good agreement with those obtained in the present study. The effect of Hg° atoms is more pronounced in the determination by the mass spectrometric technique, however.

CHAPTER V

REACTIONS OF Hg($^3P_0$) ATOMS WITH PROPANE

1. Results

Since propane quenches Hg* atoms to the Hg° level with a quantum yield of 0.38 at room temperature (44), the observed *n*- and isopropyl radicals formed in pure propane are the result of both Hg* and Hg° sensitized decomposition. In order to distinguish between the reactivity of these two species, various ratios of nitrogen and propane were photosensitized at a constant total pressure of 1000 torr. The effect of temperature was also studied in a series of experiments between 27° and 200°C. The quantum yield of propyl radical formation has been determined at 65° and 200°C. The results are summarized in Table XIV together with calculated quantities based on the data (*vide infra*).

Initial radical yields in the mercury photosensitized decomposition of a mixture of nitrogen and propane have been evaluated in terms of the following reactions:

$$\mathrm{Hg} + h\nu(2537\mathring{A}) \longrightarrow \mathrm{Hg}^* \qquad [I]$$

$$\mathrm{Hg}^* + C_3H_8 \longrightarrow (\mathrm{Hg}C_3H_8)^* \qquad [25]$$

$$(\mathrm{Hg}C_3H_8)^* \longrightarrow i\text{-Pr} + H + \mathrm{Hg} \qquad [26]$$

$$\longrightarrow n\text{-Pr} + H + \mathrm{Hg} \qquad [27]$$

$$\longrightarrow C_3H_8 + \mathrm{Hg}^\circ \qquad [28]$$

$$\longrightarrow C_3H_8 + \mathrm{Hg} + h\nu' \qquad [29]$$

TABLE XIV

Mercury Photosensitization of Propane-Nitrogen Mixtures

Time min	C_3H_8 torr	N_2 torr	DMB µM	$\frac{2R_{(n)}}{R_{(n+i)}}$	F	β	χ^a	y^b
		T = 27°C		$k_{13}/(k_{12}+k_{13}) = 0.0439$				
12.2	30.0	910	0.083	0.0855	0.172	0.125	-	0.0417
20.1	29.9	910	0.782	0.0935	0.172	0.125	-	0.0494
6.0	30.2	920	0.217	0.0948	0.172	0.125	-	0.0510
7.0	15.1	963	0.151	0.0810	0.087	0.073	-	0.0370
6.0	49.9	901	0.268	0.0914	0.276	0.172	-	0.0475
5.0	74.1	868	0.177	0.0975	0.401	0.213	-	0.0537
		T = 63°C		$k_{13}/(k_{12}+k_{13}) = 0.0616$				
15	17.2	1123	0.263	0.0981	0.076	0.070	-	0.0366
14	9.5	1140	0.221	0.103	0.046	0.044	-	0.0412
14	32.6	1127	0.295	0.0957	0.132	0.115	-	0.0342
12	58.5	1097	0.258	0.104	0.226	0.181	-	0.0419
10	81.3	1074	0.240	0.108	0.307	0.229	-	0.0464
12	28.9	910	0.244	0.119	0.143	0.124	-	0.0561
6	28.2	927	0.257	0.167	0.138	0.120	-	0.0533
6	12.4	990	0.181	0.107	0.065	0.060	-	0.0447
5	68.8	867	0.205	0.114	0.319	0.236	-	0.0519
5	50.5	905	0.154	0.189	0.235	0.187	-	0.0563
24	12.1	995	0.127	0.105	0.063	0.059	0.308	0.0423
25	19.4	990	0.248	0.104	0.093	0.085	0.647	0.0414
25	9.9	1038	0.177	0.114	0.052	0.049	0.459	0.0520
27	4.9	1052	0.076	0.125	0.031	0.030	0.201	0.0622
25	41.1	1007	0.157	0.107	0.179	0.149	0.471	0.0448
25	33.2	1004	0.148	0.125	0.148	0.128	0.480	0.0626
20	17.2	1004	0.144	0.110	0.084	0.077	0.360	0.0470
25	16.4	910	0.234	0.109	0.087	0.080	0.536	0.0468

TABLE XIV (cont'd)

Mercury Photosensitization of Propane-Nitrogen Mixtures

Time min	C_3H_8 torr	N_2 torr	DMB μM	$\frac{2R_{(n)}}{R_{(n+i)}}$	F	β	χ^a	y^b
21	26.3	908	0.200	0.105	0.132	0.115	0.550	0.0429
25	12.6	906	0.198	0.105	0.070	0.065	0.420	0.0429
20	40.0	906	0.230	0.112	0.192	0.158	0.640	0.0495
20	20.3	906	0.203	0.117	0.105	0.094	0.585	0.0549
23	9.9	906	0.178	0.106	0.058	0.054	0.456	0.0436
6.5	61.0	912	0.230	0.115	0.275	0.212	0.694	0.0526
20	88.6	906	0.260	0.117	0.381	0.269	0.883	0.0545
19	88.1	906	0.257	0.110	0.379	0.268	0.951	0.0477
13	156.2	820	0.183	0.123	0.647	0.379	0.1087	0.0608
13	234.4	740	0.193	0.123	0.922	0.459	0.303	0.0610
25	321.0	680	0.240	0.128	1.187	0.497	1.724	0.0686
60	470.0	480	0.694	0.139	1.642	0.587	1.99	0.0782
73	640.0	240	0.686	0.149	2.154	0.641	2.29	0.0894
		T = 124°C		$k_{13}/(k_{12}+k_{13})$ = 0.0944				
12	17.8	1137	0.206	0.163	0.082	0.078	-	0.0691
12	30.8	1124	0.230	0.159	0.120	0.111	-	0.0661
14	9.7	1141	0.197	0.154	0.058	0.055	-	0.0606
11	53.1	1100	0.242	0.152	0.185	0.163	-	0.0580
11	78.1	1077	0.218	0.168	0.257	0.216	-	0.0751
14	11.6	1120	0.217	0.162	0.065	0.062	-	0.0674
100	29.8	1135	1.546	0.169	0.117	0.108	-	0.0750
11	60.8	1108	0.178	0.165	0.206	0.178	-	0.0727
11	27.8	908	0.119	0.168	0.131	0.119	-	0.0738

TABLE XIV (cont'd)

Mercury Photosensitization of Propane-Nitrogen Mixtures

Time min	C_3H_8 torr	N_2 torr	DMB µM	$\frac{2R_{(n)}}{R_{(n+i)}}$	F	β	χ^a	y^b
		T = 166°C		$k_{13}/(k_{12}+k_{13}) = 0.1175$				
14	8.2	1160	0.184	0.214	0.075	0.072	-	0.0969
12	17.2	1175	0.148	0.210	0.097	0.091	-	0.0949
11	38.1	1133	0.196	0.214	0.151	0.137	-	0.0992
11	59.6	1105	0.202	0.217	0.206	0.181	-	0.1043
12.8	82.3	1082	0.244	0.224	0.264	0.224	-	0.1127
12.7	29.1	1135	0.247	0.215	0.128	0.118	-	0.1000
11.5	30.4	910	0.198	0.218	0.151	0.137	-	0.1016
		T = 200°C		$k_{13}/(k_{12}+k_{13}) = 0.1358$				
25	66.3	820	0.189	0.239	0.285	0.240	1.05	0.1148
25	151.0	784	0.198	0.229	0.517	0.387	1.22	0.1168
23	239.0	680	0.199	0.232	0.778	0.516	1.49	0.1324
22	349.0	605	0.191	0.221	1.054	0.625	1.65	0.135
22.1	428.0	514	0.182	0.226	1.28	0.699	1.71	0.155
60	555.0	350	0.511	0.213	1.68	0.802	1.87	0.153
72	700.0	125	0.614	0.206	2.27	0.916	2.26	0.163

[a] $$\chi = \Phi_T\left[1 + \frac{k_{10}}{k_{30}}\,\frac{[Hg][N_2]}{[C_3H_8]} + F(1 - \Phi' + \frac{k_{-I}}{k_{25}[C_3H_8]})\right]$$

[b] $$y = 2R_{(n)}/R_{(n+i)} - k_{13}/(k_{12}/k_{13}) + \delta Q_3$$

$$\mathrm{Hg}^{\circ} + \mathrm{C_3H_8} \longrightarrow (\mathrm{HgC_3H_8})^{\circ} \qquad [30]$$

$$(\mathrm{HgC_3H_8})^{\circ} \longrightarrow i\text{-Pr} + \mathrm{H} + \mathrm{Hg} \qquad [31]$$

$$\longrightarrow n\text{-Pr} + \mathrm{H} + \mathrm{Hg} \qquad [32]$$

$$\longrightarrow \mathrm{C_3H_8} + \mathrm{Hg} + h\nu'' \qquad [33]$$

$$\mathrm{H} + \mathrm{C_3H_8} \longrightarrow i\text{-Pr} + \mathrm{H_2} \qquad [12]$$

$$\longrightarrow n\text{-Pr} + \mathrm{H_2} \qquad [13]$$

$$n\text{-Pr} + \mathrm{C_3H_8} \longleftrightarrow i\text{-Pr} + \mathrm{C_3H_8} \qquad [14]$$

$$2n\text{-Pr} \longrightarrow n\text{-Hexane} \qquad [16]$$

$$\longrightarrow \mathrm{C_3H_6} + \mathrm{C_3H_8} \qquad [17]$$

$$n\text{-Pr} + n\text{-Pr} \longrightarrow \text{2-methylpentane} \qquad [18]$$

$$\longrightarrow \mathrm{C_3H_6} + \mathrm{C_3H_8} \qquad [19]$$

$$2i\text{-Pr} \longrightarrow \text{2,3-dimethylbutane} \qquad [20]$$

$$\longrightarrow \mathrm{C_3H_6} + \mathrm{C_3H_8} \qquad [21]$$

$$\mathrm{Hg}^{*} + \mathrm{N_2} \longleftrightarrow \mathrm{Hg}^{\circ} + \mathrm{N_2} \qquad [44]$$

$$\mathrm{Hg}^{\circ} + \mathrm{Hg} + \mathrm{A} \longrightarrow \mathrm{Hg}_2^{*} + \mathrm{A} \qquad [10]$$

where A is either N_2 or C_3H_8. Further reactions of Hg_2^* are not included since they do not lead to production of propyl radicals (81). The ratio of twice the rate of *n*-propyl to total propyl radicals produced, $R_{(n)}/R_{(n+i)}$, was calculated from the kinetic treatment of reactions [16]-[21] for each experiment (see Appendix A). Quenching of Hg^* atoms by nitrogen in its v=0 level, reaction [44], probably produces vibrationally excited (v=1) nitrogen, but

at the low light intensities used in the present system reaction [44] is appropriate (58).

As shown by Back (129), the effect of self-scavenging by the reaction

$$H + C_3H_6 \longrightarrow \textit{n} \text{ or } \textit{i}\text{-Pr} \qquad [24]$$

is important in the Hg* photosensitization of propane even at conversions of 0.5% or less. Since $(k_{12}+k_{13})/k_{24} = 1.4 \exp(-4.8x10^3/RT)$ (123), at most about 11% of the hydrogen atoms are consumed in reaction [24] (at 27°C, 10 torr propane, and 1000 torr nitrogen). At higher temperatures and propane pressures its contribution is less than 5% and can be neglected in the following calculations. Note that reaction [24] has no effect on quantum yield determinations because it also leads to the production of a propyl radical.

The occurrence of the reaction

$$2H + M \longrightarrow H_2 + M \qquad [45]$$

where M is either the walls of the reaction vessel or an inert gas molecule, could interfere with the basic kinetic scheme. At the pressures used in these experiments (1000 torr) the wall reaction could not compete effectively with recombination or abstraction (134). Making the tentative assumption that recombination is not significant and solving the steady state equation for [H] gives

$$R_{45}/R_{12+13} = k_{45}[M]R_{(n+i)}/2[C_3H_8]^2(k_{12}+k_{13})^2$$

Larkin (109) has found k_{45} (M=Ar) to be $4.6x10^{15}$ cc^2 $mole^{-2}$ sec^{-1} at 291°K with a temperature dependence of $T^{-\frac{1}{2}}$ or larger (135,136).

Assuming $k_{12} + k_{13} = 10^{12.7} \exp(-7.4\text{x}10^3/RT)$ cc mole^{-1} sec^{-1} (122) and conditions most favorable to reaction [45] (27°, 10 torr propane, and 1000 torr nitrogen), $R_{45}/R_{12+13} = 1.6\text{x}10^{-2}$ and about 2% of the hydrogen atoms react by recombination rather than abstraction from propane. Since k_{45} decreases and $k_{12}+k_{13}$ increases with increasing temperature, R_{45}/R_{12+13} decreases rapidly with increasing temperature or propane pressure. Consequently even an error of a factor of two or three in the value used for k_{45} ($M = N_2$), would be compensated for by the square terms and therefore it is reasonable to neglect H-atom recombination.

a. Calculation of the Decomposition Quantum Yields of Propane by Hg* and Hg° Atoms

The overall quantum yield of decomposition of propane in a mixture of mercury, nitrogen, and propane irradiated by 2537Å light is given by

$$\Phi_T = \frac{R_{26+27} + R_{31+32}}{R_{-I}+R_{25}+R_{30}+R_{10}-R_{28}}$$

where R_{26+27} is the combined rate of reactions [26] and [27], R_{-I} is the rate of spontaneous emission of the Hg* atom, etc. This can be written in terms of measurable quantities and known rate constants as follows (see Appendix B for derivation):

$$\Phi_T \left[1 + \frac{k_{10}[Hg][N_2]}{k_{30}[C_3H_8]} + F\left(1 - \Phi' + \frac{k_{-I}}{k_{25}[C_3H_8]}\right)\right] = \Phi^*F + \Phi° \qquad [49]$$

where

$$F = \left[\frac{\sigma^{2*}}{\sigma^{2°}}\right]_{C_3H_8} \left\{\frac{[Hg*]}{[Hg°]}\right\}$$

$$= \frac{\left\{\left(\frac{\sigma^{2*}}{\sigma^{2°}}\right)_{C_3H_8} K_{44}^{-1} + \frac{k_{25}}{k_{44}} \frac{[C_3H_8]}{[N_2]} + \left(\frac{\sigma^{2*}}{\sigma^{2°}}\right)_{C_3H_8} \frac{k_{10}[Hg][A]}{k_{44}[N_2]}\right\}}{\left\{1 + \Phi' \frac{[C_3H_8]}{[N_2]} \frac{k_{25}}{k_{44}}\right\}}$$

Thus $\Phi*$ and $\Phi°$ can be evaluated if the terms on the left hand side of equation [49] are known. There are several values available in the literature for the rate constants required for the calculation. The most reliable ones, listed in Table XV, have been employed in the present computations which are summarized in Table XIV. Plots of the left hand side of equation [49] against F at 63° and 200°C are shown in Figure 8. The curvature observed in this plot at 63°C below F = 0.2 is probably due to loss of radicals by the radical-radical reactions

$$H + n\text{-}Pr \longrightarrow C_3H_8 \qquad [46]$$

$$H + i\text{-}Pr \longrightarrow C_3H_8 \qquad [47]$$

An estimate of the rates of reactions [46] and [47], compared to abstraction of H-atoms from propane by hydrogen, has been made from the rate of the analogous reaction with ethyl radicals:

$$H + C_2H_5 \longrightarrow C_2H_6 \qquad [48]$$

Assuming $k_{46}+k_{47} \approx k_{48} = 2.3\text{x}10^{13}$ cc mole^{-1} sec^{-1} (137) and $k_{16} = 10^{13.8}$ cc mole^{-1} sec^{-1} (133), the ratio

TABLE XV

Quenching Cross Sections and Rate Constants Used in the Calculation of k_{32}/k_{31}

Quantity	Value	Reference
$\sigma^{2*}_{C_3H_8}$	3.1 $\mathring{A}^2$	1
$(\sigma^{2*}/\sigma^{2°})_{C_3H_8}$	5.6	58
k_{25}/k_{44}	5.57 $\exp[(1/300-1/T)1.6\text{x}10^3/R]$	78
k_{10}	$3.8\text{x}10^{18}$ cc^2 $mole^{-2}$ sec^{-1}	58
K_{44}	3 $\exp(-5.0\text{x}10^3/RT)$	80
k_{-I}	Calculated from τ_o = $1.145\text{x}10^{-7}$ sec with the correct imprisonment formula applied (5,9,14)	7
Φ'	0.38	44
k_{17}/k_{16}	0.154	130
k_{19}/k_{18}	0.408	130
k_{21}/k_{20}	0.69	130
k_{36}/k_{35}	0.118	130
k_{38}/k_{37}	0.306	130

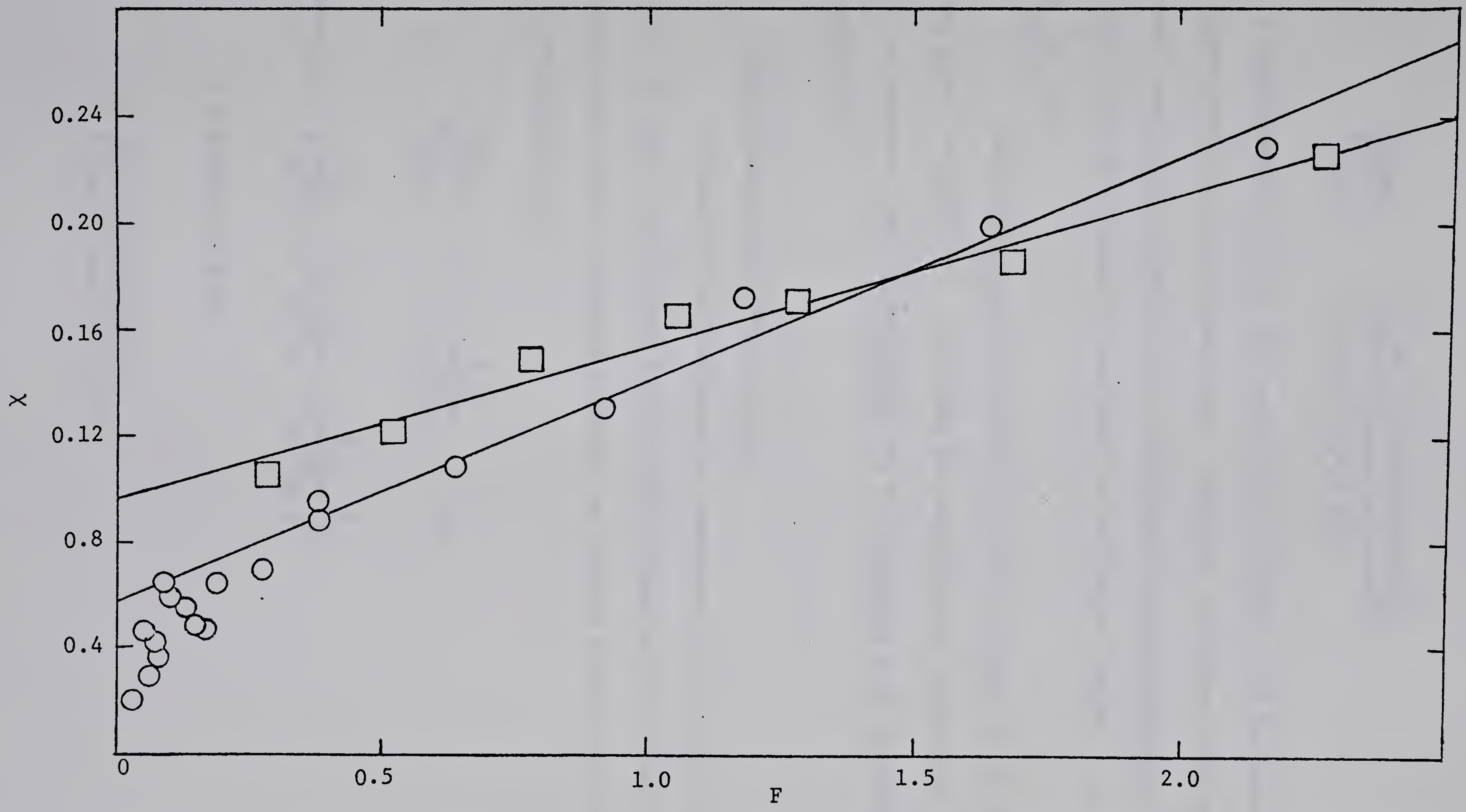

FIGURE 8: Variation of the quantum yield equation [49] with F from the mercury sensitized decomposition of propane at 63°C (○) and 200°C (□) from Table XIV.

$$\frac{R_{46+47}}{R_{12+13}} = \frac{(k_{46}+k_{47})[n\text{-Pr}]/[i\text{-Pr}]R_{Hx}^{\frac{1}{2}}}{(k_{12}+k_{13})[C_3H_8]\ k_{16}^{\frac{1}{2}}}$$

is approximately 0.3 at 25°C and 10 torr propane, and decreases at higher pressures.and temperatures. However, reactions [46] and [47] would have little effect on the calculated *n*-propyl/isopropyl ratio since both rate constants are near the collision frequency and $k_{46}/k_{47} \approx 1$.

The slopes and intercepts of plots in Figure 8 for $F > 0.2$ are given in Table XVI. Although the experimental errors are large, it is apparent that Φ^* decreases and Φ° increases with increasing temperature.

b. Calculation of the Ratio k_{32}/k_{31}

A steady state treatment of reactions [25] - [33], [12] - [14], and [16] - [21] leads to the same expression for twice the fractional yield of *n*-propyl radicals as derived before (see Chapter IV and Appendix B):

$$\frac{2R_{(n)}}{R_{(n+i)}} = Q_4 + \frac{k_{13}}{k_{12}+k_{13}} - \delta Q_3 \qquad [43]$$

where $Q_4 = \dfrac{k_{32}}{k_{31}+k_{32}} + \left[\dfrac{k_{27}}{k_{26}+k_{27}} - \dfrac{k_{32}}{k_{31}+k_{32}}\right]\beta$

$$\beta = F\Phi^*/(\Phi^\circ + F\Phi^*)$$

$$\delta = \frac{2\{1-\exp(-\varepsilon[\mathrm{Hg}]L/2)\}}{\{\varepsilon[\mathrm{Hg}](1-\exp(-\varepsilon[\mathrm{Hg}]L))\}}$$

TABLE XVI

Calculation of Φ^* and Φ° at 63° and 200°C from the Data shown in Figure 8 for Points Greater than F = 0.2[a]

T(°C)	Slope (Φ^*)	Intercept (Φ°)
63	0.84 ± .05	0.57 ± .06
200	0.58 ± .04	0.95 ± .06

[a] Errors given are one standard deviation

and $$Q_3 = \frac{R^{1/2}_{DMB}}{R_{(n+i)}} \frac{R_{MP}}{R_{DMB}} - 2K^{-1}_{14} \frac{k_{14}}{k^{1/2}_{20}} [C_3H_8]$$

This mechanism predicts a linear dependence of the quantity $2R_{(n)}/R_{(n+i)} - k_{13}/(k_{12}+k_{13}) + \delta Q_3$ on the expression β, with the intercept given by $k_{32}/(k_{31}+k_{32})$. Computed quantities from experiments at five temperatures are summarized in Tables XIV and XVII and displayed in Figures 9 and 10. An Arrhenius plot of k_{32}/k_{31} calculated from these values is shown in Figure 11 and each point is assigned the accompanying error limit from Table XVII. A least mean square calculation of these points gives:

$$\log k_{32}/k_{31} = -0.06\pm0.070 - \frac{(1.90\pm0.12)\times10^3}{2.30RT}$$

where the errors given are for one standard deviation. Thus

$$k_{32}/k_{31} = 0.78 \exp(1.90\times10^3/RT).$$

TABLE XVII

Summary of Results from Figures 9 and 10

T(°C)	No. of Points	Slope[a]	Intercept; $k_{32}/(k_{31}+k_{32})$[a]
27	6	0.10 ±.04	0.0328±.006
63	31	0.057±.008	0.0412±.002
124	9	0.038±.04	0.0641±.005
166	7	0.107±.02	0.0867±.002
200	7	0.078±.01	0.0921±.006

[a] Errors given are one standard deviations.

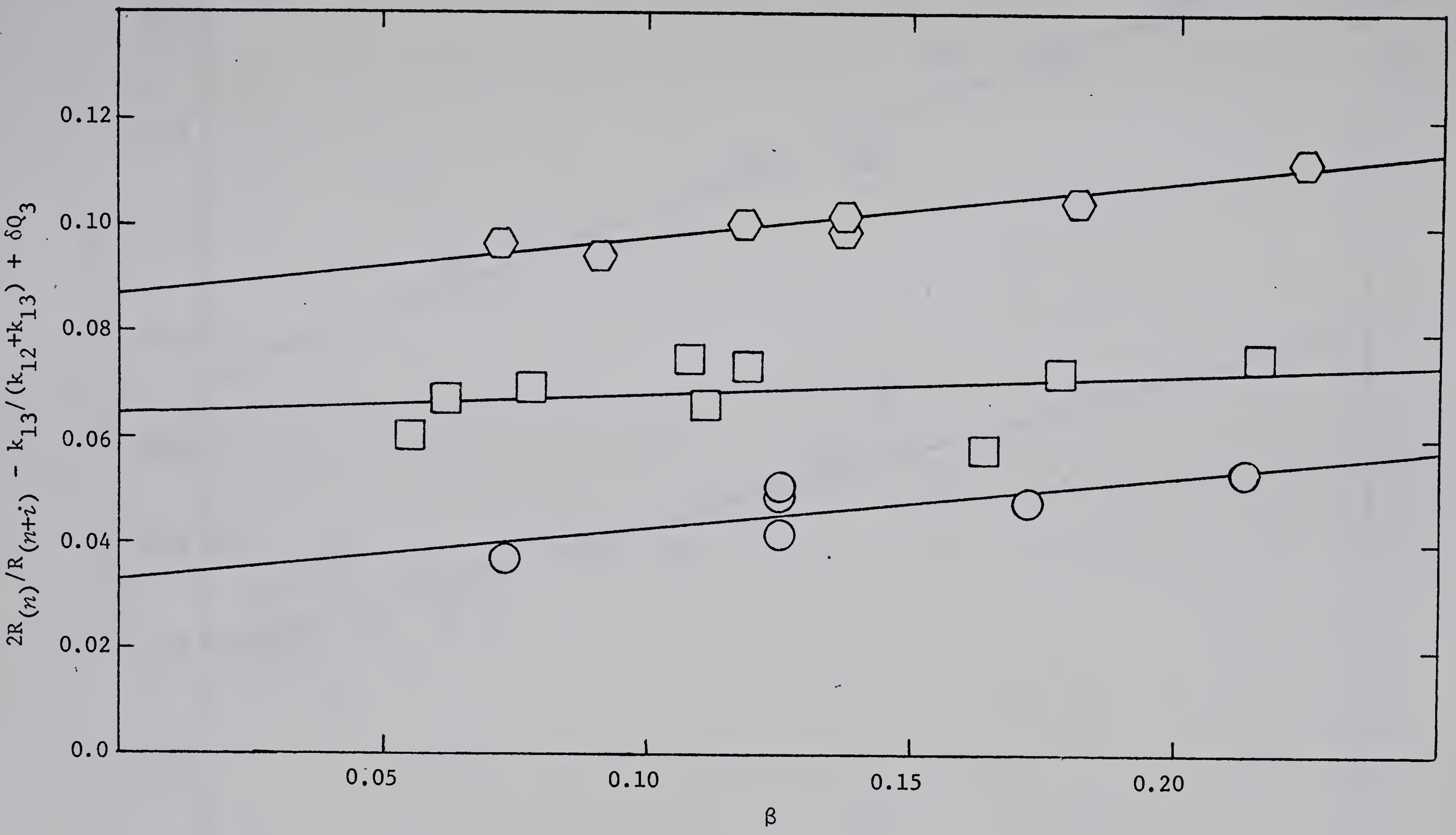

FIGURE 9: Plots of $2R_{(n)}/R_{(n+i)} - k_{13}/(k_{12}+k_{13}) + \delta Q_3$ against β at 27°C, ○; 124°C, □; 166°C, ⬡ from Table XIV.

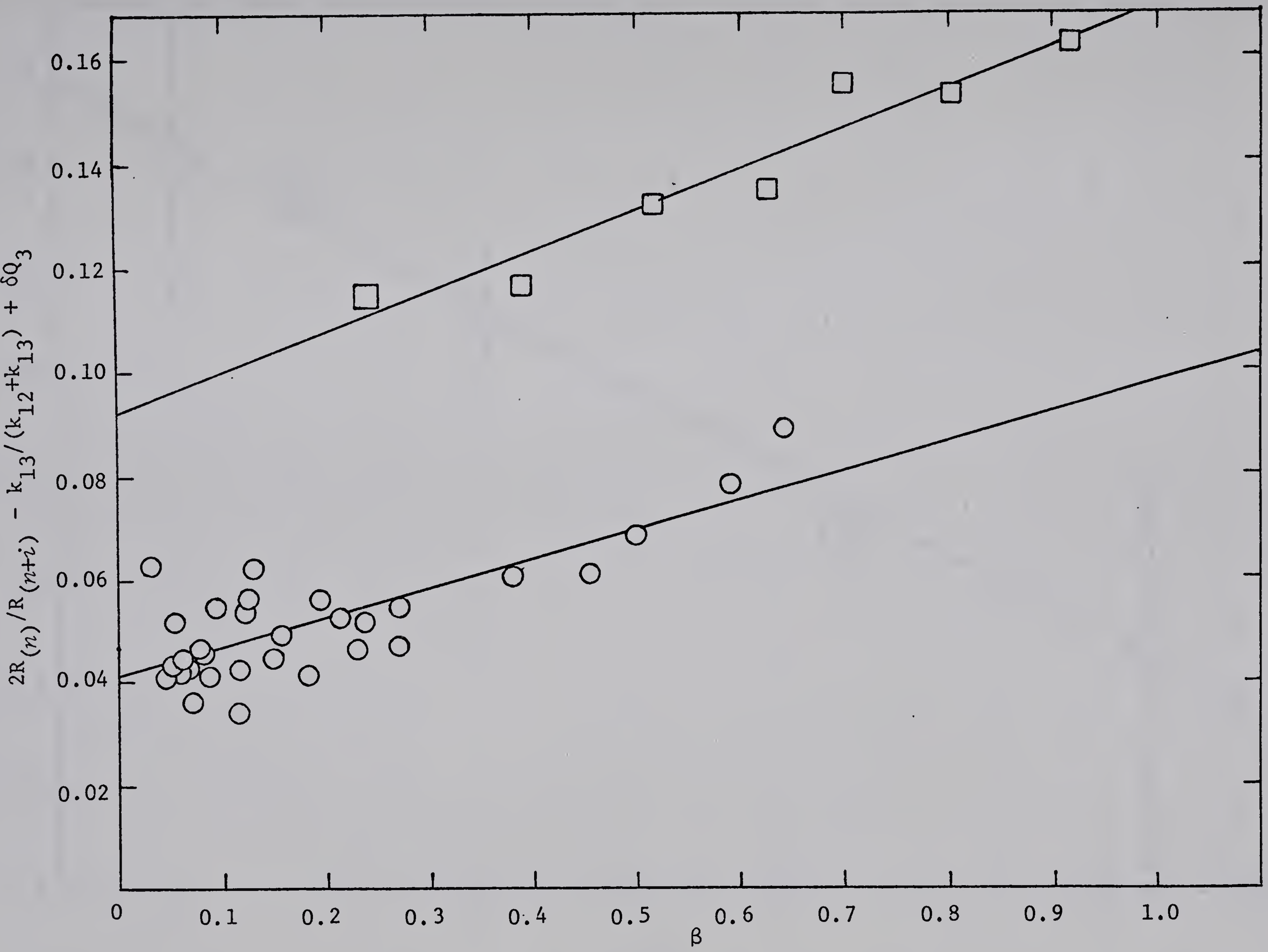

FIGURE 10: Plots of $2R_{(n)}/R_{(n+i)} - k_{13}/(k_{12}+k_{13}) + \delta Q_3$ against β at 63°C, ○; and 200°C, □ from Table XIV.

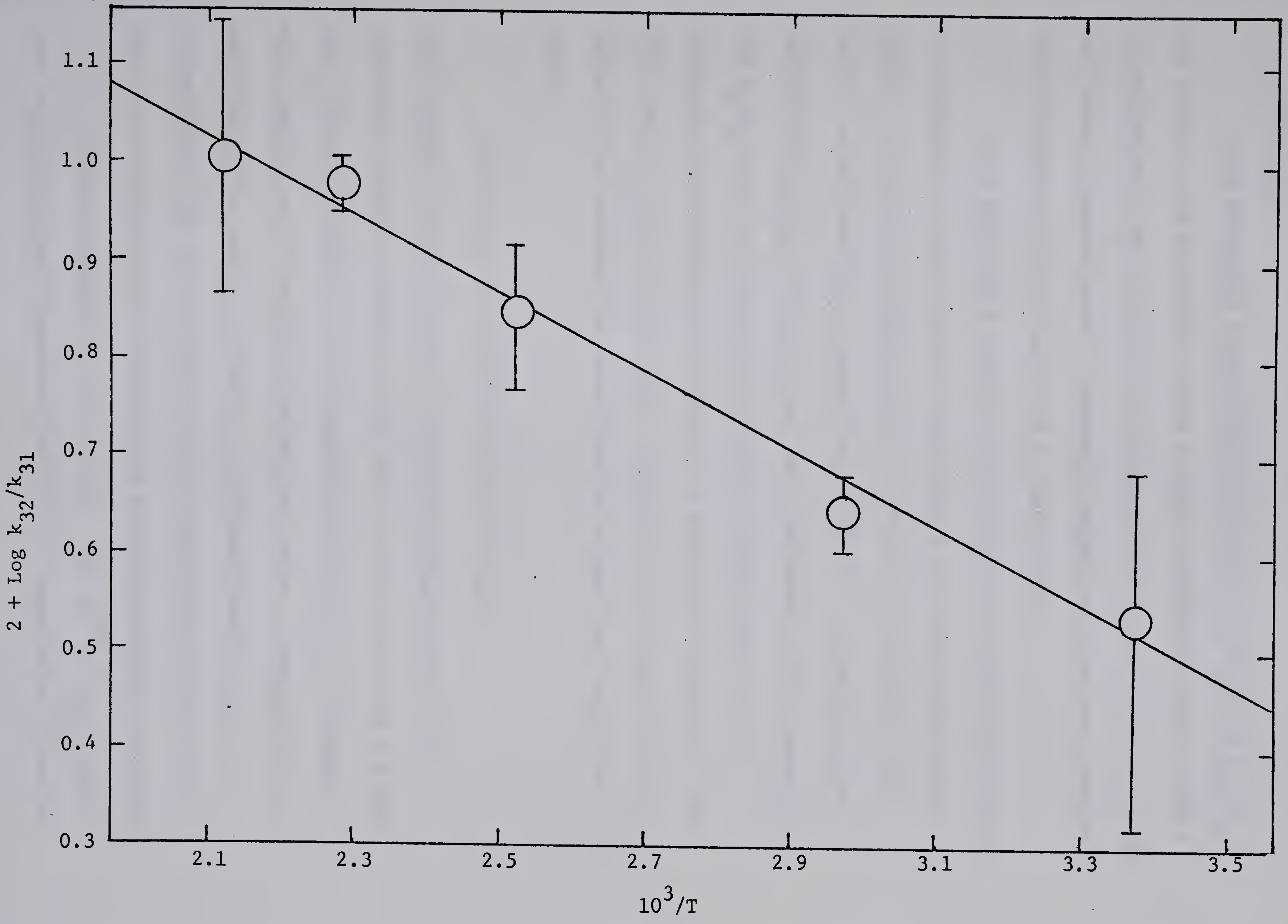

FIGURE 11: Arrhenius plot of the k_{32}/k_{31} ratio for the Hg° sensitized decomposition of propane including the error limits from Table XVII.

2. Discussion

The foregoing computations of Φ^*, Φ°, k_{27}/k_{26} and k_{32}/k_{31} are based on the preferred values of rate constants listed in Table XV (referred to as the basic rate constant set). The effect of varying these parameters over a reasonable range have also been examined. These computations are summarized in Table XVIII.

The basic rate constant set includes the disproportionation to recombination rate constant ratios (k_d/k_r) of Terry and Futrell (130). If the k_d/k_r values of 0.15, 0.35 and 0.55 for $n+n$, $n+i$, and $i+i$ propyl radicals, respectively (138,139) are employed the quantities k_{27}/k_{26} and k_{32}/k_{31} are only decreased by 5%. Recently the k_d/k_r ratio for isopropyl radicals has been shown to be independent of temperature (within ±0.5 kcal/mole) between 26° and 207°C with a value of 0.61 (140). However, if we assume the k_d/k_r ratios to be dependent on temperature by as much as 1 kcal/mole in the form of

$$[k_d/k_r]_{n+n} = 0.15 \exp[(1/300-1/T)\times\Delta E_{nn}/R]$$

and similarly for $n+i$ and $i+i$, the absolute magnitudes of the activation energies change, but $\Delta E^\circ-\Delta E^*$ is never less than 0.6 kcal/mole. Note also that if it is assumed that $[k_d/k_r]_{i+i}$ increases with temperature, Φ° becomes greater than unity. Consequently a small activation energy in favor of disproportionation over recombination has little effect on the calculated rate ratios and leads to an unreasonable quantum yield of decomposition of propane.

Values ranging from 5.6 to 290 for $(\sigma^{2*}/\sigma^{2\circ})_{C_3H_8}$ have been reported in the literature (Table IV). Computations given in

Tables XIV and XVI are based on a value of 5.6. Employing a larger value reduces the difference between ΔE° and ΔE* and increases the difference in the A-factor ratios (Table XVIII). Quenching cross section ratios larger than 30 however, are incompatible with the present experiments since they lead to values of $k_{32}/(k_{31}+k_{32})$ at 27°C less than zero (the intercept of Figure 9). Furthermore making $(\sigma^{2*}_{C_3H_8}/\sigma^{2*}_{N_2})$ a constant rather than a temperature dependent variable (to the extent of 1.6 kcal/mole) does not alter the calculated results significantly.

Callear and McGurk (44) reported a value of Φ', the quantum yield of Hg° formation by propane, of 0.38 at room temperature. Assuming that emission from the $(HgC_3H_8)^*$ complex is negligible compared to reactions [26] - [28].

$$(HgC_3H_8)^* \longrightarrow i\text{-Pr} + H + Hg \qquad [26]$$

$$\longrightarrow n\text{-Pr} + H + Hg \qquad [27]$$

$$\longrightarrow C_3H_8 + Hg^\circ \qquad [28]$$

$$\longrightarrow C_3H_8 + Hg + h\nu' \qquad [29]$$

$(\Phi^* = 1 - \Phi')$ and allowing Φ' to vary, a value for ΔE° - ΔE* of 0.9 kcal/mole is obtained at $\Phi' = 0.2$ and 0.2 kcal/mole with $\Phi' = 0.6$ (Table XVIII). Therefore, the quantum yield of spin-orbit relaxation must be greater than 0.6 so that $\Delta E^\circ \approx \Delta E^*$ (within experimental error) in the present system. This is an extremely high value of Φ' in view of Callear and McGurk's observations.

If we consider the following reactions for the deactivation of Hg° atoms by propane,

$$Hg^\circ + C_3H_8 \longrightarrow (HgC_3H_8)^\circ \qquad [30]$$

$$(HgC_3H_8)^\circ \longrightarrow \textit{i}\text{-Pr} + H + Hg \qquad [31]$$

$$\longrightarrow \textit{n}\text{-Pr} + H + Hg \qquad [32]$$

$$\longrightarrow C_3H_8 + Hg + h\nu'' \qquad [33]$$

we have

$$\Phi^\circ = (k_{31}+k_{32})/(k_{31}+k_{32}+k_{33}).$$

From Φ° values at 63° and 200° (Table XVI), the ratio k_{32}/k_{31} determined above and the basic rate constant set, the following relationship has been derived:

$$k_{31}/k_{33} = 1.4\text{x}10^4 \exp(-6.2\text{x}10^3/RT)$$

Therefore decomposition of propane by Hg° atoms via reactions [31] and [32] proceeds with an average activation energy of 6.2 kcal/mole larger than fluorescence from the mercury-propane complex. The values of k_{31}/k_{33} have also been computed employing rate constants other than those of the basic set and these are included in Table XVIII.

Similarly, from the reactions

$$(HgC_3H_8)^* \longrightarrow \textit{i}\text{-Pr} + H + Hg \qquad [26]$$

$$\longrightarrow \textit{n}\text{-Pr} + H + Hg \qquad [27]$$

$$\longrightarrow C_3H_8 + Hg^\circ \qquad [28]$$

$$\longrightarrow C_3H_8 + Hg + h\nu' \qquad [29]$$

we have,

$$\Phi^* = (k_{26}+k_{27})/(k_{26}+k_{27}+k_{28}+k_{29}),$$

and $\Phi' = k_{28}/(k_{26}+k_{27}+k_{28}+k_{29})$.

Since emission from $(HgC_3H_8)^*$ is much less important than spin-orbit relaxation, $k_{29} << k_{28}$, (44,67); Φ^* has been determined at 63° and 200°C (Table XVI) and the ratio k_{27}/k_{26} given above, we have

$$k_{28}/k_{26} = 31 \exp(-3.3\text{x}10^3/RT).$$

From this expression, Φ^* and Φ' (since $\Phi' = 1 - \Phi^*$ when $k_{29} << k_{28}$) can be determined at any temperature. Furthermore, since Φ' was required for the calculation of F in Equation [49]

$$\Phi_T\left[1 + \frac{k_{10}[Hg][N_2]}{k_{30}[C_3H_8]} + F\left(1 - \Phi' + \frac{k_{-I}}{k_{25}[C_3H_8]}\right)\right] = \Phi^*F + \Phi° \qquad [49]$$

$$F = \frac{\left\{\left(\frac{\sigma^{2*}}{\sigma^{2°}}\right)_{C_3H_8} \cdot K_{44}^{-1} + \frac{k_{25}}{k_{44}}\frac{[C_3H_8]}{[N_2]} + \left(\frac{\sigma^{2*}}{\sigma^{2°}}\right)_{C_3H_8} \frac{k_{10}[Hg][A]}{k_{44}[N_2]}\right\}}{\left\{1 + \Phi' \frac{[C_3H_8]}{[N_2]}\frac{k_{25}}{k_{44}}\right\}}$$

an iterative computation has been carried out by placing the resulting values of Φ' into F and redetermining the quantities Φ^* and $\Phi°$ through equation [49]. A self-consistent set of values was obtained when

$$k_{28}/k_{26} = 1.1\text{x}10^3 \exp(-6.5\text{x}10^3/RT)$$

(Table XVIII). Both A^*_{27}/A^*_{26} and ΔE^* calculated in this manner decrease somewhat but $A°_{32}/A°_{31}$ and $\Delta E°$ are unchanged from the results computed by keeping Φ' constant. Therefore the crossover from the Hg^*-C_3H_8 to the $Hg°$-C_3H_8 potential surface lies between 3 and 6 kcal/mole above the crossover to decomposition.

TABLE XVIII

Computed Quantities Employing Various Values of Input Rate Constants[a]

k_d/k_r[b]	J dep. kcal/mole *nn-ni-ii*	Φ* Used	Φ* 63°/200°C	Φ° 63°/200°C	k_{32}/k_{31} $A^\circ_{32}/A^\circ_{31}$	k_{32}/k_{31} ΔE° kcal/mole	k_{27}/k_{26} A^*_{27}/A^*_{26}	k_{27}/k_{26} ΔE* kcal/mole	k_{31}/k_{33} log A_{31}/A_{33}	k_{31}/k_{33} ΔE kcal/mole
A	0-0-0	0.62	0.84/0.58	0.57/0.95	0.78	1.90	0.89	1.25	4.1	6.2
A	1-.5-0	0.62	0.84/0.59	0.57/0.98	1.17	2.16	1.06	1.35	5.2	7.9
A	0-.5-1	0.62	0.90/0.76	0.61/1.2	0.58	1.75	0.53	0.95		
B	0-0-0	0.62	0.78/0.54	0.52/0.88	0.74	1.83	0.97	1.30	2.8	4.4
B	0-.5-1	0.62	0.83/0.67	0.56/1.1	0.68	1.84	0.64	1.06		
A	0-0-0	0.40	0.74/0.39	0.55/0.94	0.72	1.83	1.86	1.64	3.8	5.7
A	0-0-0	0.80	0.92/0.74	0.58/0.97	0.84	2.00	0.62	1.06	4.6	6.8
A[c]	0-0-0	0.62	0.85/0.58	0.56/0.96	0.53	1.67	0.99	1.31	4.3	6.4
A[d]	0-0-0	0.62	0.85/0.59	0.53/0.94	0.62	1.76	0.94	1.29	4.0	6.2
A	0-0-0	e	0.95/0.54	0.59/0.94	0.83	1.95	0.55	1.00	3.9	6.8

[a] Preferred values given in the first row.

[b] Disproportionation to recombination ratios: A, Table A-I; B, 0.15, 0.35, 0.55 for *n+n*, *n+i* and *i+i*, respectively.

[c] $(\sigma^{2*}/\sigma^{2\circ})_{C_3H_8} = 16.8$

[d] $(\sigma^{2*}_{C_3H_8}/\sigma^{2*}_{N_2}) = 5.57$ independent of temperature

[e] Using the calculated values of Φ* dependent on temperature with $k_{28}/k_{26} = 1.1\text{x}10^3 \exp(-6.5\text{x}10^3/RT)$.

It can be concluded from Table XVIII that either $\Delta E^\circ - \Delta E^*$ $= 0.6$ kcal/mole and $A^\circ_{32}/A^\circ_{31} = A^*_{27}/A^*_{26}$ or $\Delta E^\circ = \Delta E^*$ and $(A^\circ_{32}/A^\circ_{31})/(A^*_{27}/A^*_{26}) \approx 2 - 3$ depending on which set of input parameters are used. The first alternative occurs over a reasonable range of k_d/k_r (both dependent and independent of temperature), whether or not $(\sigma^{2*}_{C_3H_8}/\sigma^{2*}_{N_2})$ is a constant or temperature-dependent, and when Φ^*, as found by experiment, is temperature dependent. The second alternative only becomes possible for the extreme cases when $\Phi' \geqslant 0.6$ or $(\sigma^{2*}/\sigma^{2\circ})_{C_3H_8} > 30$. Therefore the first alternative is more reasonable. In addition, there is no evidence at present which would suggest that $A^\circ_{32}/A^\circ_{31}$ and A^*_{27}/A^*_{26} should be different, whereas a difference in ΔE° and ΔE^* can be readily visualized as a difference in potential energies of crossing between the Hg°- and Hg*-propane complex surfaces and the surfaces leading to decomposition of the propane. A correlation of potential energy surfaces with the activation energy differences measured in the present study will be discussed in Chapter VII.

CHAPTER VI

EMISSION FROM EXCITED MERCURY-SUBSTRATE COMPLEXES

It has been shown from this laboratory (67) and by others (49,71-75) that the measurement of band fluorescence gives pertinent information about the nature of the excited mercury-quencher interaction. The early work by Oldenberg (65), Kuhn (64) and others (63, 66) has long been overlooked by those chemists interested in understanding the electronic energy transfer process. Since the quantum yield of paraffin decomposition is not always unity (16) and in view of the temperature dependent *n*-propyl to isopropyl ratio observed in the mercury photosensitzation of propane (Chapters IV and V) it is of interest to study this band fluorescence in more detail. Emission from excited mercury-substrate complexes using a series of related compounds has been examined as a possible mode of deactivation of the excited mercury atom.

1. Results

The fluorescence spectra observed from a system containing mercury and a quencher irradiated with 2537Å light can be divided into three characteristic regions: *a*) bands appearing a few angstroms on either side of the 2537Å resonance line (±20Å); *b*) structureless bands appearing as a broadening, or a partially resolved shoulder, extending several hundred angstroms to the long wavelength side of the resonance line; and *c*) structureless bands toward longer wavelengths separated completely from the 2537Å line. For comparison,

a microdensitometer trace of the mercury resonance lamp emission is shown in Figures 12 and 13. The sharp lines observed in some of the spectra are due to scattered light. Table XIX summarizes the separation of the band maxima from the 2537Å resonance line for all the compounds which gave separate emission band maxima.

Figure 14 gives the trace of the fluorescence spectra obtained with mercury in the presence of nitrogen. The 3350Å and 4850Å emission bands attributed to the $A(^3 1_u)$ and $A(^3 0_u^-)$ states of Hg_2 (22) are clearly seen, as well as a broadening of the 2537Å resonance line to the long wavelength side. There is also a band close to the resonance line in the *a* region (Figure 15).

The fluorescence spectra in the presence of ammonia, water and ethanol (Figure 16-18) each have one structureless band in the *c* region. The emission intensity increase markedly in the order $NH_3 > H_2O >> C_2H_5OH$. The carbon monoxide spectrum is somewhat different (Figure 19) in that it is extremely weak with the intensity increasing uniformly towards longer wavelengths to the limit of plate sensitivity at 5000Å.

The emission spectra observed in the presence of various rare gases around atmospheric pressure and room temperature are displayed in Figures 20-27. With Ar and Xe, at least two, and with Kr, three bands appear in the *a* region of the spectra. With He and Ne, asymmetrical broadening of the resonance line toward the short wavelength side indicates that these gases also give weak band fluorescence in this region. An experiment with 10 torr Xe indicated that the *a* band positions were independent of pressure between 10 and

800 torr. There is a consistent trend in the band positions throughout the noble gas series. Going from He to Xe, the maxima of the *a* region bands shift toward the resonance line and become more intense. In addition, Ar, Kr, and Xe give one band in the *b* region extending to 2600, 2700, and 3000Å, respectively. Xenon has a broad maxima at $\lambda \sim 2690$Å while Kr and Ar broaden the resonance line extensively toward longer wavelengths. These gases show a faint though definite fine structure superimposed on the continuum near the resonance line (Figure 27) while Xe in addition shows a slight indication of structure throughout the continuum (marked of Figure 26).

A trend similar to that found in the rare gases is observed in the presence of paraffins around atmospheric pressure and room temperature (Figures 28-40). A single, short wavelength band converges on the resonance line, while the *b* region band shifts progressively to longer wavelengths as the molecular weight of the substrate increases. Paraffins containing less than three carbon atoms give only an asymmetrical broadening of the resonance line toward longer wavelengths while larger molecules give a broad maximum beyond 2650Å. Reducing the total pressure of isobutane or neopentane to 8 torr (Figures 34-36) shifts the emission spectra slightly to shorter wavelengths. Cyclopropane appears to differ significantly from propane in that the *b* region band extends to 3000Å with a maximum at about 2690Å. However the emission spectra in the presence of larger cycloparaffins are similar to their straight chain analogs.

The fluorescence spectra observed with SF_6 and various partially and completely fluorinated methanes near 300 torr are shown in Figures 41-48. Since band fluorescence from these compounds was observed under the same experimental conditions, the emission intensities can be directly compared. Several interesting features are:

1. Replacement of all the H-atoms of methane with fluorine shifts the *a* region band further from the resonance line (Table XIX and Figures 28,44). Band fluorescence in the presence of SF_6 (Figure 45) however, is almost identical to that with CF_4 under the present conditions.

2. Replacement of successive hydrogens by fluorine atoms (Figures 41-43) shifts and *a* region band of CH_4 to longer wavelengths. The CH_3F band is completely obscured by the resonance line whereas the CH_2F_2 band can be seen as an asymmetrical broadening of the resonance line. The band of CHF_3 appears as a shoulder on the long wavelength side of the 2537Å line.

3. Emission in the *b* region in the presence of CH_3F (Figure 46) shows a band with a peak at about 2630Å extending to about 2740Å, while CH_2F_2 gives a weak band as an asymmetrical broadening of the resonance line extending to about 2660Å. Trifluoromethane gives a more intense band which extends to only about 2640Å.

TABLE XIX

Separation of Emission Band Maxima from the 2536.5Å ($39,424\ cm^{-1}$) Resonance Line[a]

Compound	Pressure torr	"a" Region Bands $\Delta\omega_1$	$\Delta\omega_2$	$\Delta\omega_3$	"b" Region $\Delta\omega$
Ar	400	∿27	77	164	
Kr	180	∿30	70	128	
Kr	750	∿30	74	128	
Xe	10		58		-1,830
Xe	860	∿36	58		-2,380
CH_4	220	65			
C_2H_6	330	29			
C_3H_8	600				-1,260
i-C_4H_{10}	645				-1,260
$C(CH_3)_4$	8				-1,560
$C(CH_3)_4$	510				-1,830
c-C_3H_6	400				-2,250
c-C_5H_{10}	210				-1,400
c-C_6H_{12}	72				-1,770
CH_3F	330				-2,000
CHF_3	280	-97			
CF_4	614	220			
SF_6	190	220			

[a] in wave numbers.

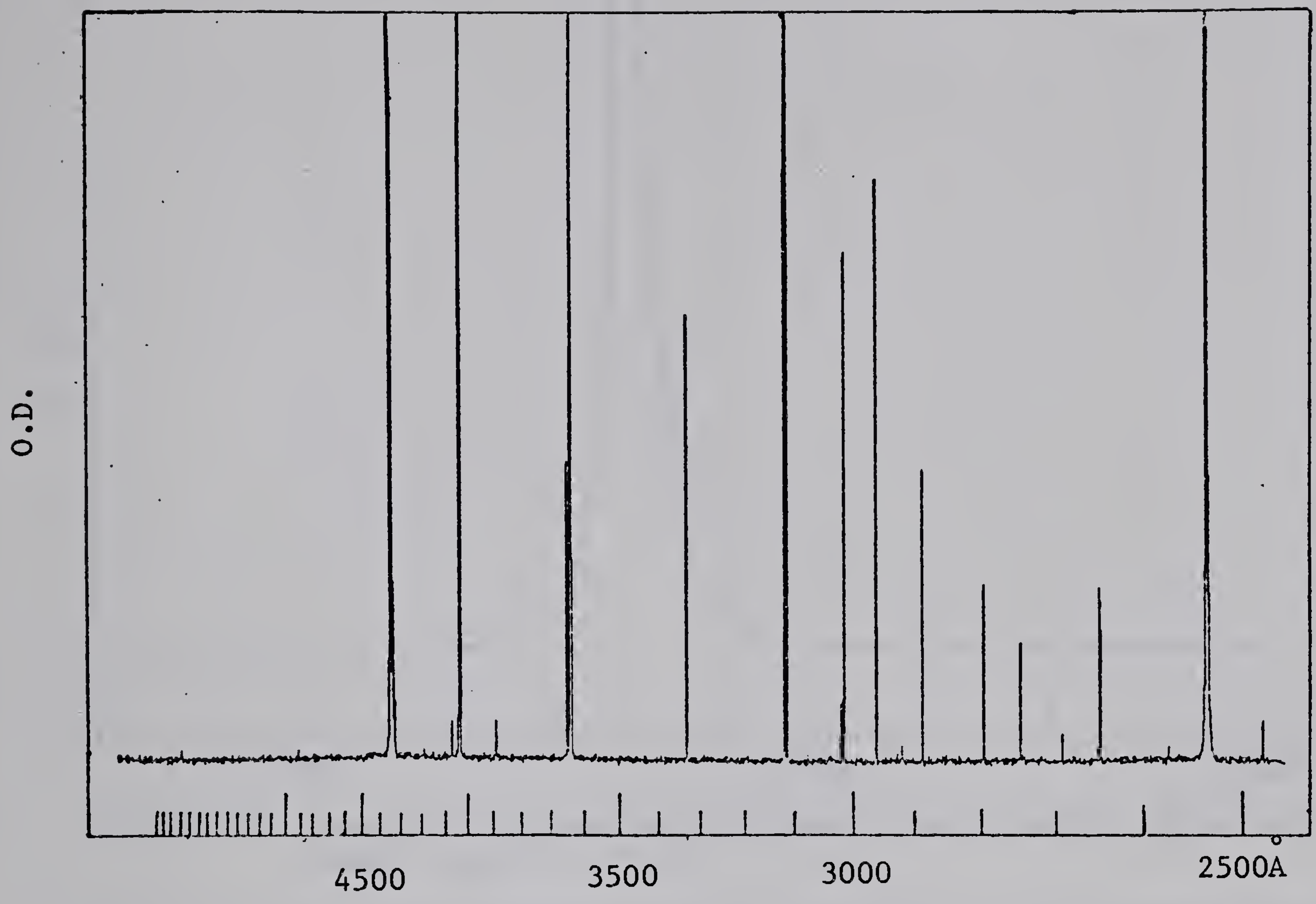

FIGURE 12: Microdensitometer trace of the emission spectra from the mercury resonance lamp used in the fluorescence studies with 1 sec exposure time. Maximum pen deflection of 2.1 optical density units (O.D.).

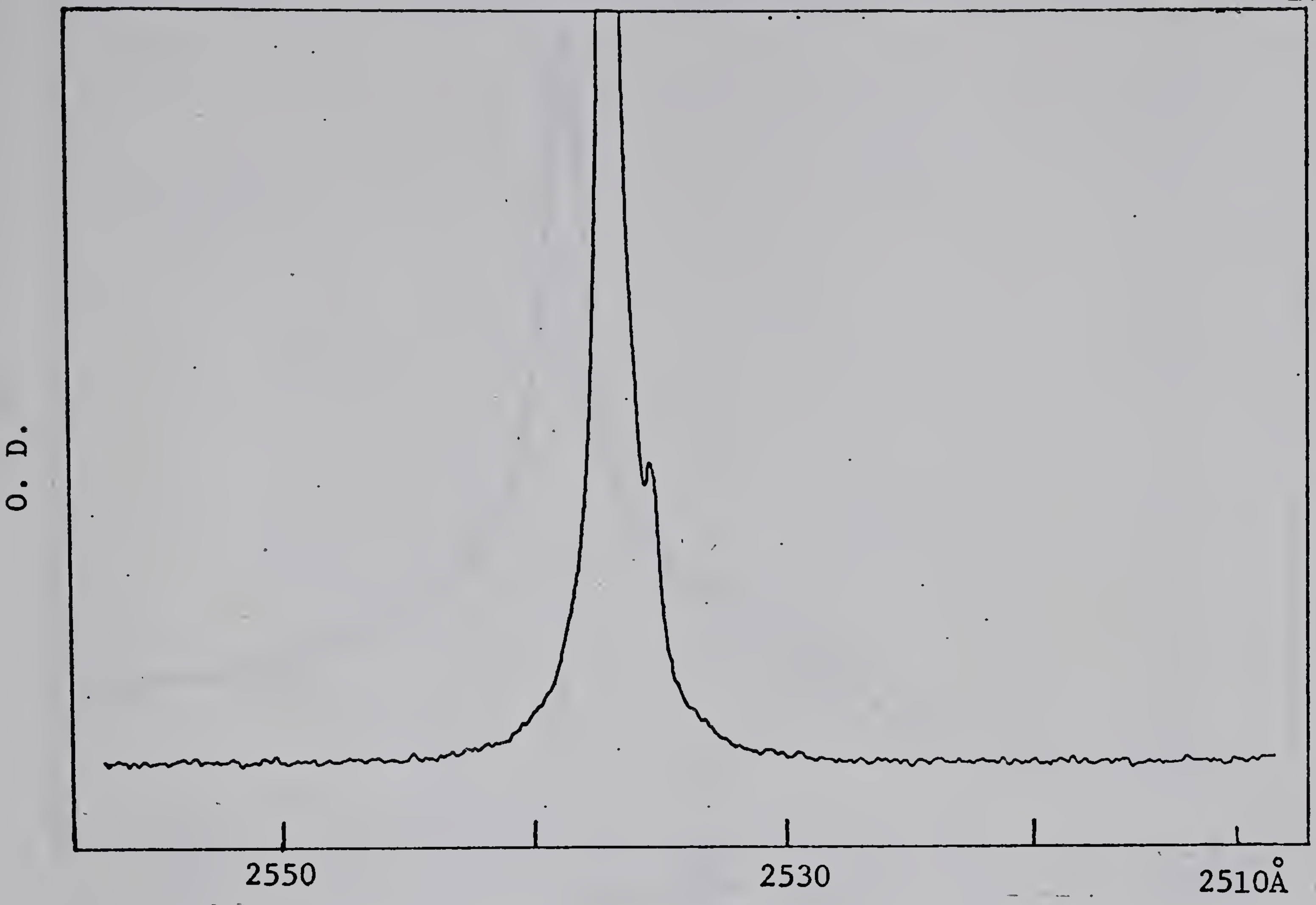

FIGURE 13: Detail of the mercury resonance line from the photolysis lamp, 1 sec, 2.1 O.D.

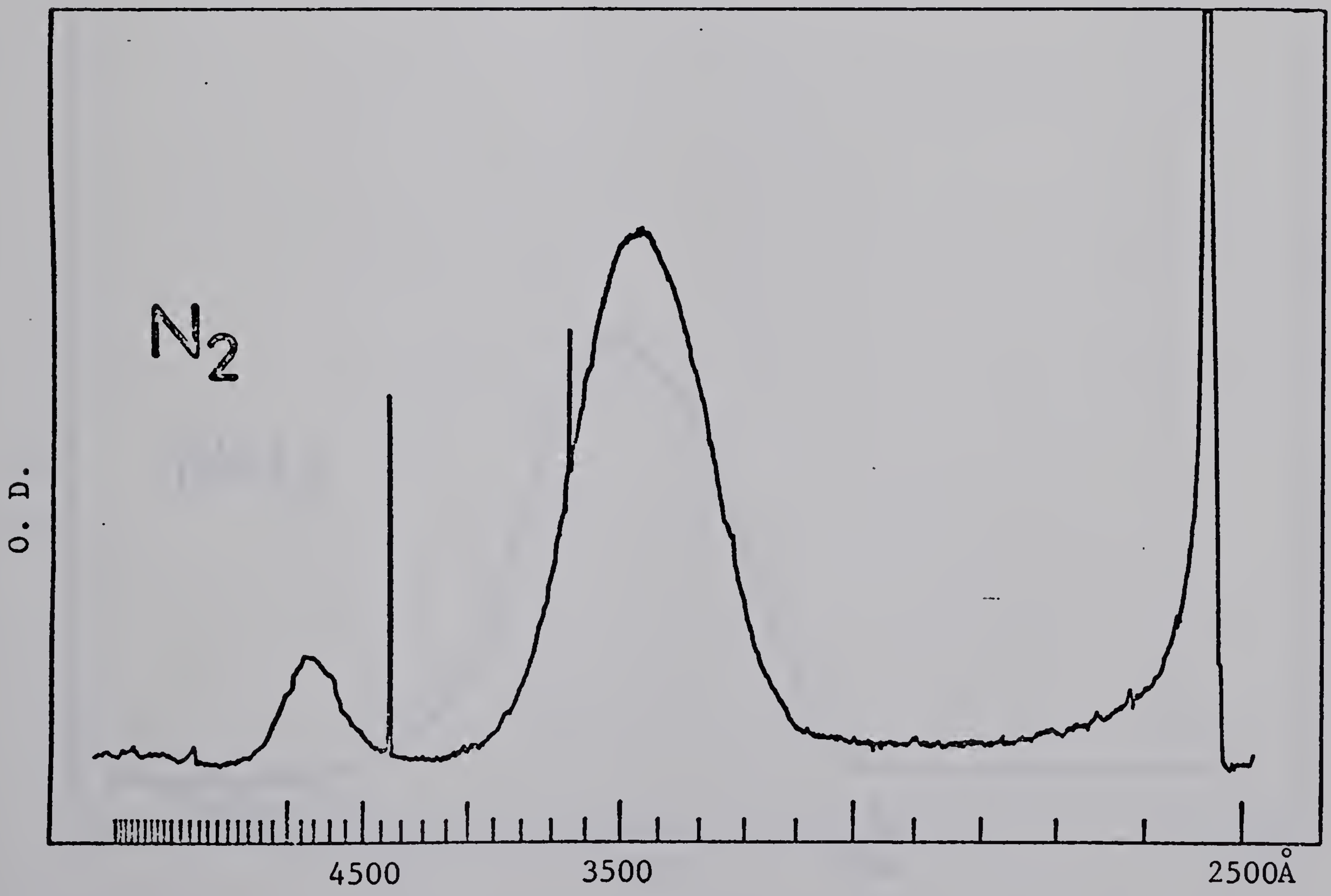

FIGURE 14: Fluorescence spectra: 728 torr N_2, 2 hours, 2.1 O.D.

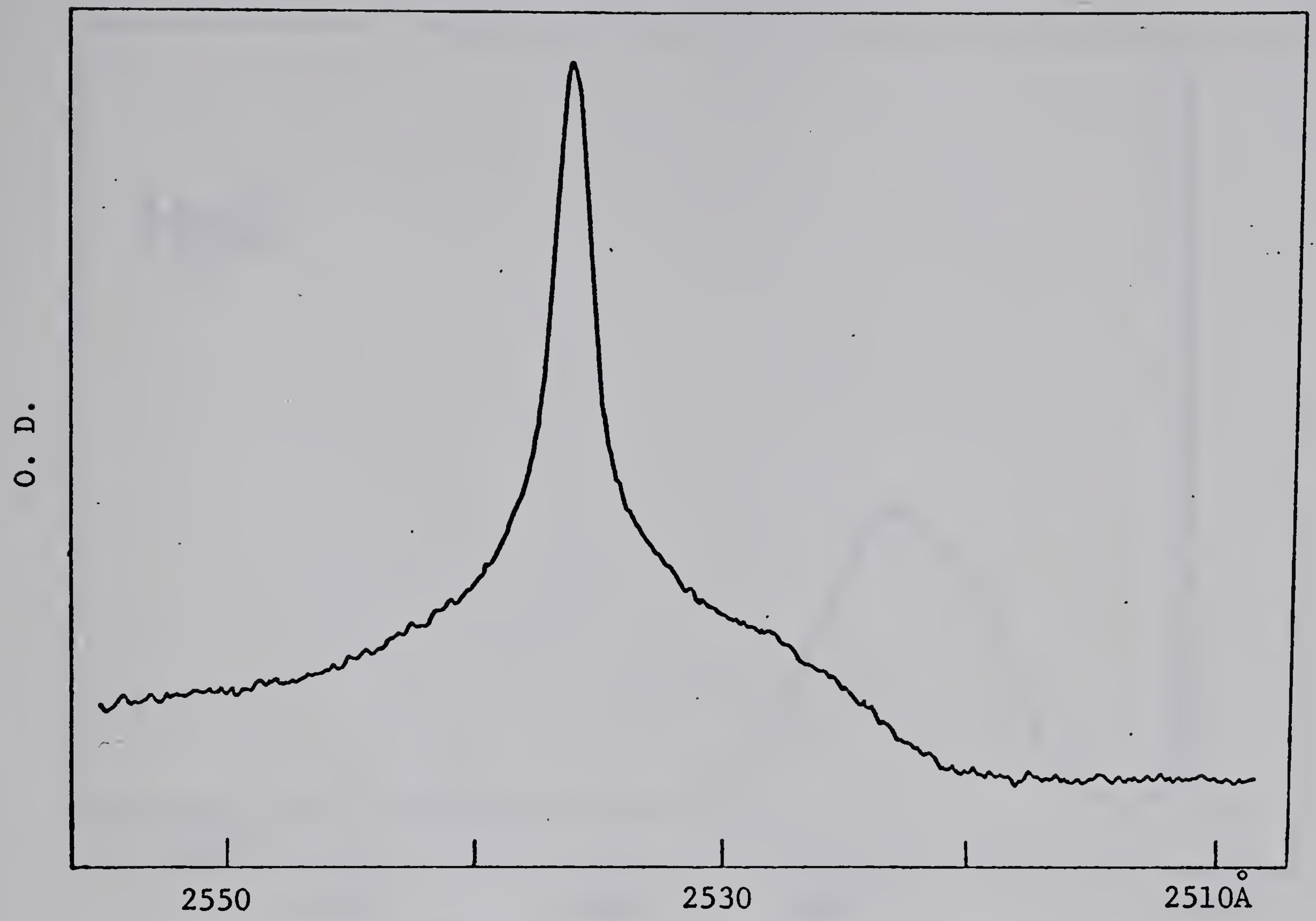

FIGURE 15: Fluorescence spectra: 600 torr N_2, 5 hours, 2.1 O.D.

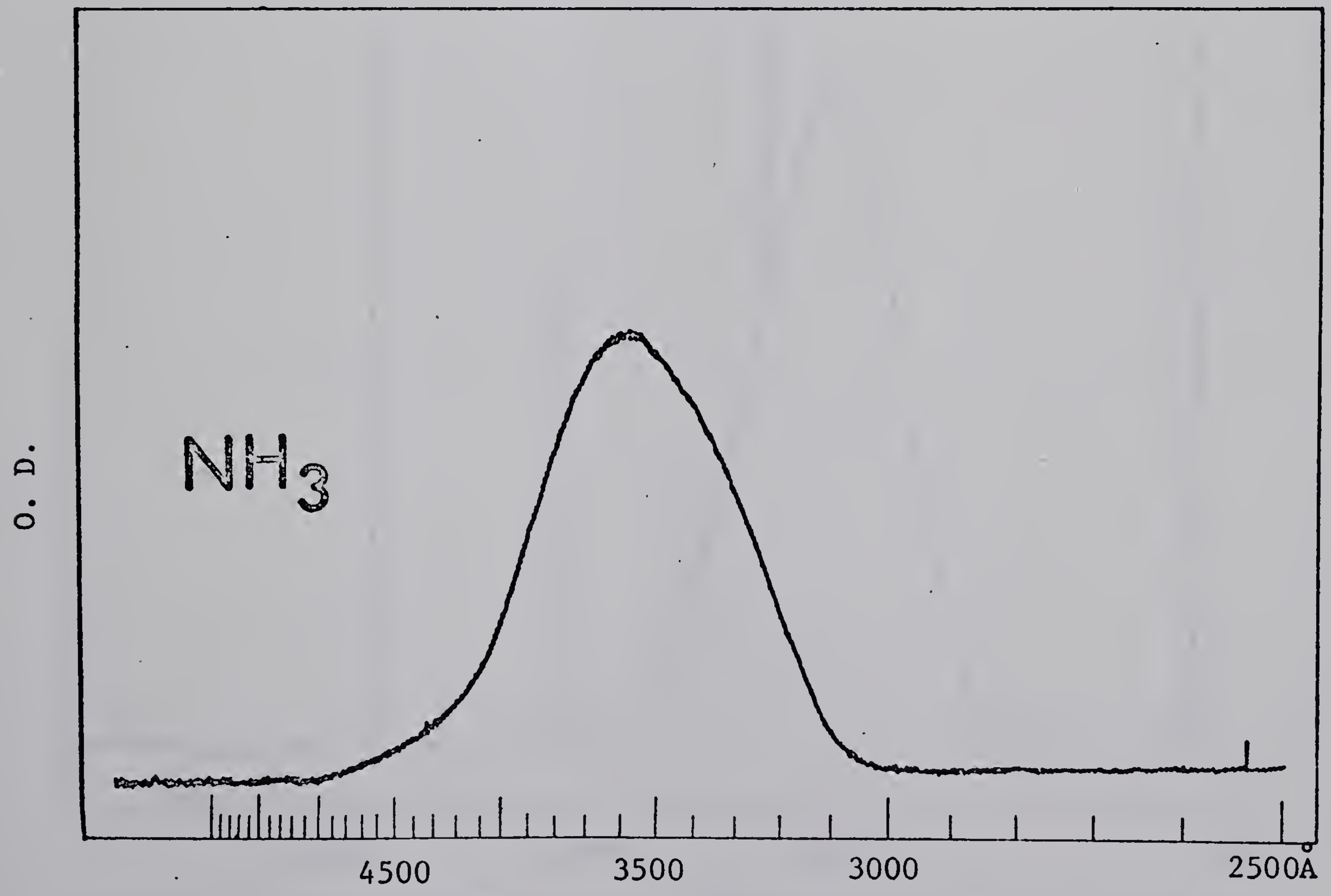

FIGURE 16: Fluorescence spectra: 400 torr NH_3, 1 min, 2.1 O.D.

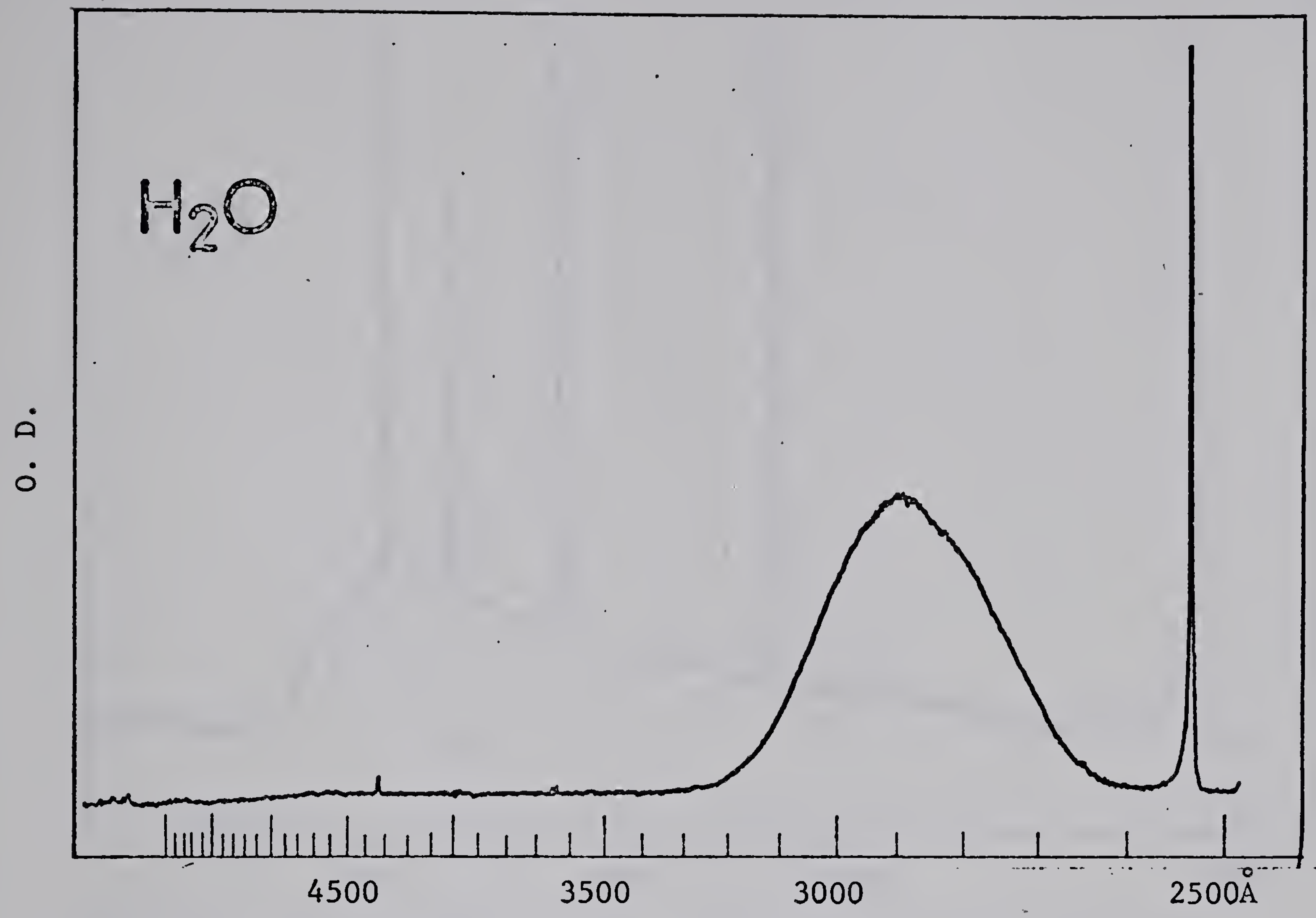

FIGURE 17: Fluorescence spectra: 14 torr H_2O, 15 min, 2.1 O.D.

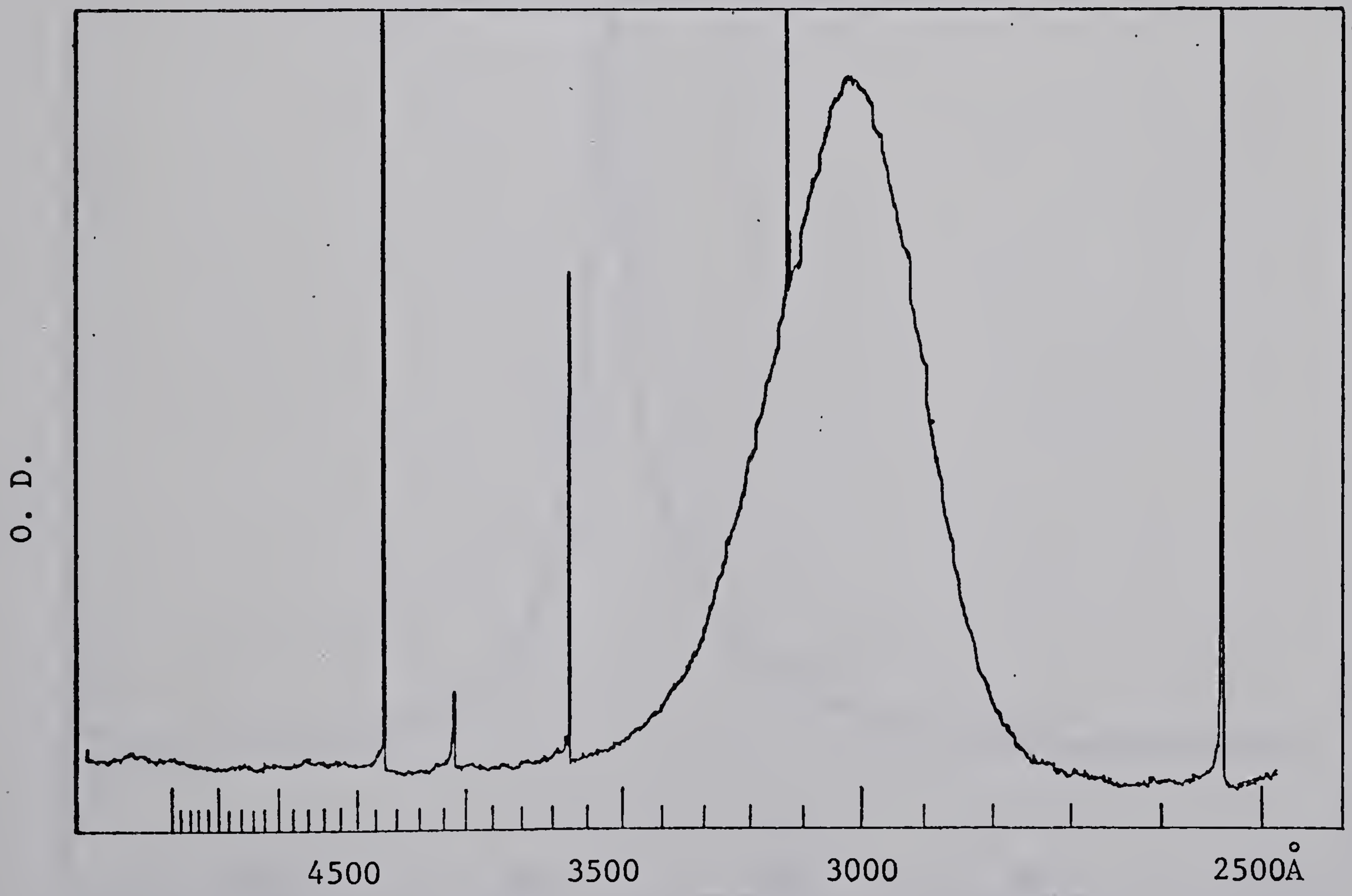

FIGURE 18: Fluorescence spectra: 40 torr C_2H_5OH, 30 min, 0.4 O.D.

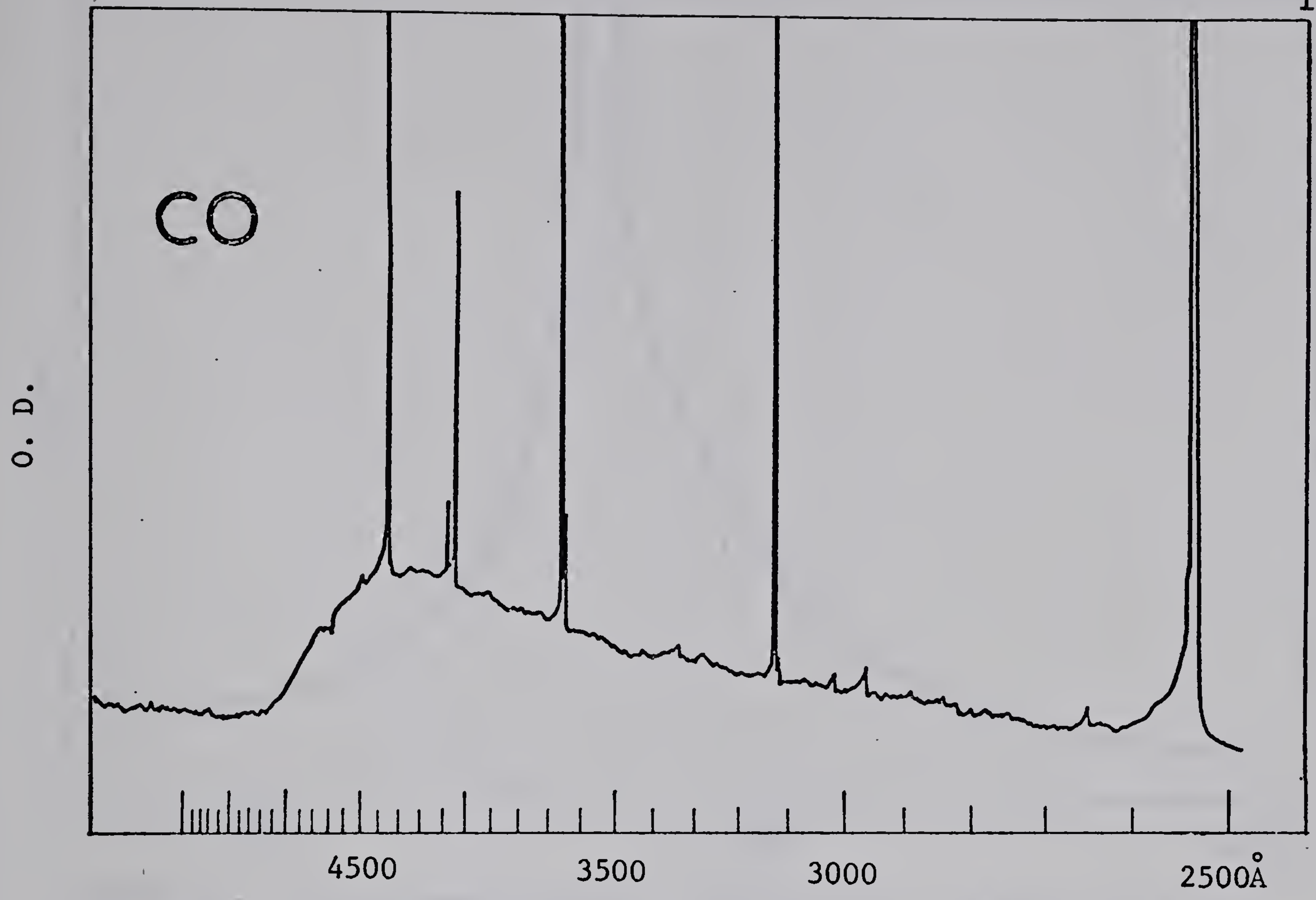

FIGURE 19: Fluorescence spectra: 420 torr CO, 4 hours, 0.4 O.D.

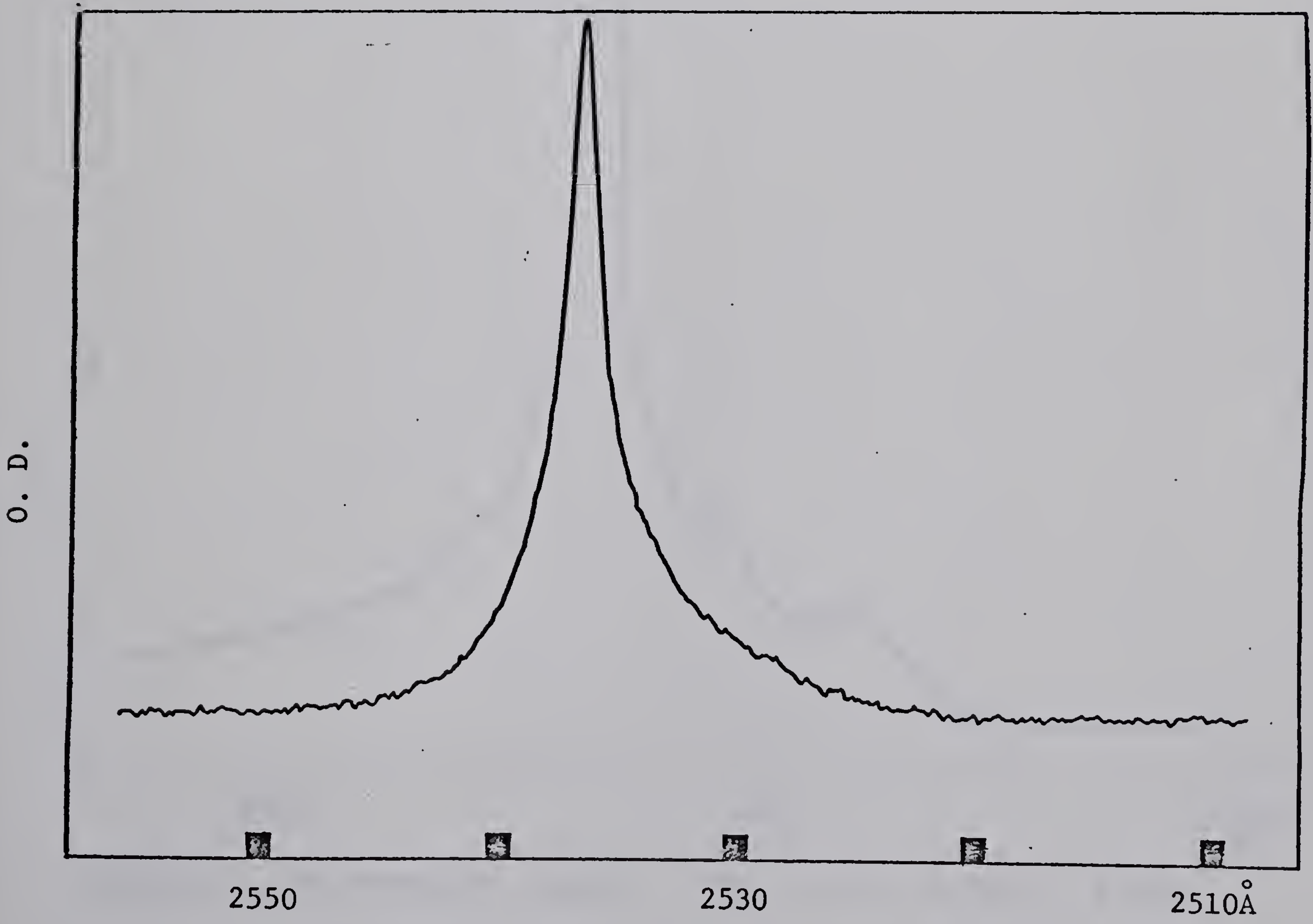

FIGURE 20: Fluorescence spectra: 430 torr He, 4.5 hours, 2.1 O.D.

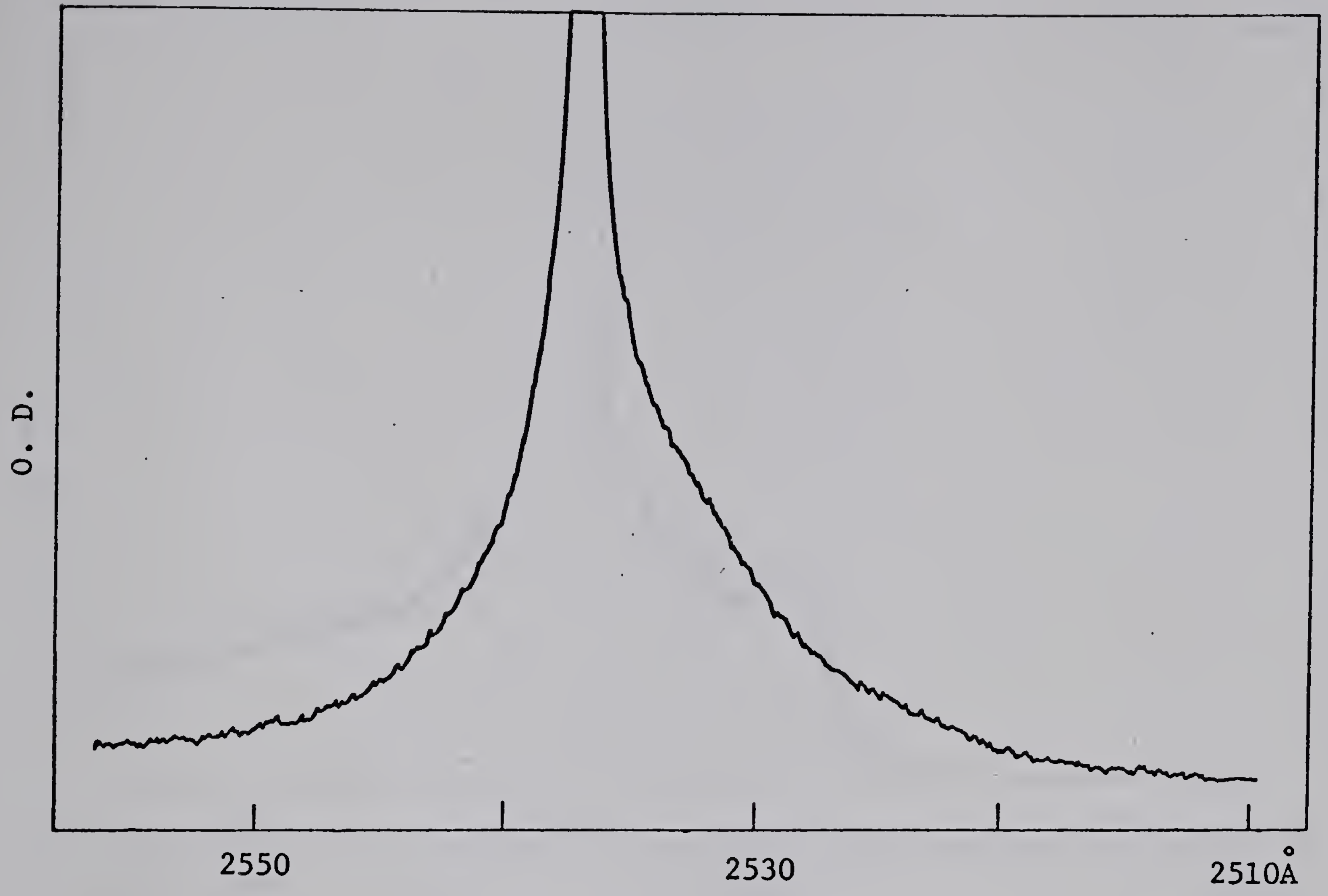

FIGURE 21: Fluorescence spectra: 440 torr Ne, 1.5 hours, 2.1 O.D.

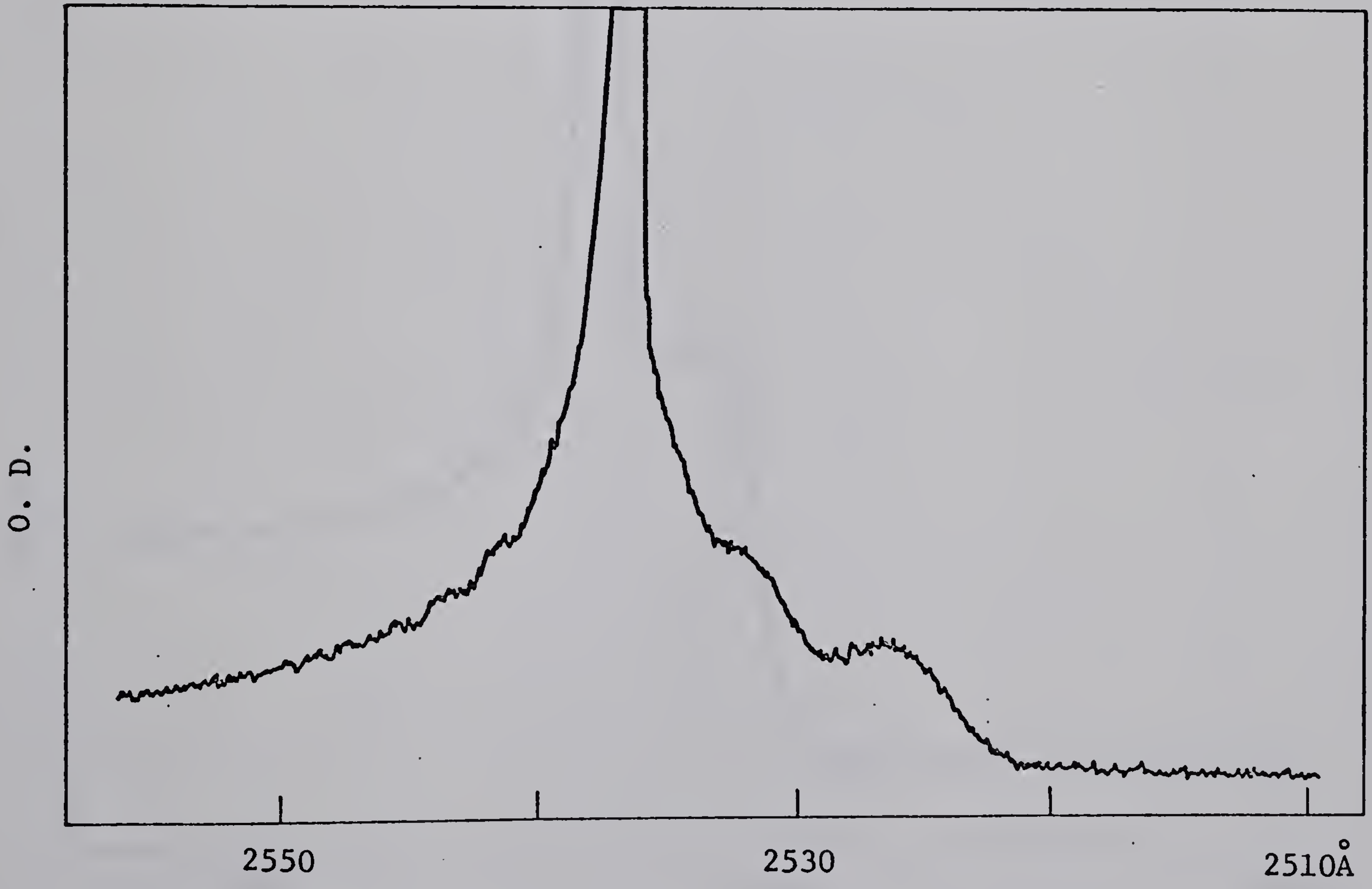

FIGURE 22: Fluorescence spectra: 600 torr Ar, 20 min, 2.1 O.D.

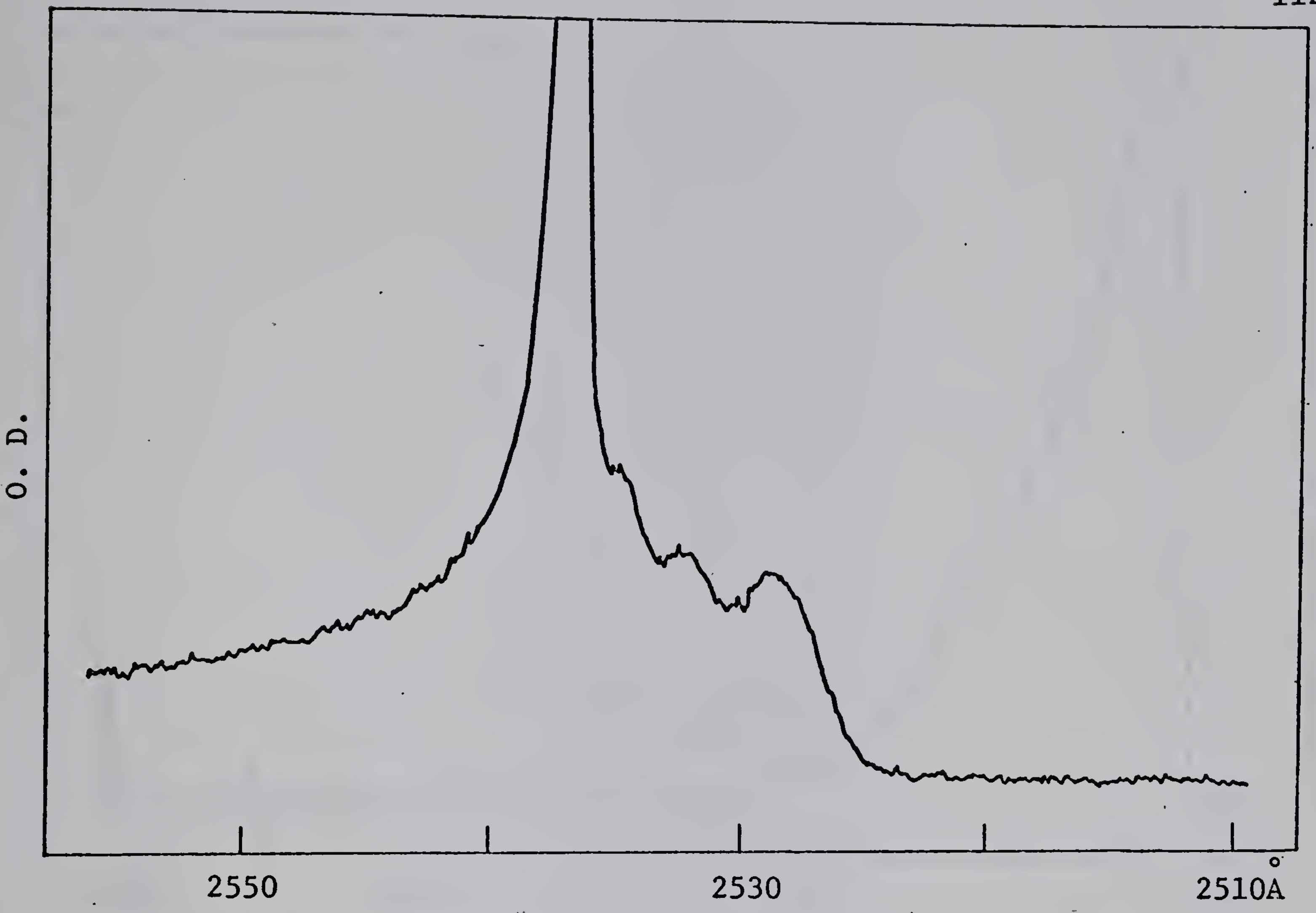

FIGURE 23: Fluorescence spectra: 750 torr Kr, 10 min, 2.1 O.D.

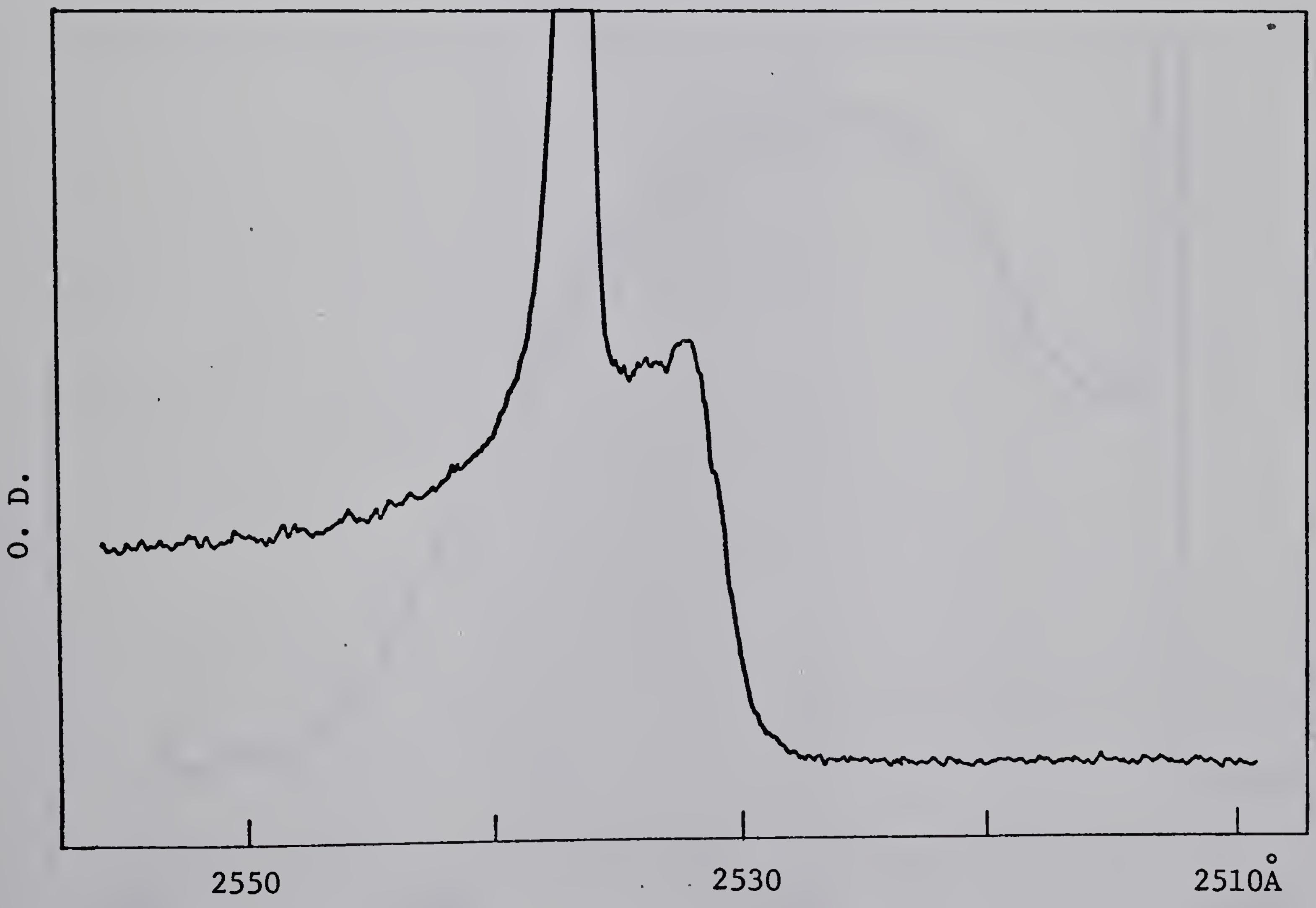

FIGURE 24: Fluorescence spectra: 860 torr Xe, 30 min, 2.1 O.D.

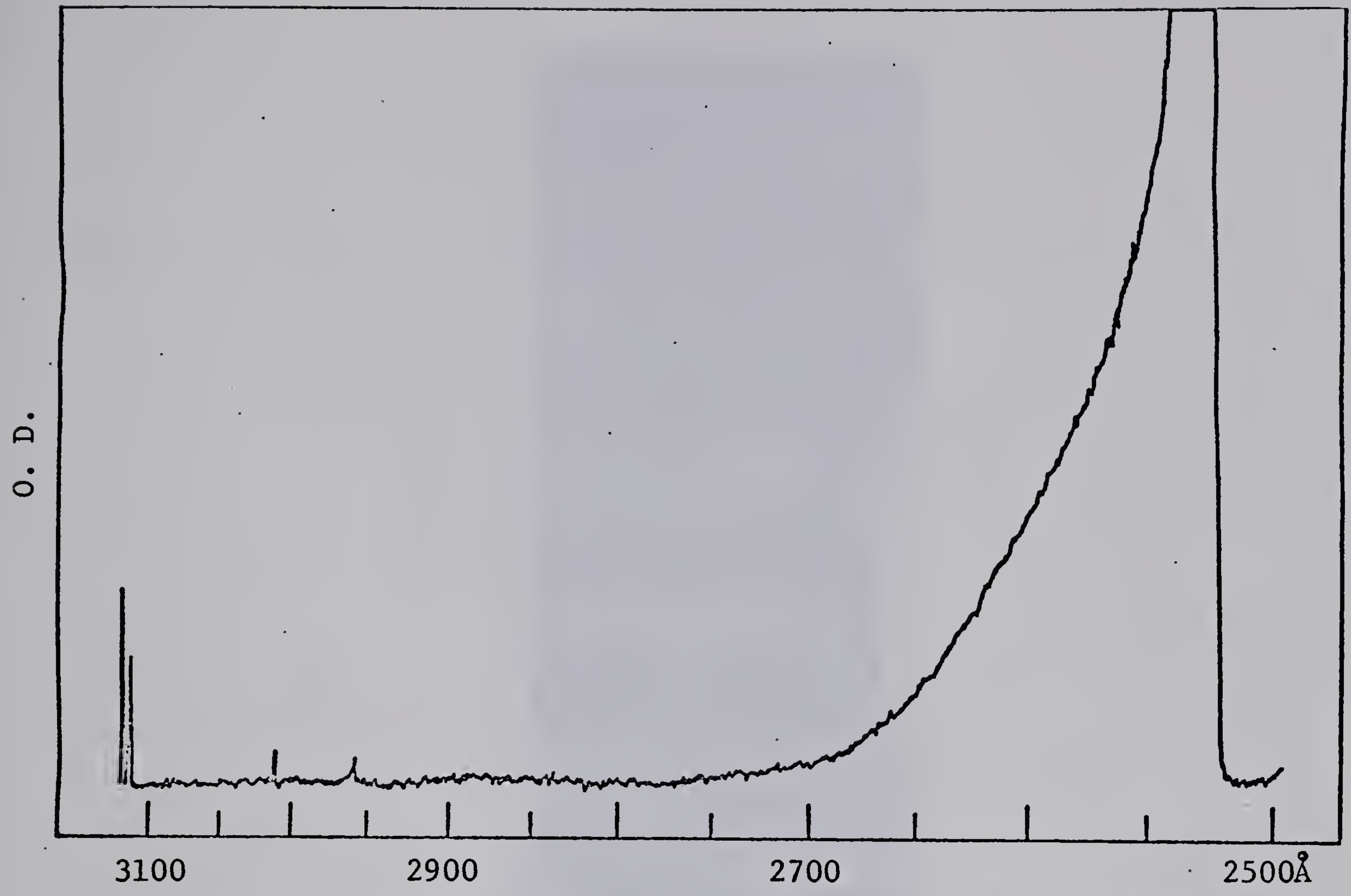

FIGURE 25: Fluorescence spectra: 750 torr Kr, 10 min, 0.8 O.D.

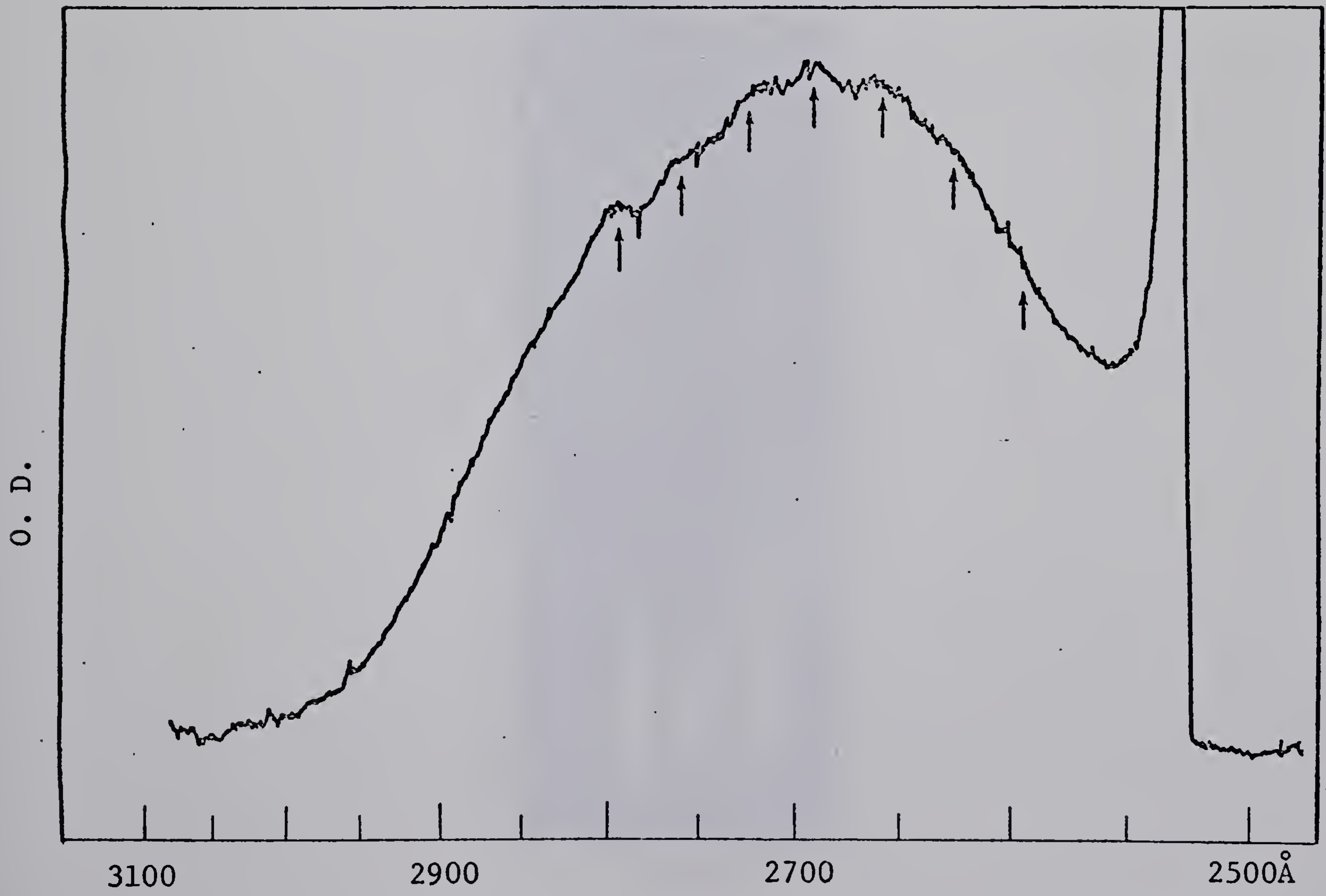

FIGURE 26: Fluorescence spectra: 830 torr Xe, 10 min, 0.8 O.D.

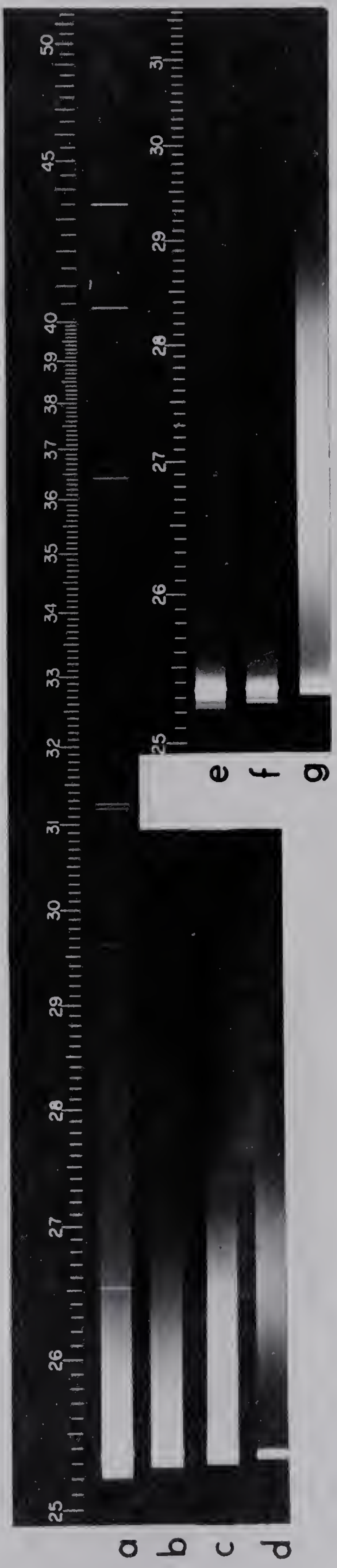

25
26
27
28
29
30
31
32
33
34
35
36
37
38
39
40
45
50
25
26
27
28
29
30
31
a
b
c
d
e
f
g

(Previous Page)

FIGURE 27: Fluorescence spectra from excited mercury-substrate complexes: a, 600 torr N_2, 5 hours; b, 400 torr C_2H_6, 15 min; c, 600 torr C_3H_8, 3 hours; d, 510 torr $C(CH_3)_4$, 1.2 hours; e, 600 torr Ar, 20 min; f, 750 torr Kr, 10 min; g, 830 torr Xe, 10 min.

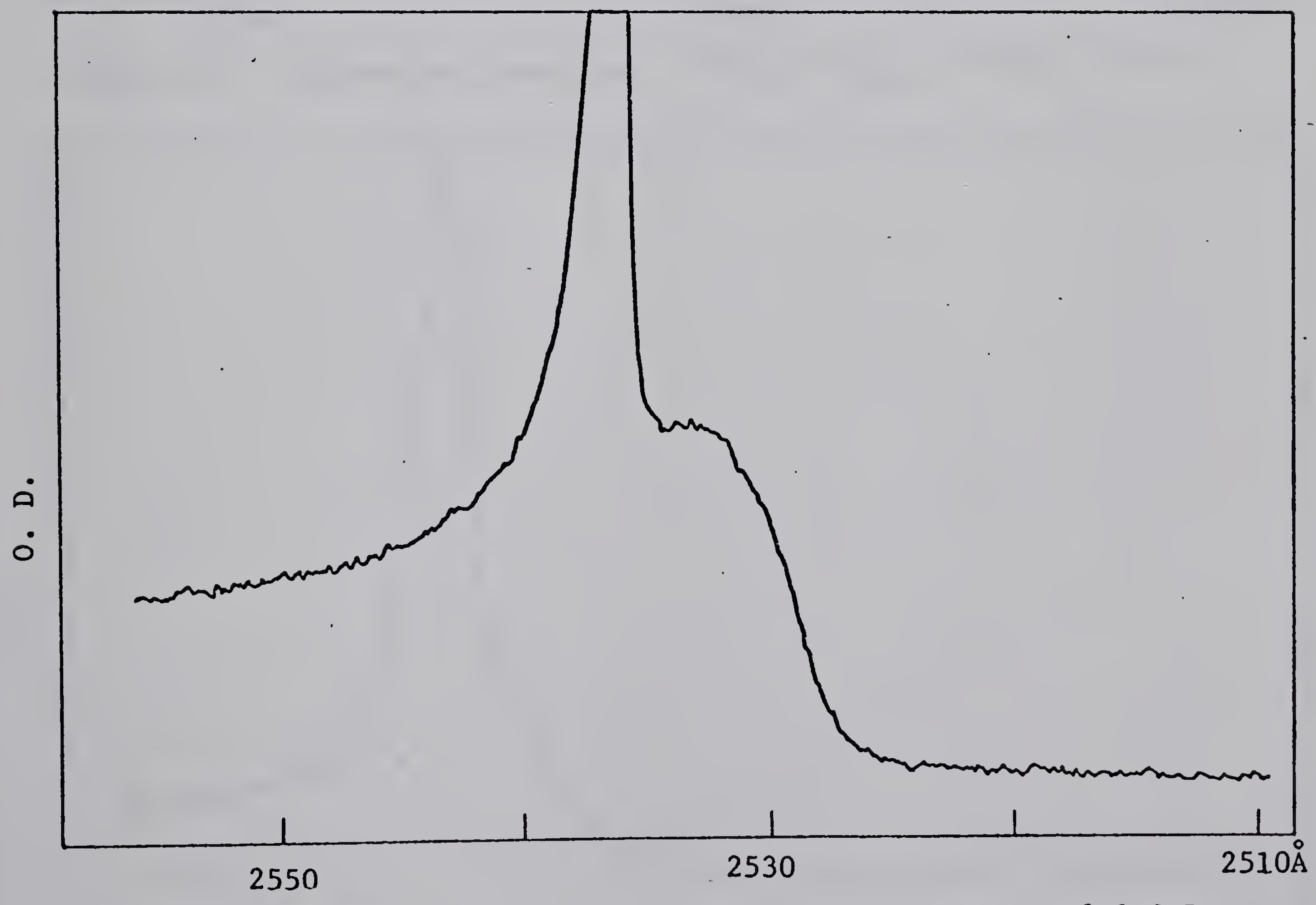

FIGURE 28: Fluorescence spectra: 500 torr CH_4, 60 min, 2.1 O.D.

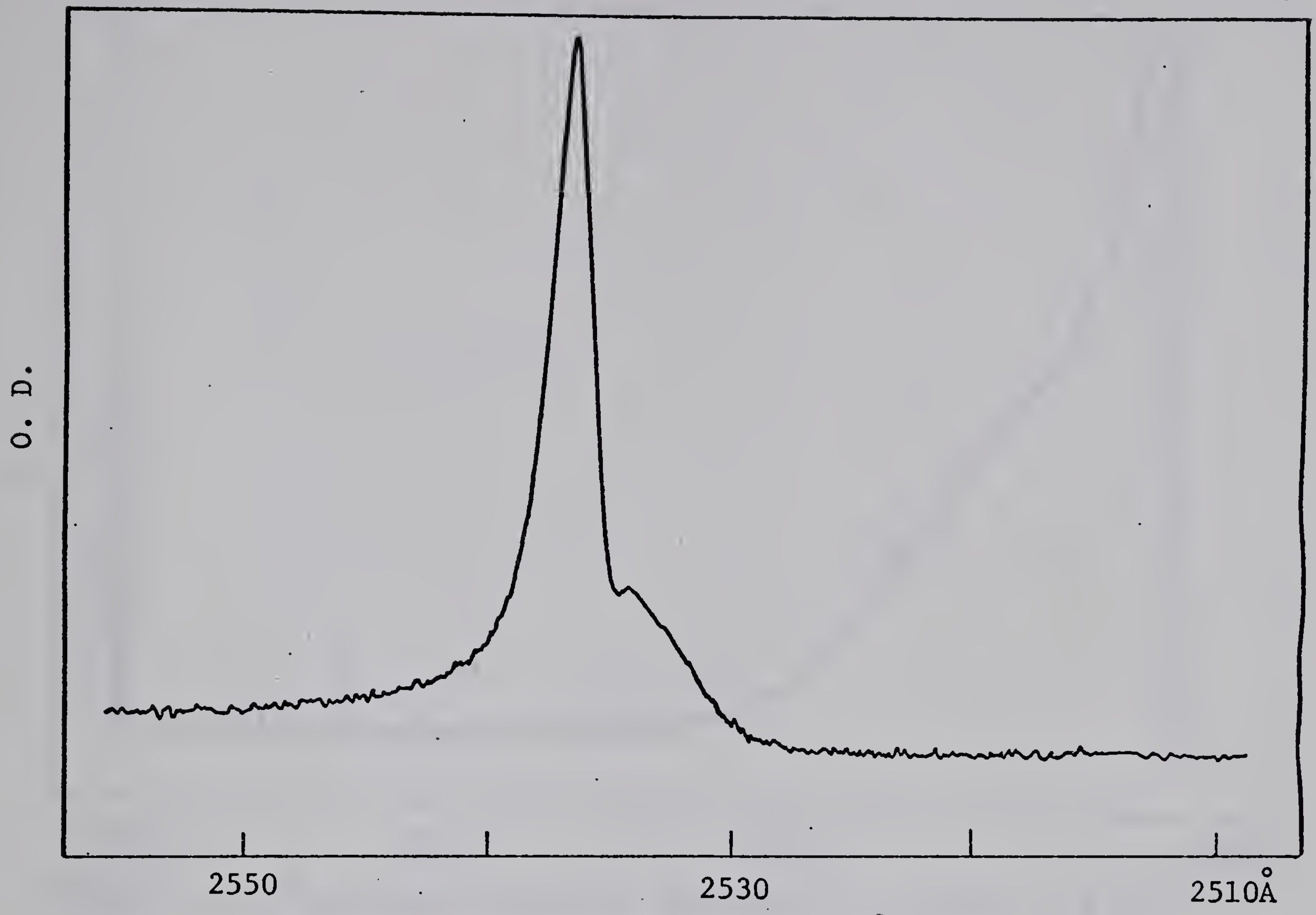

FIGURE 29: Fluorescence spectra: 400 torr C_2H_6, 15 min, 2.1 O.D.

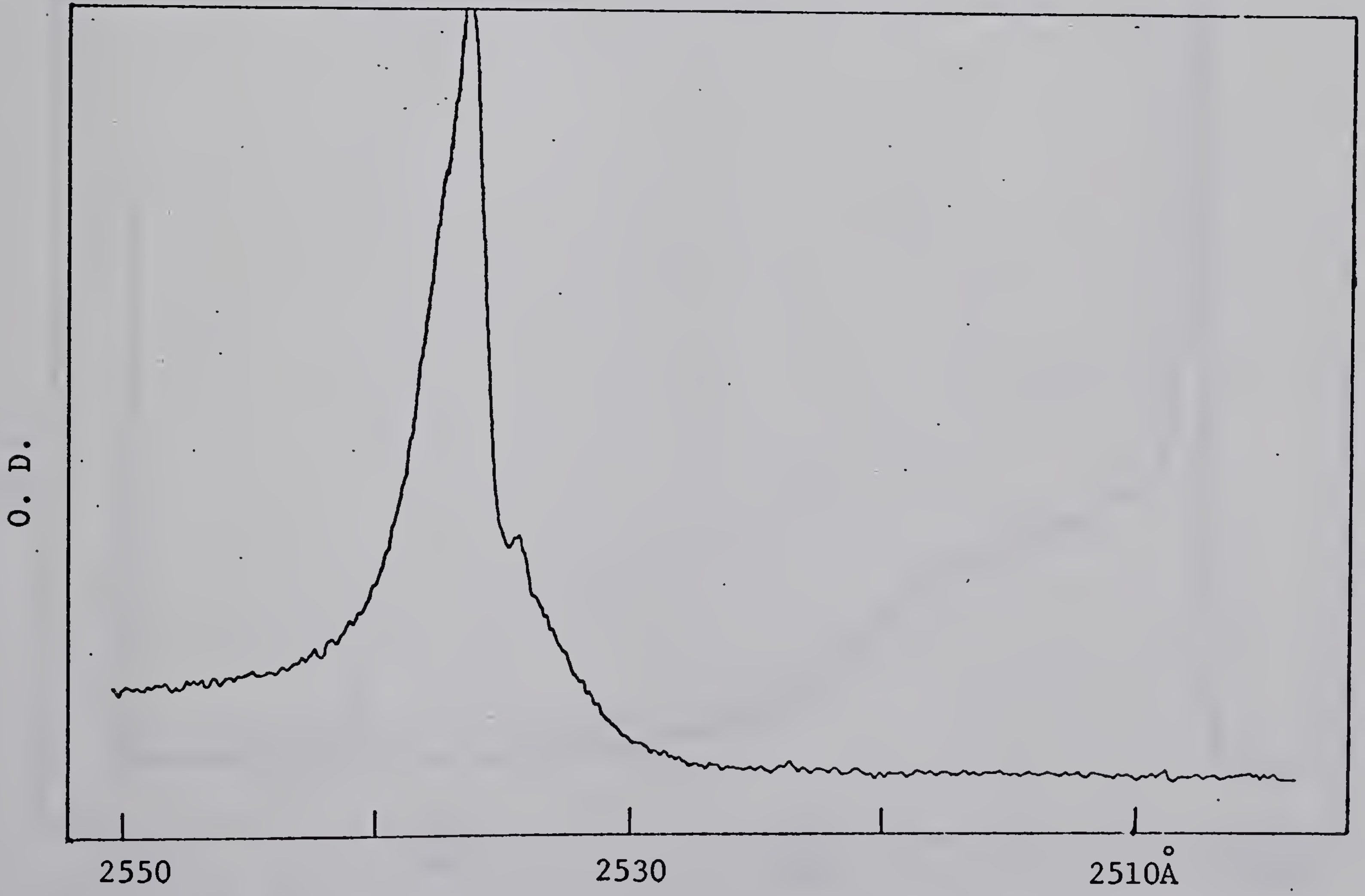

FIGURE 30: Fluorescence spectra: 600 torr C_3H_8, 3 hours, 2.1 O.D.

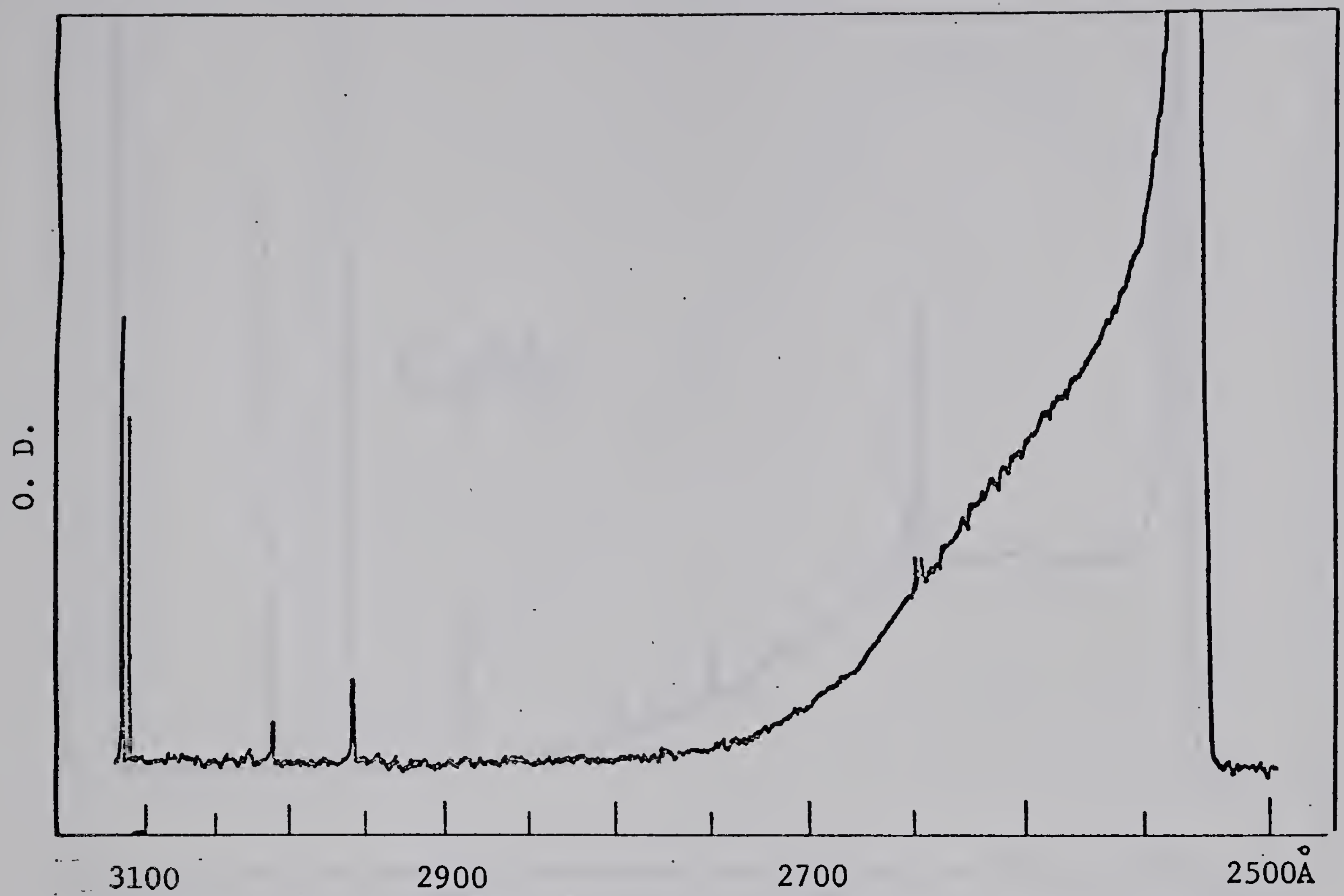

FIGURE 31: Fluorescence spectra: 500 torr CH_4, 60 min, 0.8 O.D.

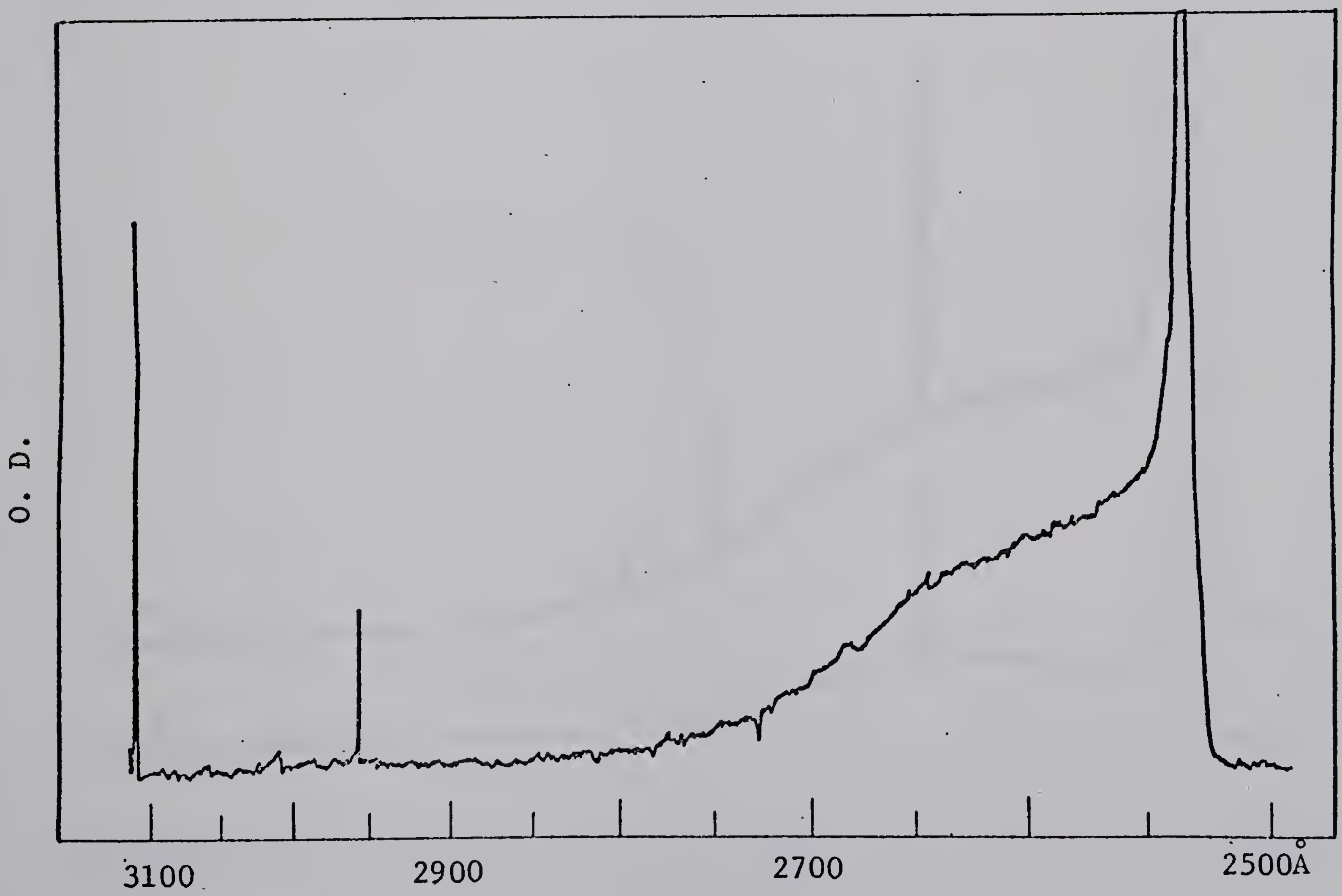

FIGURE 32: Fluorescence spectra: 400 torr C_2H_6, 15 min, 0.8 O.D.

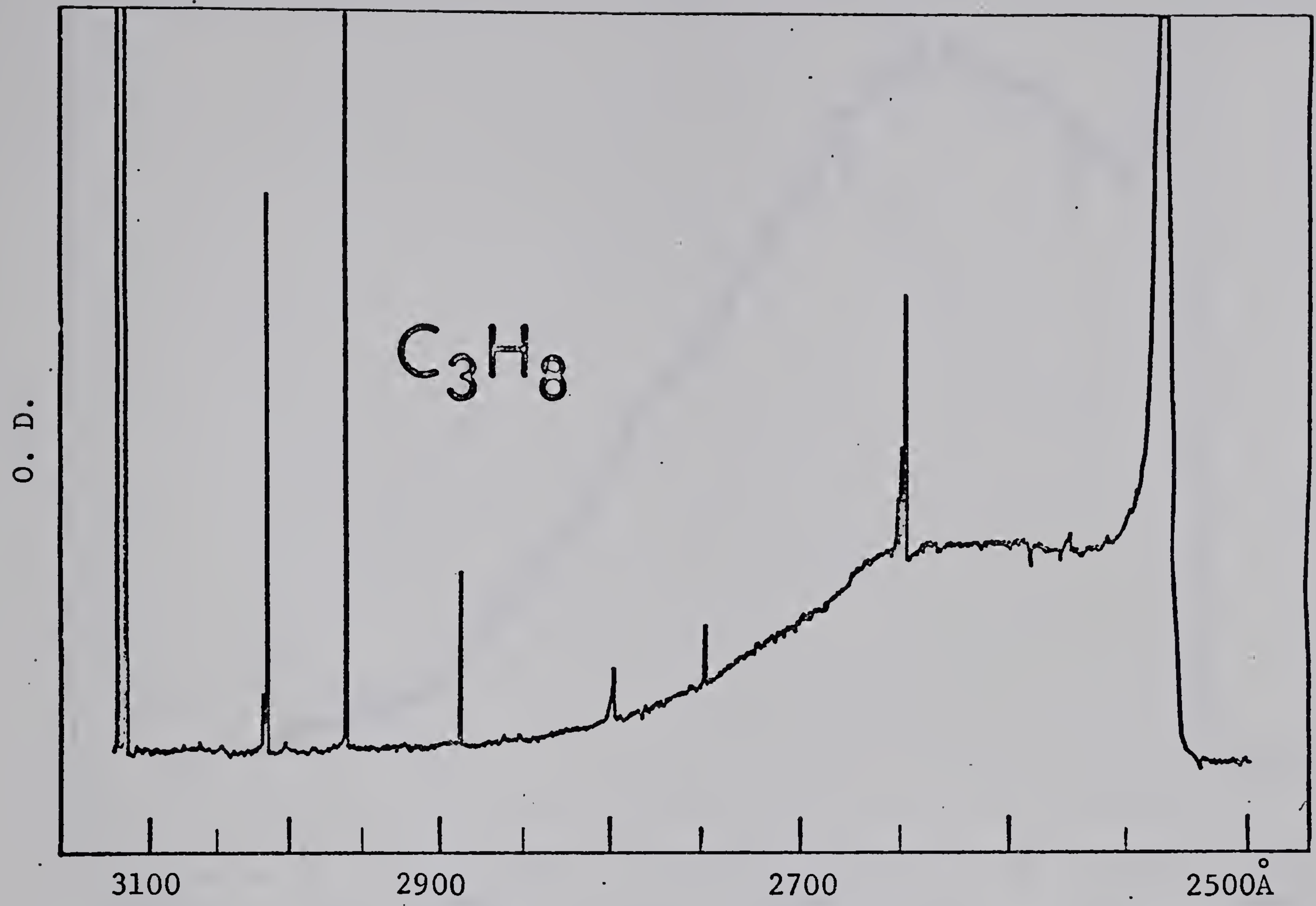

FIGURE 33: Fluorescence spectra: 600 torr C_3H_8, 3 hours, 0.8 O.D.

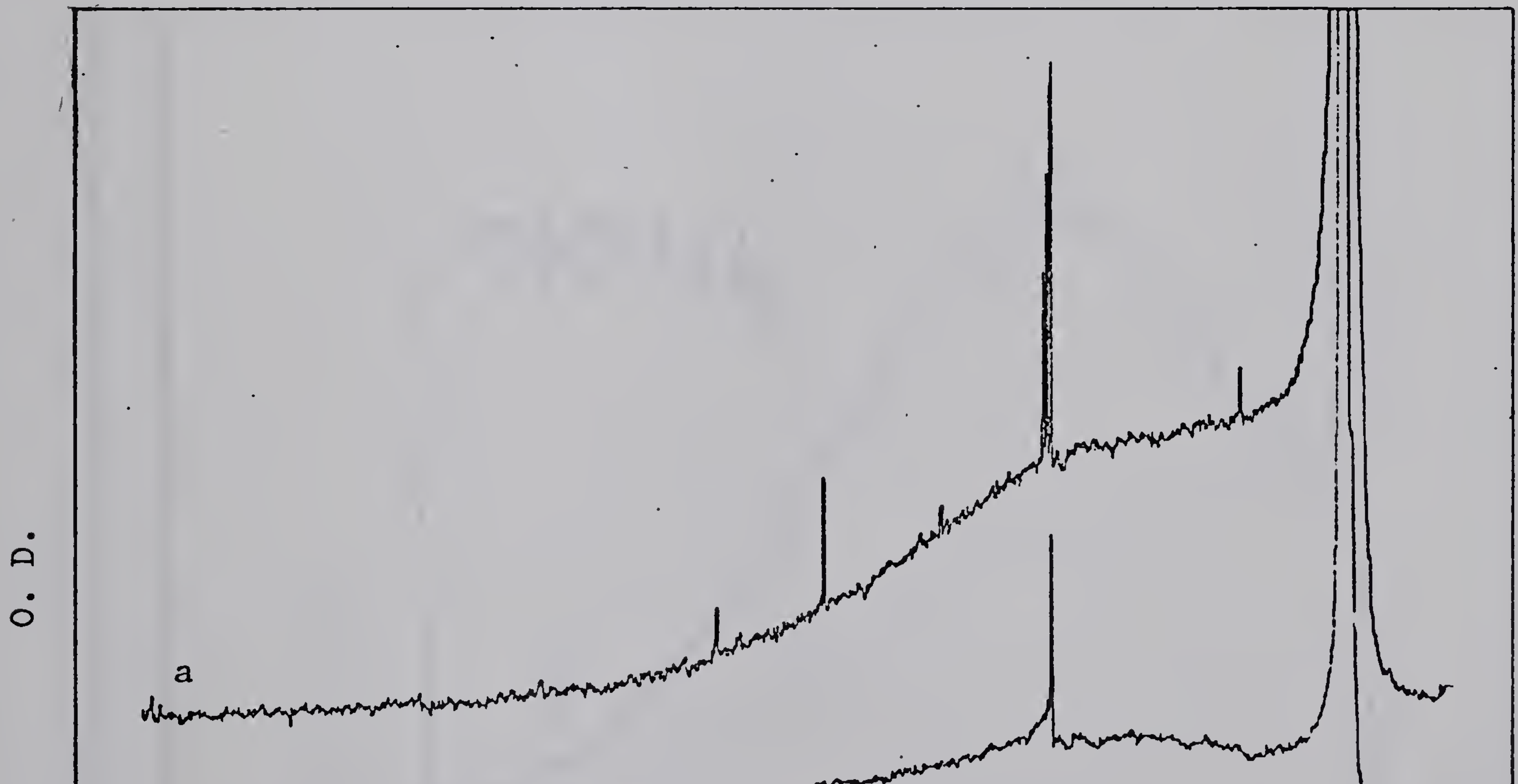

FIGURE 34: a, 8 torr $i\text{-}C_4H_{10}$, 180 min, 0.8 O.D.;

b, 645 torr $i\text{-}C_4H_{10}$, 46 min, 0.4 O.D.

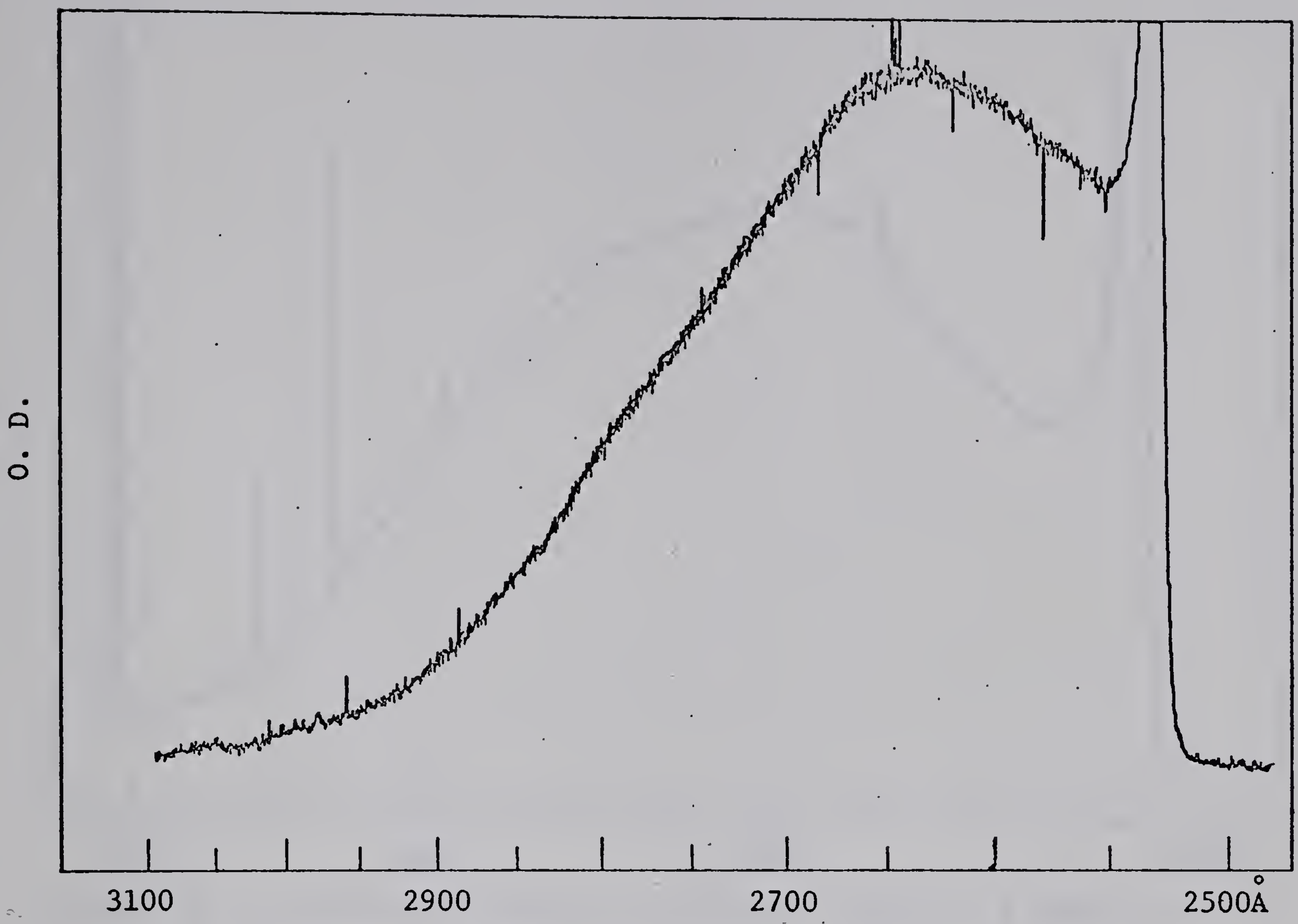

FIGURE 35: Fluorescence spectra: 8 torr $C(CH_3)_4$, 120 min, 0.4 O.D.

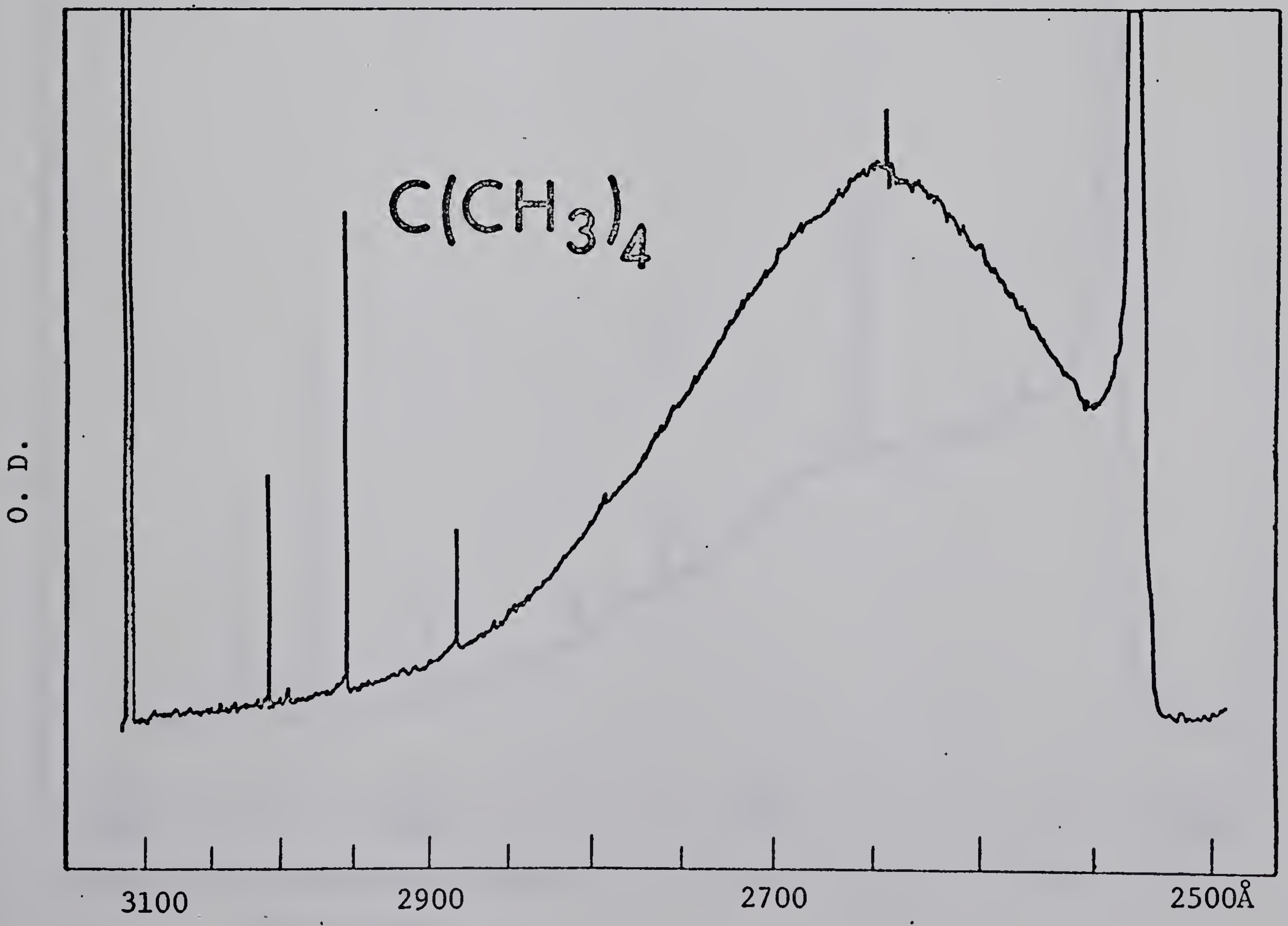

FIGURE 36: Fluorescence spectra: 510 torr $C(CH_3)_4$, 1.2 hours, 0.8 O.D.

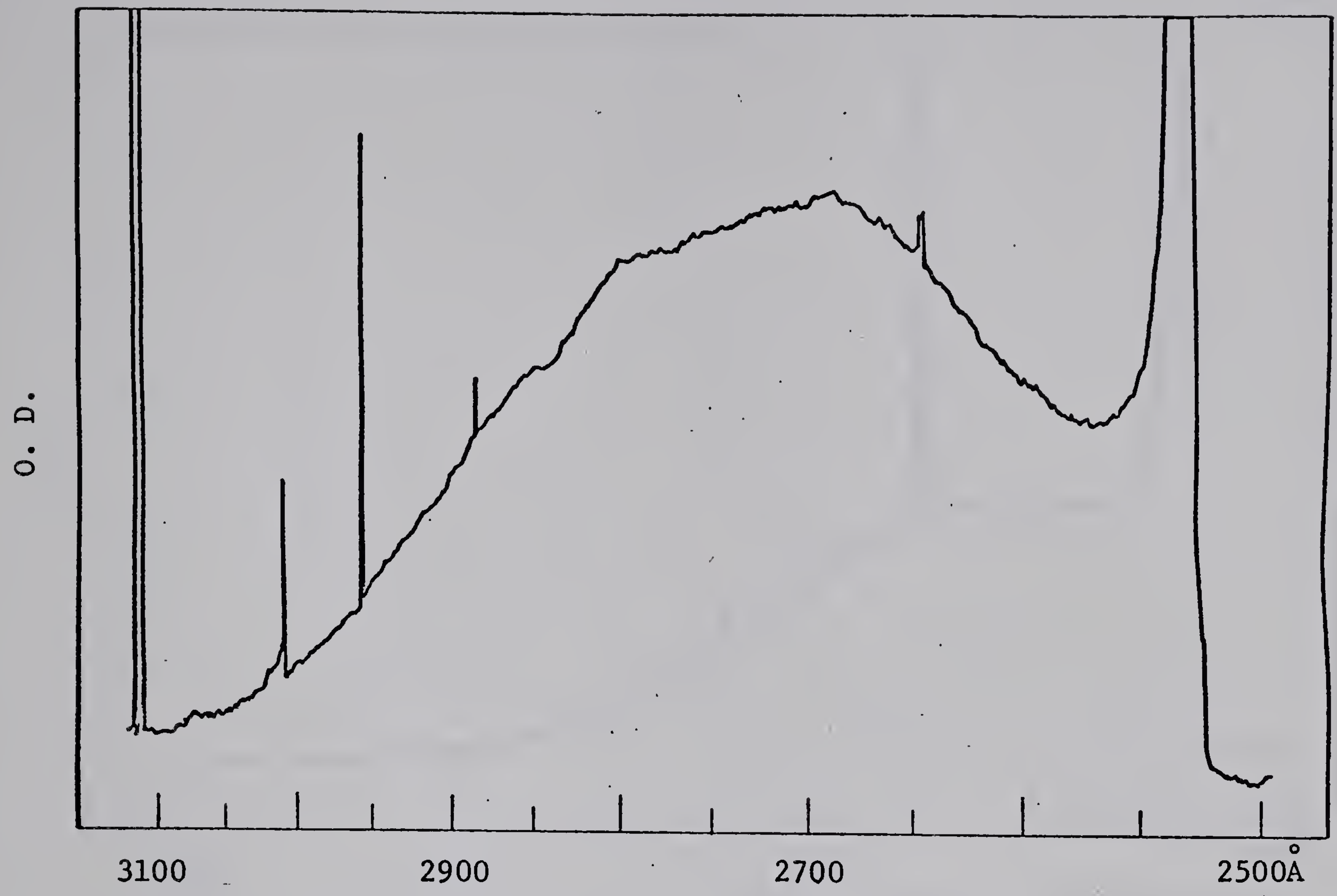

FIGURE 37: Fluorescence spectra: 400 torr c-C_3H_6, 1.5 hours, 0.4 O.D.

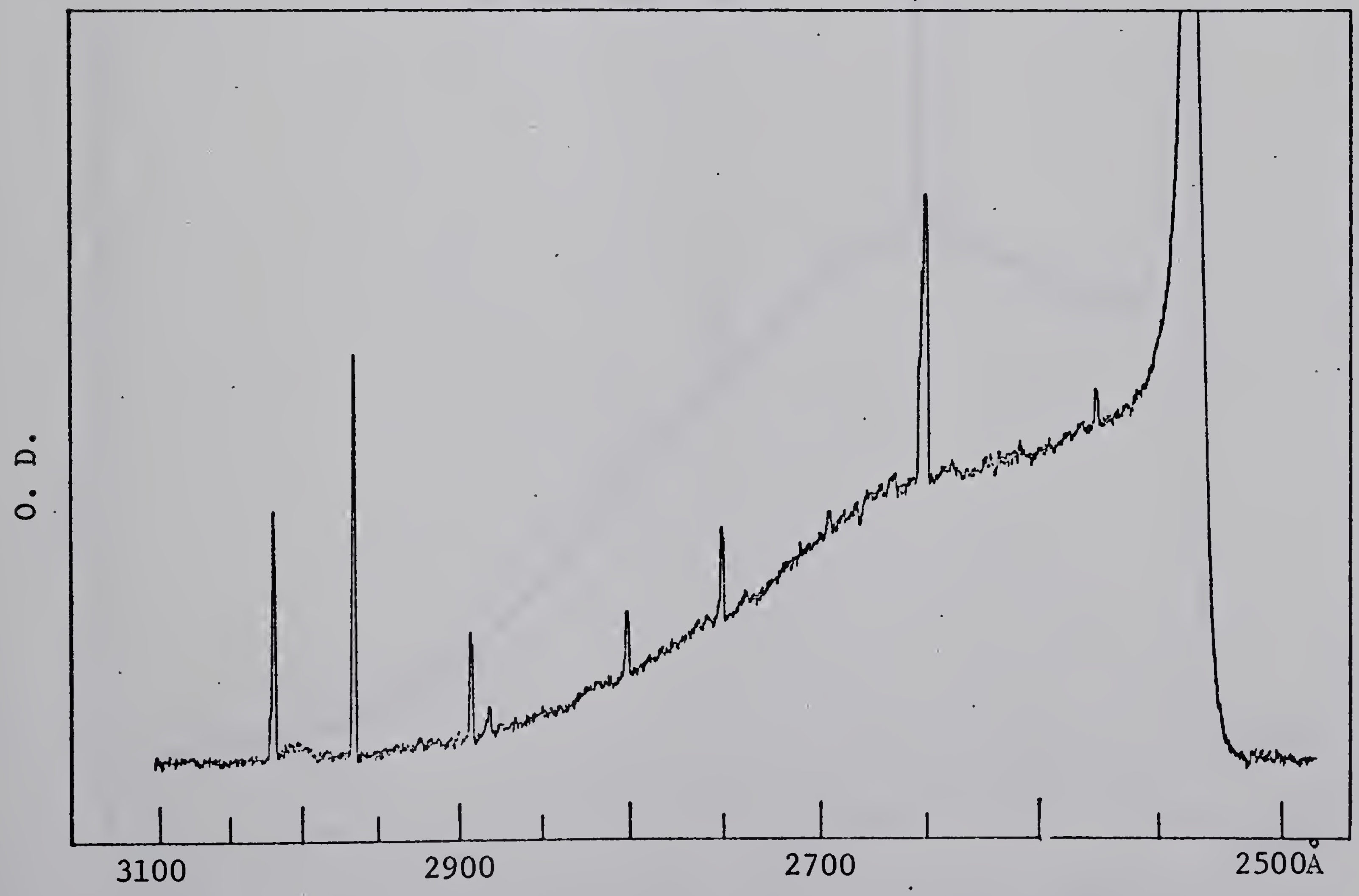

FIGURE 38: Fluorescence spectra: 720 torr c-C_4H_8, 1.5 hours, 0.8 O.D., 100 μm slit.

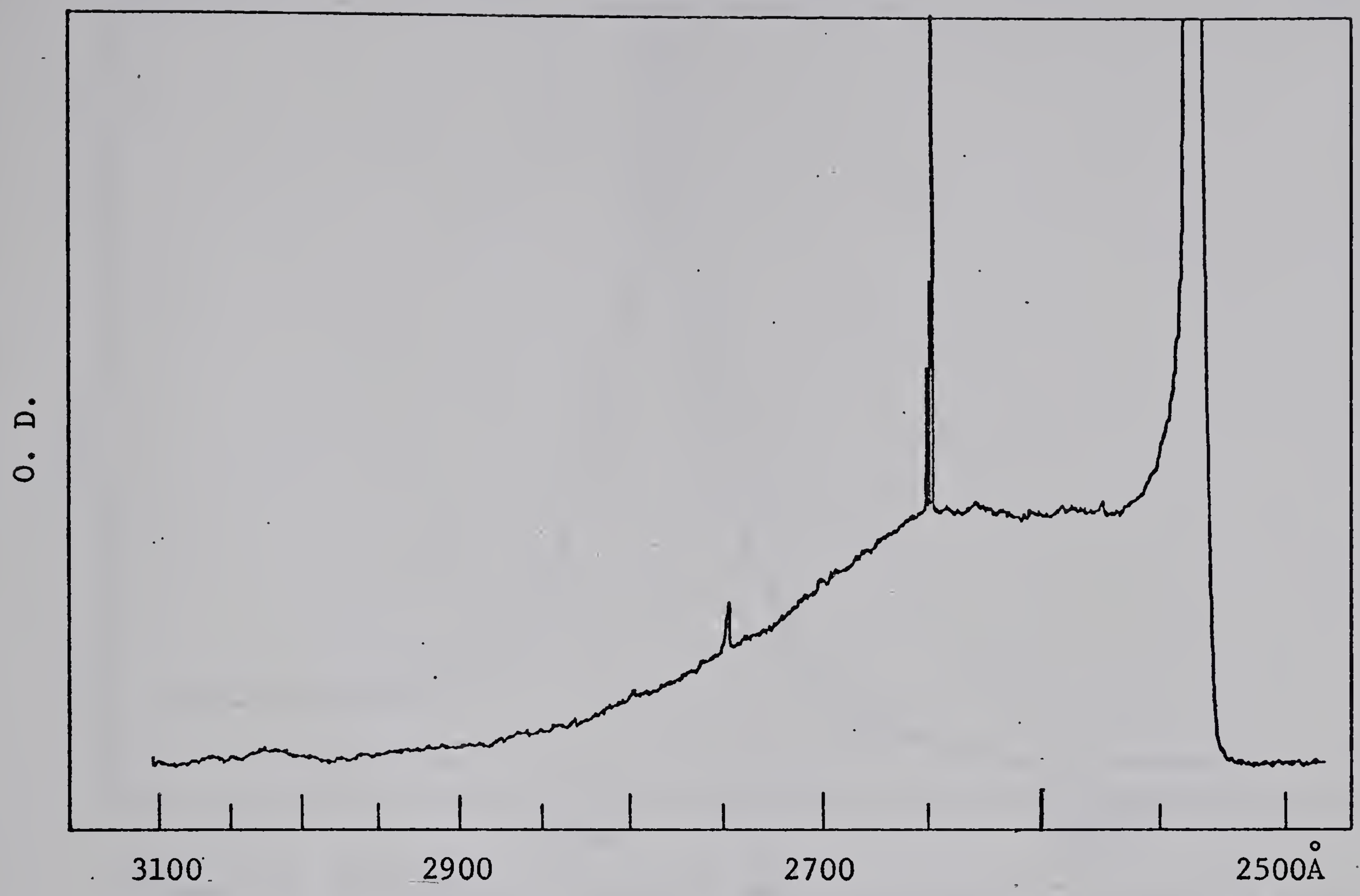

FIGURE 39: Fluorescence spectra: 210 torr c-C_5H_{10}, 55 min, 0.4 O.D.

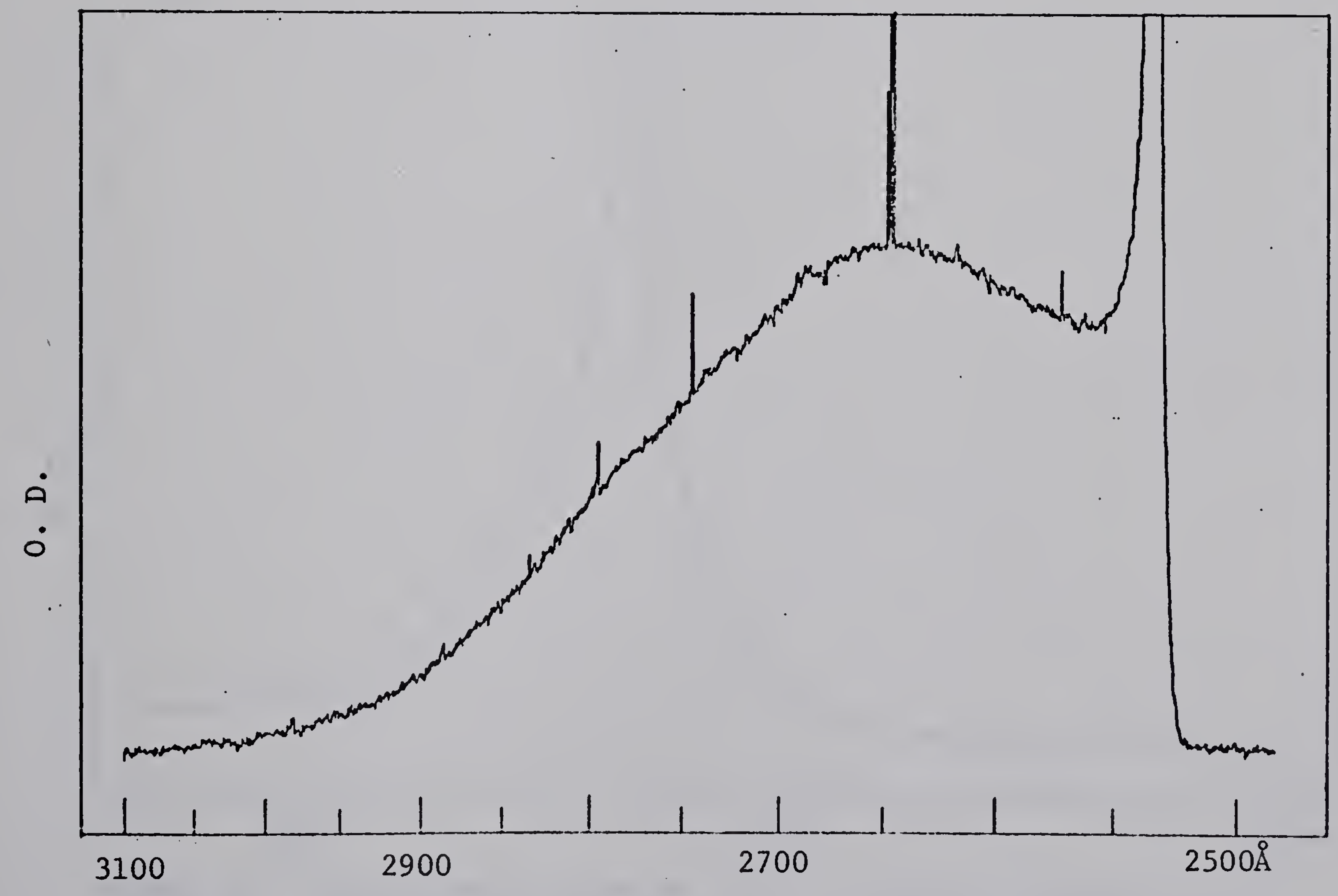

FIGURE 40: Fluorescence spectra: 70 torr c-C_6H_{12}, 180 min, 0.4 O.D.

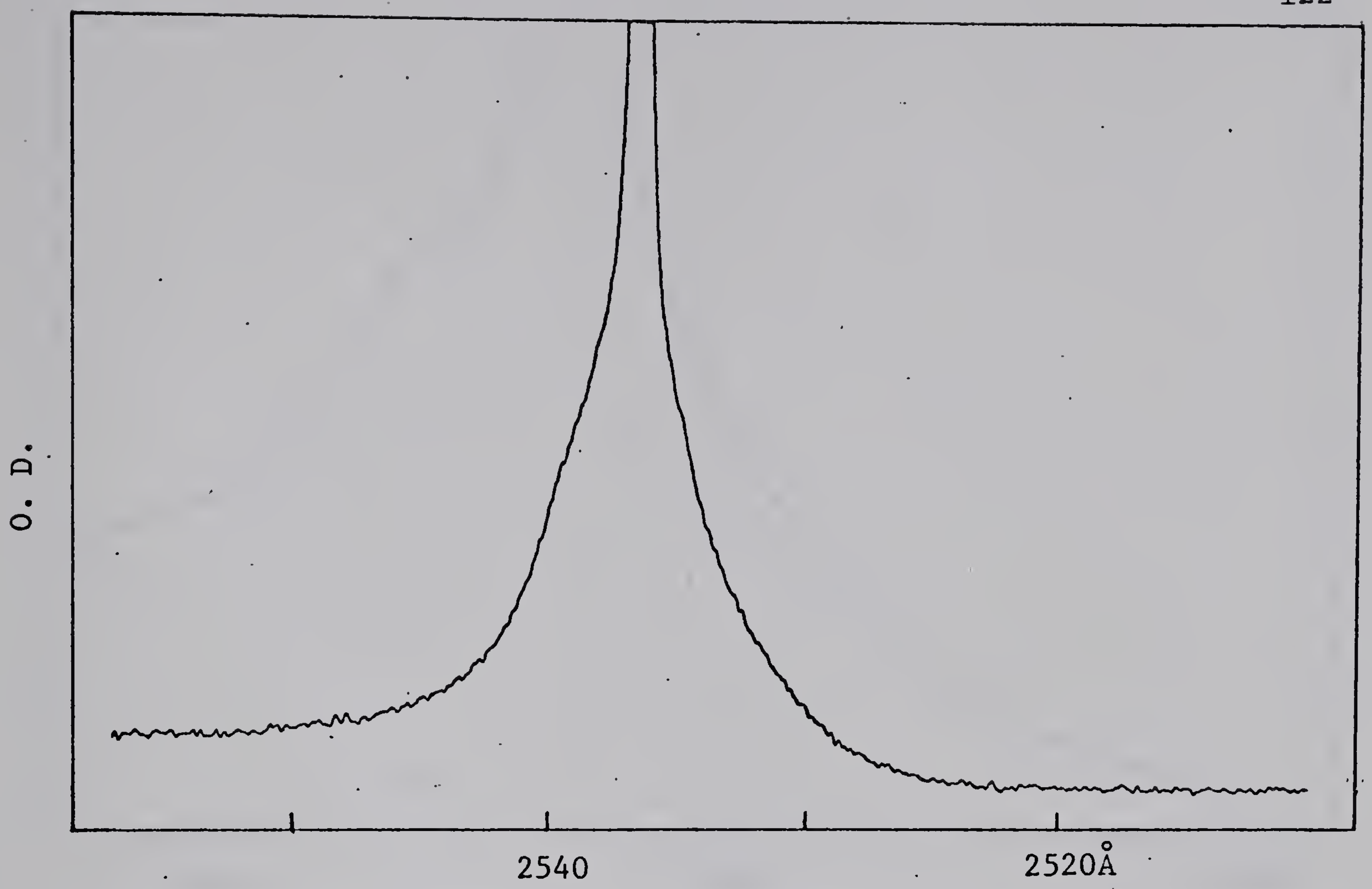

FIGURE 41: Fluorescence spectra: 330 torr CH_3F, 14.5 min, 2.1 O.D.

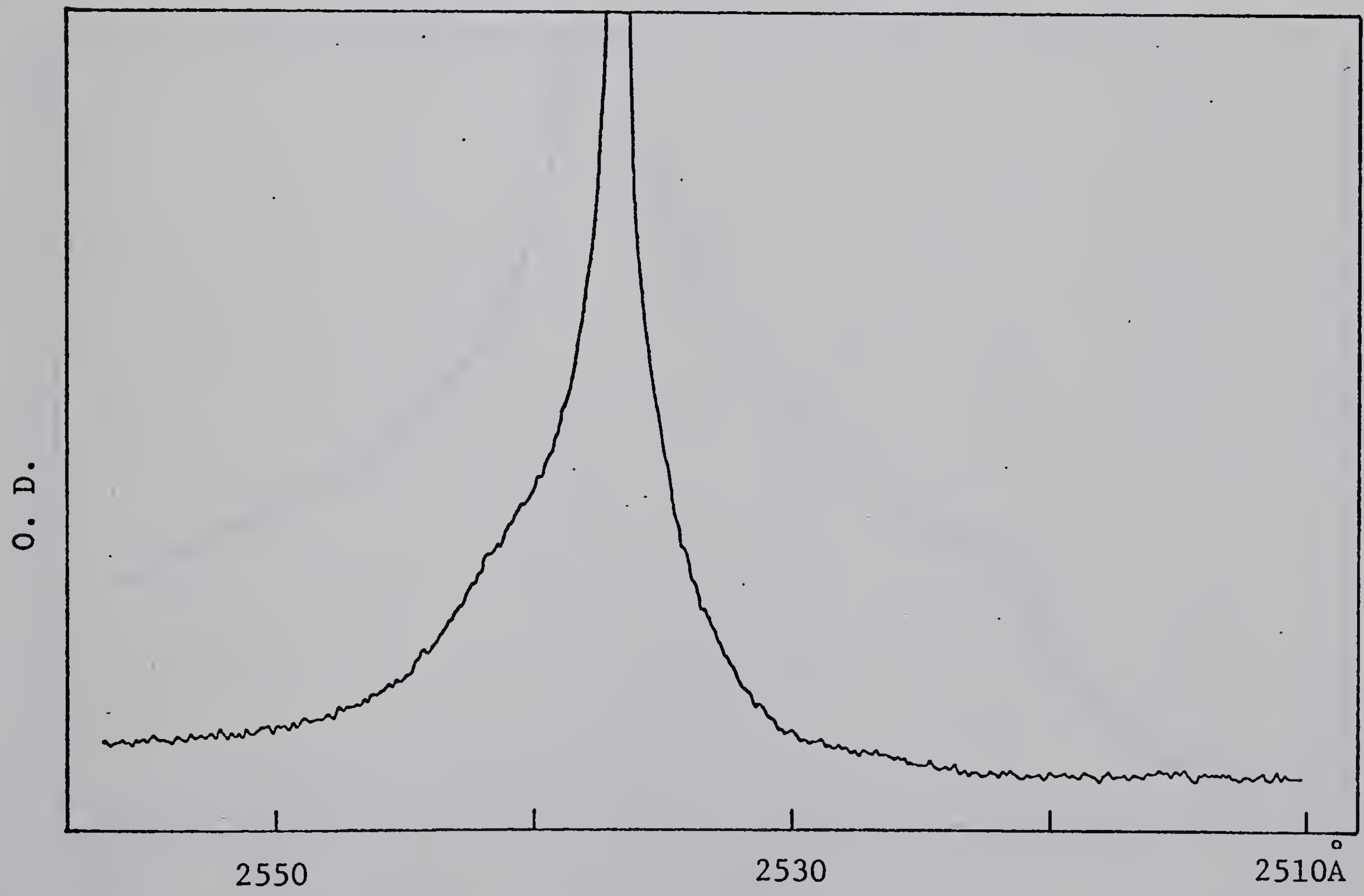

FIGURE 42: Fluorescence spectra: 310 torr CH_2F_2, 15 min, 2.1 O.D.

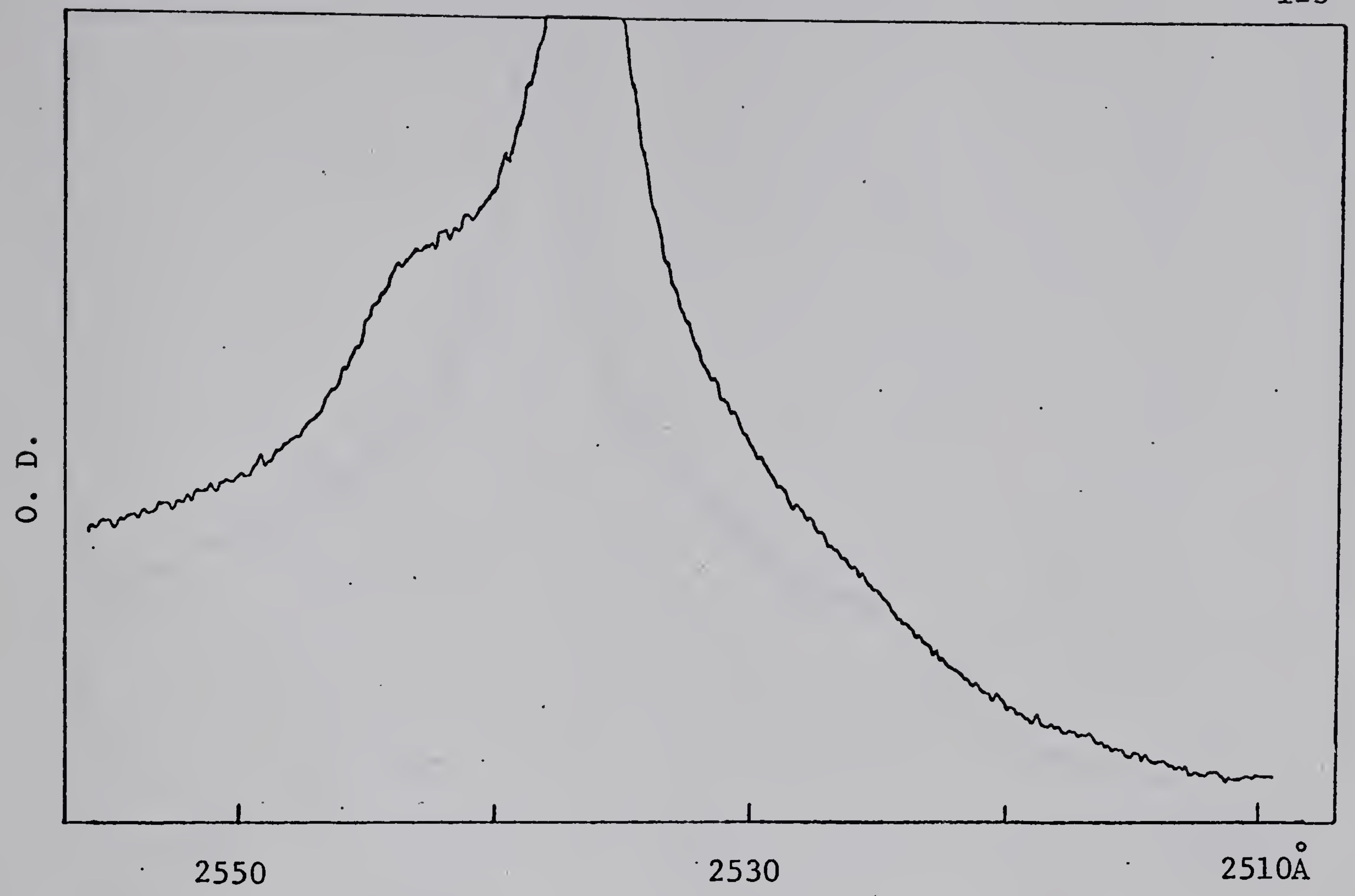

FIGURE 43: Fluorescence spectra: 280 torr CHF_3, 15 min, 2.1 O.D.

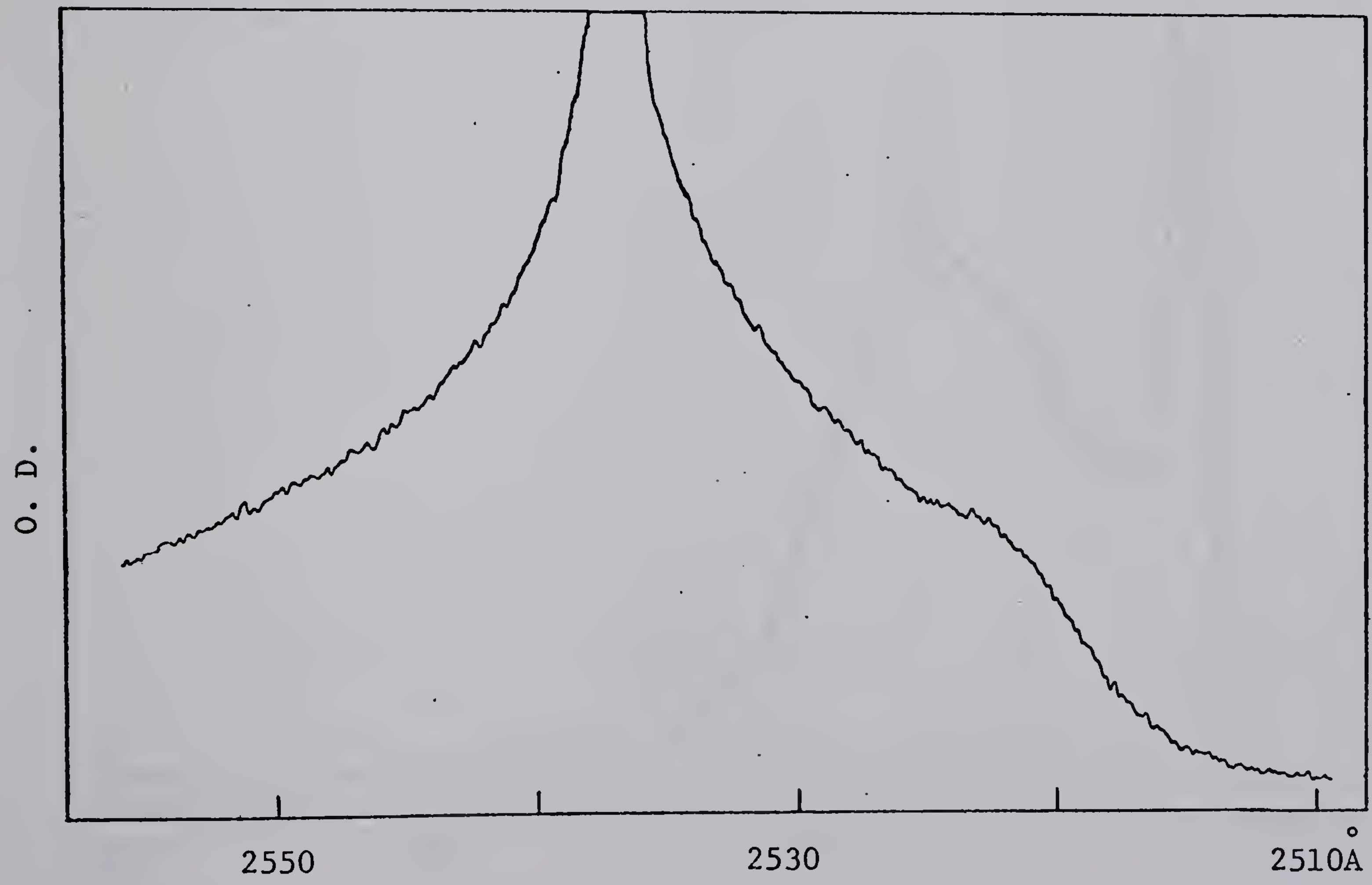

FIGURE 44: Fluorescence spectra: 614 torr CF_4, 30 min, 2.1 O.D.

[illegible]

[illegible]

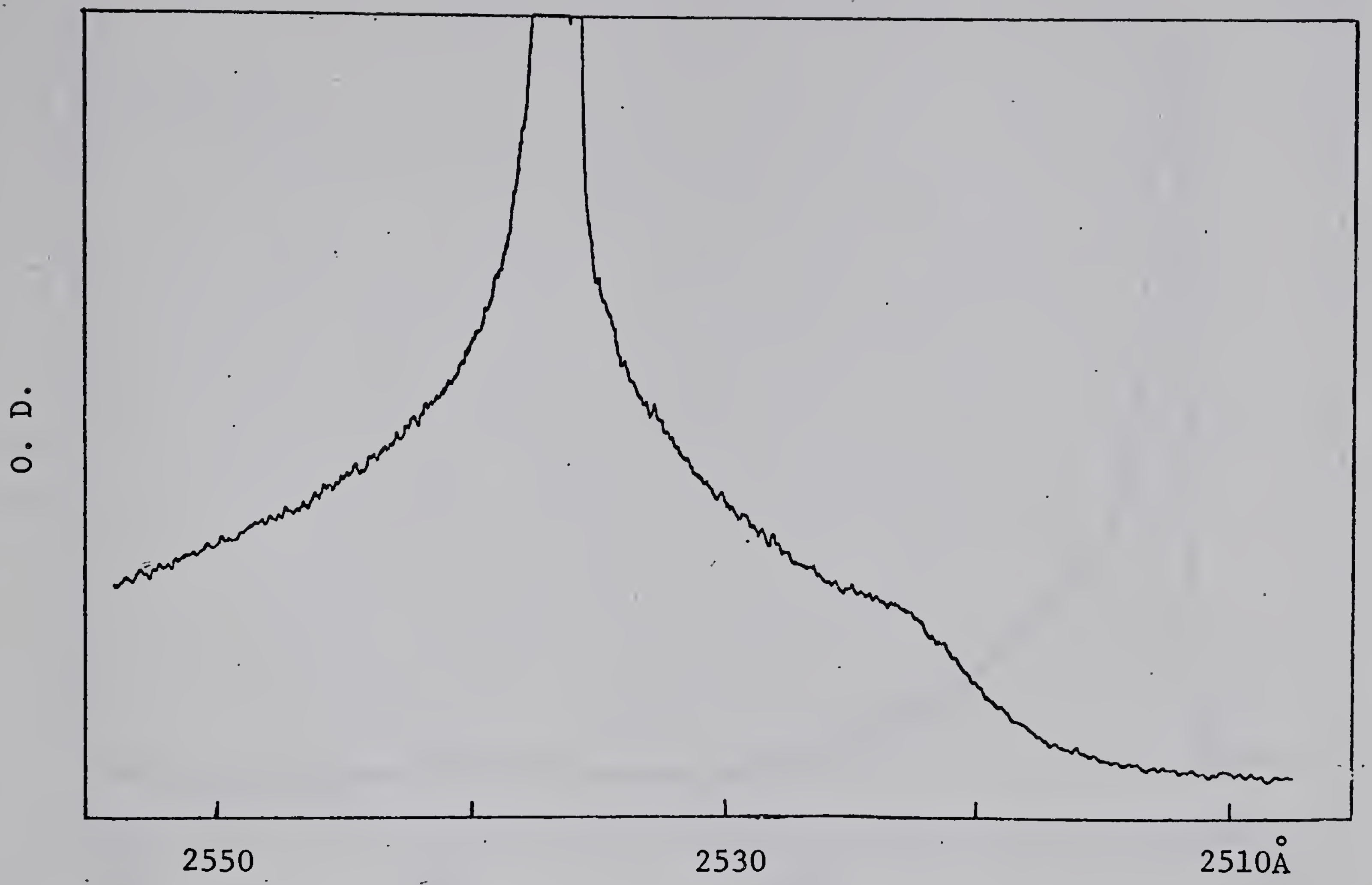

FIGURE 45: Fluorescence spectra: 190 torr SF_6, 60 min, 2.1 O.D.

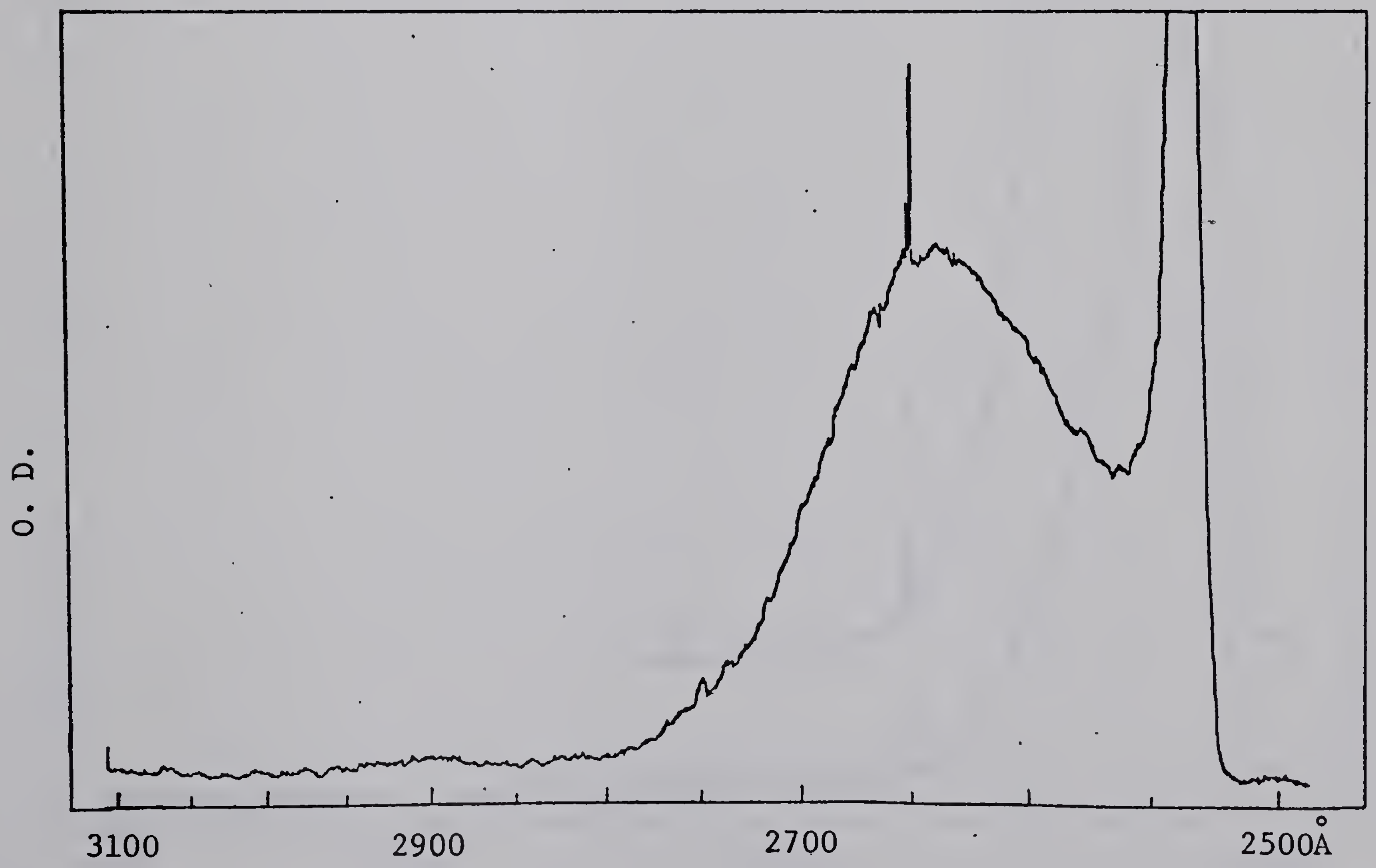

FIGURE 46: Fluorescence spectra: 330 torr CH_3F, 14.5 min, 0.4 O.D.

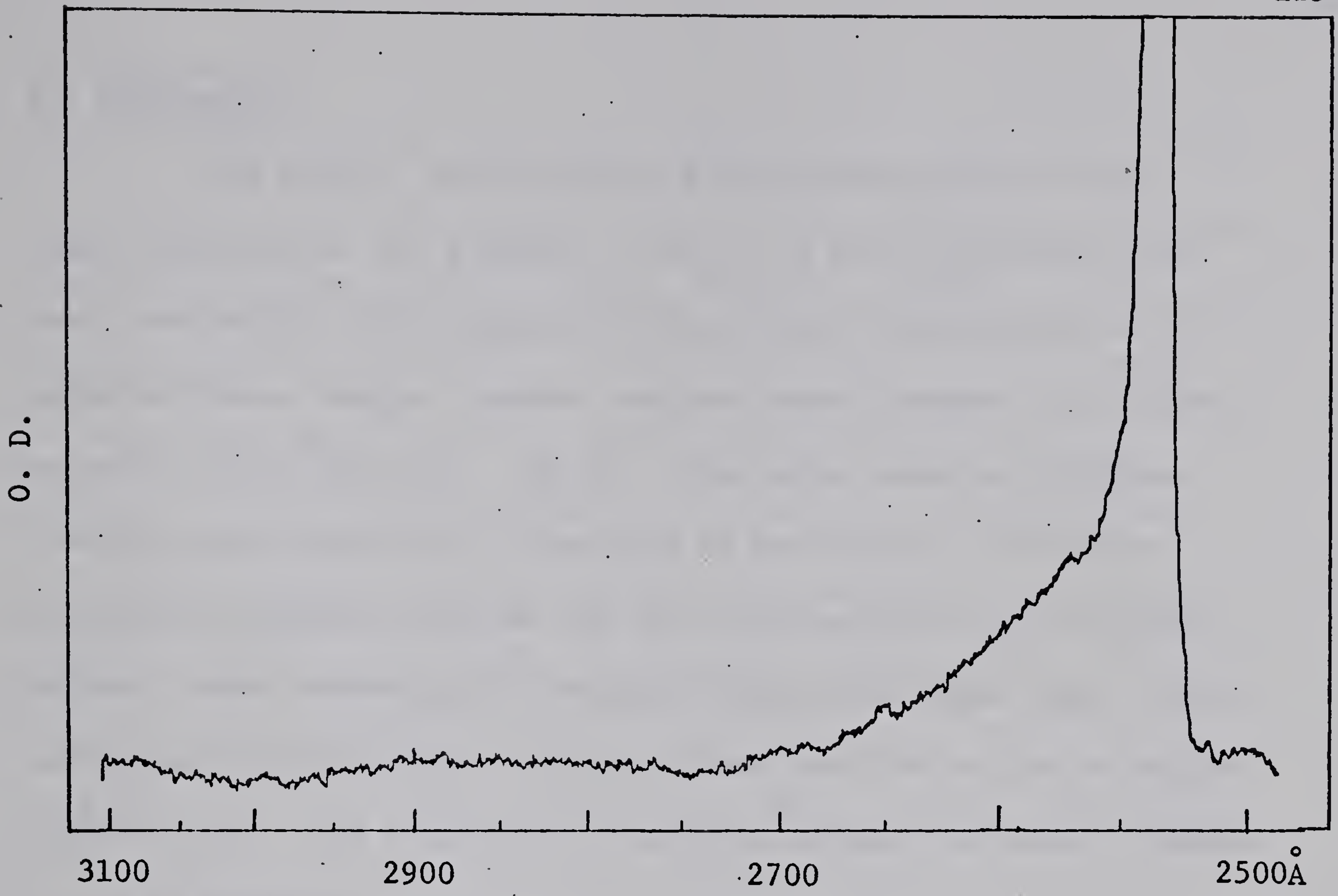

FIGURE 47: Fluorescence spectra: 310 torr CH_2F_2, 15 min, 0.4 O.D.

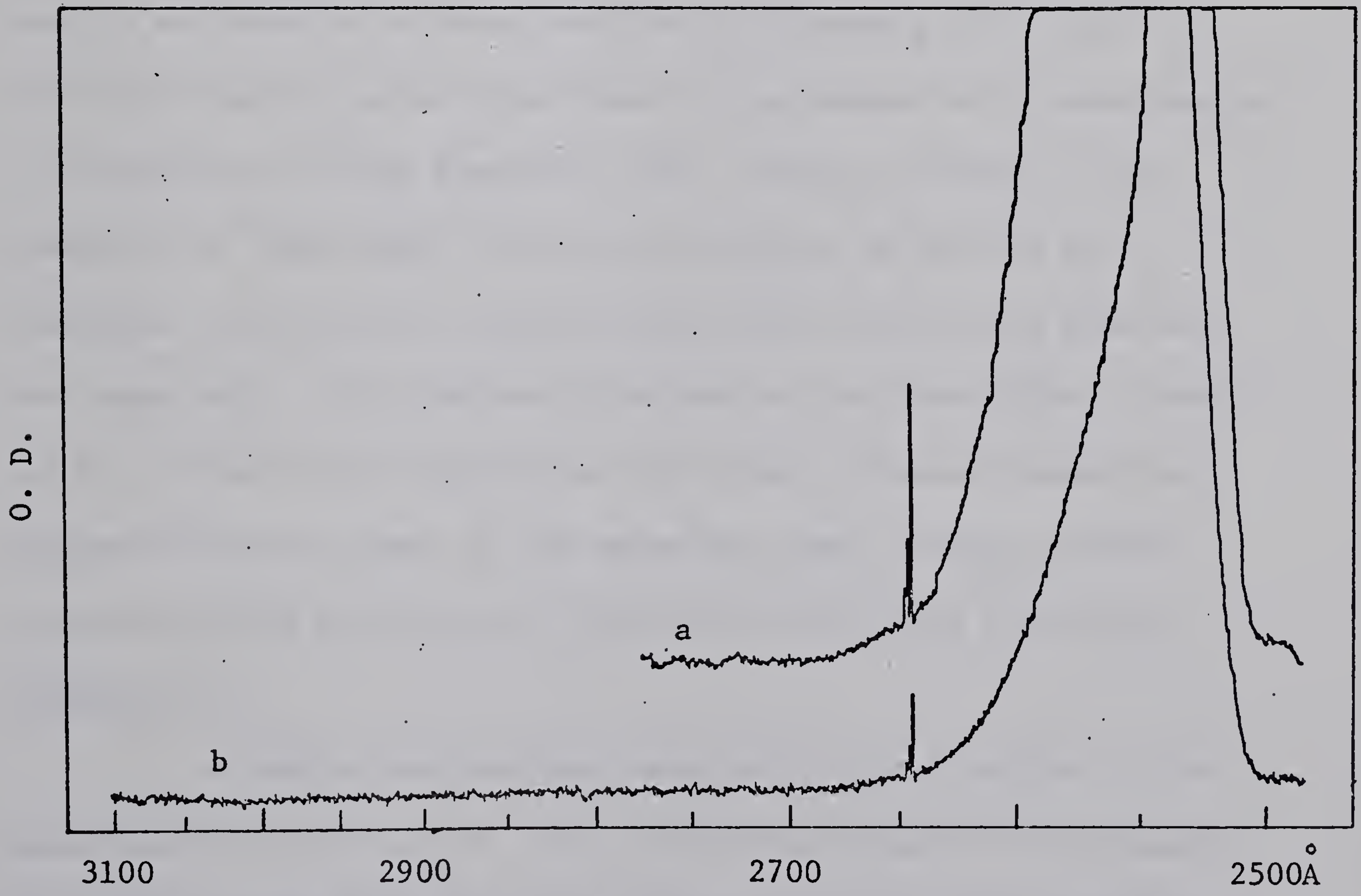

FIGURE 48: 280 torr CHF_3, 15 min; a, 0.4 O.D.; b, 0.8 O.D.

[illegible]

[illegible]

2. Discussion

The single, structureless fluorescence bands in the *c* region observed in the presence of NH_3, H_2O and C_2H_5OH have also been reported by other workers (49,50,70) and were attributed to emission from a charge transfer complex formed between a substrate molecule and an Hg° atom. The Hg° atoms were shown to originate from the rapid spin-orbit relaxation of Hg* atoms. The excited mercury-CO emission spectrum has not been observed in this region before. Since vibrationally excited CO has been found under similar conditions (83,84), the structureless band observed in the uv region indicates that some emission is occurring during the energy transfer to the CO molecule.

The *a* region bands observed in the presence of Ar, Kr and Xe are similar to those observed by Oldenberg (65) with the exception that Kr gives three bands, in agreement with measurements in absorption at high densities (63). Since no change in the position of these bands was observed between 10 and 800 torr, multiple interactions of mercury with more than one gas atom are not important. The structural features of the red-shifted *b* bands in Ar, Kr and Xe are significant since they indicate transitions between discrete levels of the upper and lower states, probably associated with vibrational levels of van der Waals molecules (Appendix C).

A single band has been observed in the *b* region of the spectrum for Ar, Kr and Xe. The fluorescence band in the presence of xenon extends from the 2537Å resonance line to about 3000Å and

attains a separate maximum at 2690±10Å independent of pressure. Since the fluorescence band extends smoothly past 2656Å but changes drastically near the 2547Å line, it has been assigned to transitions from the (Xe-Hg)* potential surface. Freeman, McEwan, Claridge and Phillips (69) have reported a peak maxima for this band at 2740Å and attributed it to emission from the (Xe-Hg)° surface. This assignment does not seem reasonable on energetic grounds because band emission from a (Xe-Hg)° complex would require up to 5 kcal/mole additional energy to be supplied from translational modes. It is very unlikely that thermal energy is sufficient to account for this *b* region band. It is also apparent that the technique used by them was not sensitive enough to detect the band fluorescence in the presence of argon or krypton.

The shift in the maxima to shorter wavelengths at low pressures of neopentane or isobutane indicates some pressure stabilization of the complex. Thus the lifetime of the complex must be greater than the collision frequency ($\tau > 10^{-9}$ sec). Determination of the interaction energy for the mercury paraffin complex from the shift in peak wavelength is not possible however, because of the proximity of the resonance line. The isobutane peak disappears at the lower pressures.

The band fluorescence associated with the mercury resonance line in the presence of the rare gases and paraffins can be compared with bands observed in the absorption spectra of the alkali metals Ne, Rb and Cs in the presence of paraffins and rare gases (62). In the case of alkali metals, the violet bands appear several hundred

wavenumbers from the resonance line, while the red bands are shifted only some 20 to 90 cm^{-1} away. The red band maxima were separated from the spectral line only for the heavier foreign gases, such as xenon, krypton and saturated hydrocarbon vapors heavier than propane. The shifts in the spectra with molecular weight and polarizability were believed to originate from van der Waals interactions in both the ground and excited states. Except for the absolute magnitudes of the band positions the trends observed in the mercury system are similar to these. Consequently it is reasonable to assume that van der Waals forces play an important role in the mercury band fluorescence as well.

Of fundamental importance to emission and absorption processes is the Franck-Condon principle (141) which, stated simply, means that the electron jump in a molecule takes place so rapidly in comparison to the motion of the nuclei that in the final state the nuclei still have very nearly the same relative position and velocity. Consequently transitions between two levels occur vertically with no change in position of the nuclei. The energy of light absorbed or emitted is then given by the vertical separation between the two levels at that particular internuclear distance.

The exact position and shape of the upper and lower potential surfaces, the vibrational and rotational energy of the upper state, and the oscillator strength of the transition will determine the shape and intensity of the emission bands. In order to understand the existence of fluorescence bands and the trends observed in the various series of gases, the parameters affecting

the potential surfaces must be examined in detail. Herzberg (142) has discussed the effect of various shapes of potential surfaces on the observed emission spectra of diatomic molecules and showed that continuous spectra are expected on both the long and short wavelength sides of the resonance line when weakly bonding van der Waals molecules are present. In general, the band fluorescence in the presence of the rare gases, paraffins, fluoromethanes and SF_6 fall into this category. Fluorescence in these systems appear as structureless bands directly associated with the 2537Å resonance line. Consequently the existence of van der Waals forces or polarization binding should be examined in more detail in these systems.

Gunning, Penzes, Sandhu and Strausz (68) have computed simple Lennard-Jones potential energy curves for the interaction of ground and excited states of mercury with Xe, Kr and Ar assuming only polarization binding between the two species. Their results are shown in Table XX. In every case, the depth of the excited potential surface was computed to be considerably larger than the ground state surface and thus transitions between these surfaces should lead to longer wavelength emission than the resonance line. The same type of calculation has been carried out for paraffins (Appendix C) and the results are given in Table XXIV. Again the depth of the well for the (RH-Hg)* interaction increases with increasing molecular weight in the range of 2 to 5 kcal/mole, while that of the ground state is only in the range of 0.5 to 1 kcal/mole. These calculations adequately explain the observed trends in the long wavelength band fluorescence spectra. It is also very important to the interpretation

TABLE XX

Calculated Values of Lennard-Jones Force Constants of Mercury-Rare Gas Pairs[a]

Collision Pair	σ Å	$\varepsilon(^1S_0)$ kcal/mole	$\varepsilon^*(^3P_0)$ kcal/mole	$\varepsilon^*(^3P_1)$ kcal/mole
Hg-Xe	3.4990[b]	0.861	1.179	2.294
Hg-Kr	3.2525[b]	0.757	1.016	1.975
Hg-Ar	3.1515[b]	0.634	0.838	1.627
Hg-Xe	3.4990[c]	0.861	2.219	4.317
Hg-Kr	3.2525[c]	0.757	1.911	3.717
Hg-Ar	3.1515[c]	0.634	1.577	3.062

Atom	σ Å[d]	ε kcal/mole[d]	α $Å^3$[e]	IP ev[f]
Xe	4.10	.439	4.0	12.08
Kr	3.607	.340	2.48	13.93
Ar	3.405	.239	1.63	15.68

[a] From reference (68).

[b] σ^* assumed equal to σ(ground).

[c] σ^* assumed 10% less than σ(ground).

[d] Reference (143)

[e] Reference (144)

[f] Reference (145)

of the observed radical yield ratio in the mercury photosensitization of propane.

The transitions occurring between two van der Waals molecules can be represented schematically in Figure 49. At very large internuclear separation (between points A and B) only the resonance line is observed. At intermediate distances along the attractive portion of the surface (C-D) transitions give rise to emission of light in the *b* region. At the repulsive turning point, emission (H-G) occurs with increased energy corresponding to the *a* region. The definite trend in the band maxima with increasing molecular weight, in both the rare gases and the paraffin systems, can be readily visualized in these terms. Considering only the *b* region first, a slight broadening of the line is observed with methane and the lighter rare gases. As the quencher size increases (increasing polarizability) the band shifts to longer wavelengths and ultimately reaches a point (Xe and paraffins higher than propane) where the band attains a separate maximum. This can be visualized as a deepening of the excited potential well (F) more than the ground state potential (E in Figure 49). The *b* region maxima for the rare gases and paraffins follow the same trend. Increasing polarizability is associated with a shift of the bands closer to the resonance line and can be attributed to a deeper minimum in the upper surface in the region of the H-G transition. Since the band maxima of SF_6 and CF_4 are the same, the repulsive portions of these potential surfaces seems to be less influenced by the overall polarizability of the molecule.

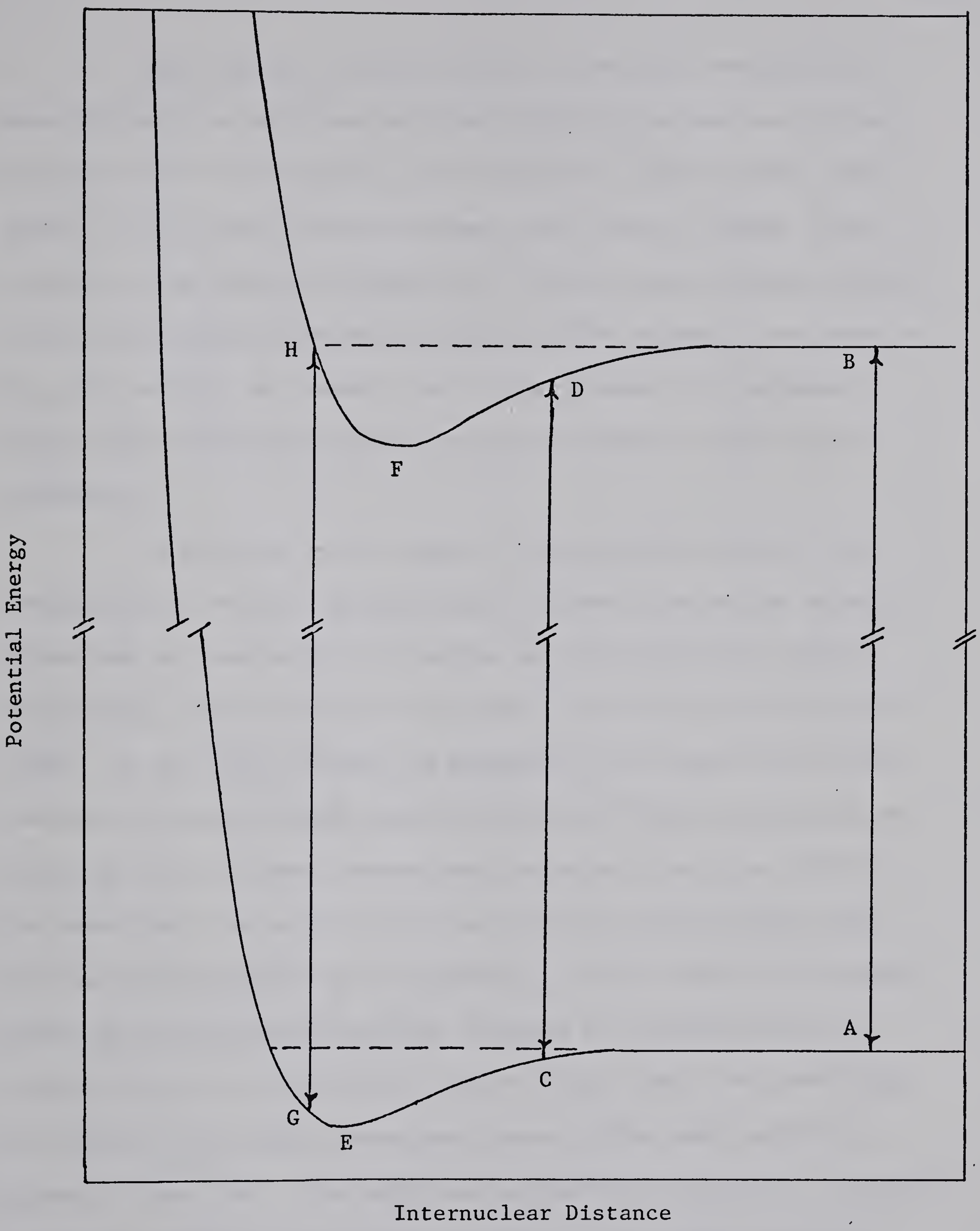
Potential Energy
Internuclear Distance
H
B
D
F
A
C
G
E

FIGURE 49: Schematic potential energy diagram for the optical transitions between the van der Waals molecules (Hg*-X) and (Hg-X) ground state.

Band spectra obtained with the fluorinated methanes are more difficult to correlate with their physical properties, listed in Table XXI. For compounds with no permanent dipole moment, the shift of the a band from the resonance line does not appear to be related to the total polarizability. The fact that the band spectra from the partially fluorinated methanes differ markedly from those of CH_4, CF_4 and SF_6, is probably due to the presence of a permanent dipole since the dipole-dipole interactions occur at much larger distances.

In addition to the shape of the potential surface, the probability of emission originating at various internuclear separations must be considered. In bonding molecules there are several vibrational levels between the zero point level and the dissociation limit. In the higher levels the probability of finding the molecule near the classical turning points is high and therefore transitions normally occur at these internuclear distances. Mulliken (145-147) has shown that the turning points are not the only positions which give a maximum probability of emission. For the simplified situation where the upper potential surface is given by a parabola and the lower surface by a Lennard-Jones curve (Figure 50a), the probability of emission from a high vibrational level of the upper surface is given by Figure 50b. The additional probability maximum as a function of ν arises from emission near the centre of the upper electronic state where the kinetic energy is a maximum. If the present system is considered analoges to the one discussed by Mulliken and the emission lifetime of the complex is assumed to be near the collision

TABLE XXI

Physical Parameters of Some Fluorinated Compounds

Cpd.	Hg* Quenching Cross Section[a] Å	Dipole Moment[c] $\mu \times 10^{18}$ esu	Polarizability[d] α, Å^3	I.P.[e] ev	L-J Force Constants[h]		ε^*[i] kcal/mole
					σ Å	ε kcal/mole	
SF_6	very small	0.0	$\sim$4.5[g]	19.3	5.128	0.441	2.18
CF_4	very small	0.0	2.85[c]	17.8	4.662	0.262	1.71
CHF_3	0.0094	1.59	2.80[c]	13.84[f]	4.33	0.477	2.37
CH_2F_2	-	1.97	2.73[c]	12.55[f]	4.08	0.632	2.76
CH_3F	$\sim 2\times10^{-5}$ [b]	1.85	2.63	12.80[f]	3.73	0.662	2.82
CH_4	0.115	0.0	2.6	12.95[f]	3.758	0.295	1.88

[a] Reference (1).

[b] Reference (154).

[c] Reference (155).

[d] Reference (144), p. 509.

[e] Reference (144), p. 360.

[f] Reference (156).

[g] Estimated from electron polarization in reference (144), p. 509.

[h] Lennard-Jones Force Constants from reference (152).

[i] Interaction energy between $Hg(^3P_1)$ and the molecule calculated by the method described in Appendix C and assuming σ(excited) = σ(ground).

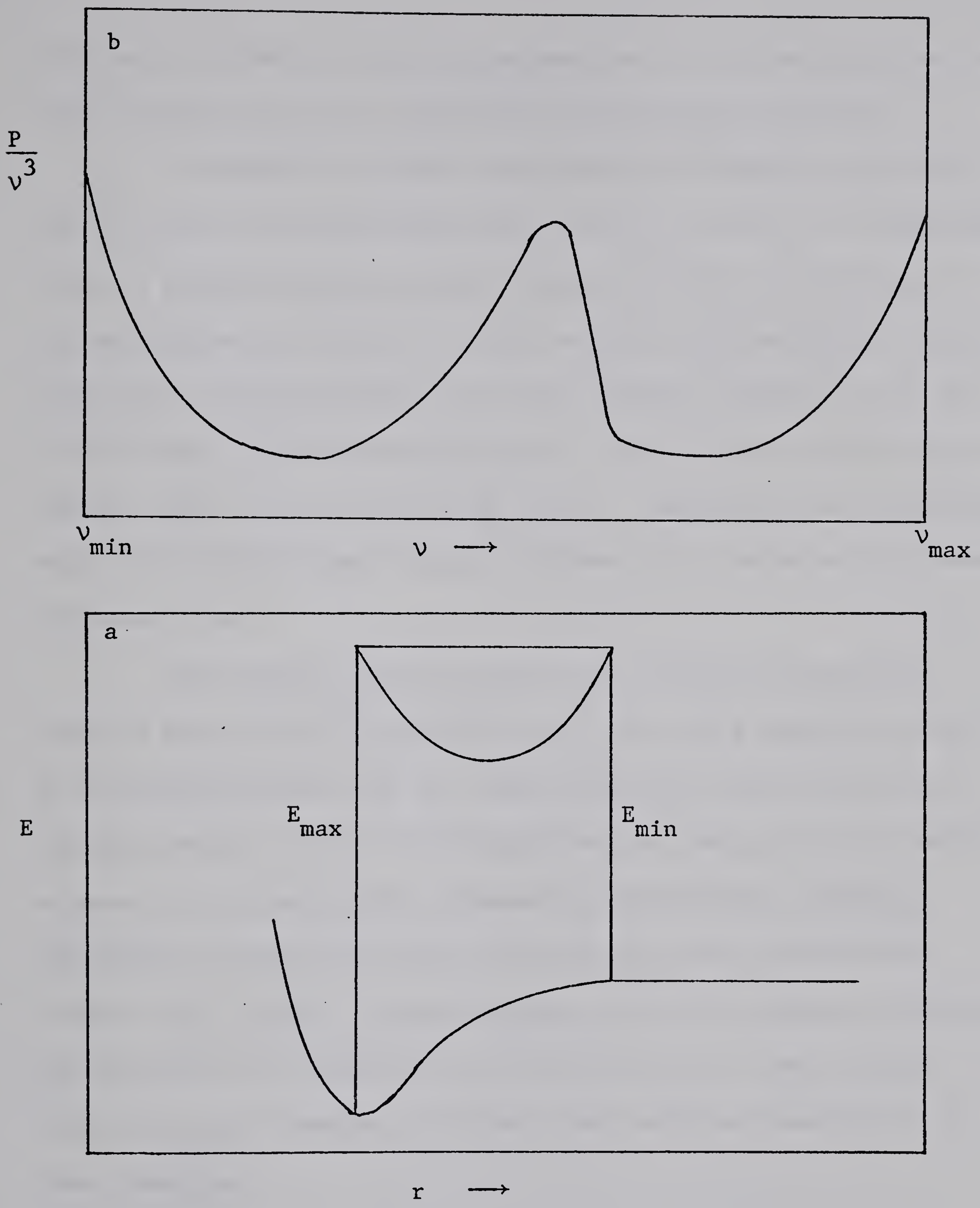
b
P/ν³
ν min
ν →
ν max
a
E
E max
E min
r →

FIGURE 50: Schematic potential surfaces representing emission from a high vibrational level (a) and the accompanying emission probability (b) assuming the oscillator strength of the transition does not change with r.

frequency, the emission spectra can have one or more intensity maxima near the resonance line, consistent with the present studies.

In addition to these considerations, it must be noted that the $^3P_1$ state of mercury splits into its $M_J = 0$ and $M_J = \pm 1$ components during a collision with an atom or molecule (148). At close internuclear approaches, the $M_J = 0$ state combines with the Hg($^3P_0$) state. Thus there are three separate potential surfaces involved, each with its own shape and emission probability. Two of these correlate with the Hg* level and one with the Hg° level. Consequently the possibility exists for more than one intensity maximum due to emission from these different levels.

The present study has shown that the band fluorescence observed near the 2537Å resonance line (the *a* and *b* regions) are due to transitions between van der Waals molecules formed between Hg* and the quencher. This is different from the charge transfer complex between Hg° and the quencher proposed by Phillips and coworkers (49,50,70) to explain the band fluorescence at much larger wavelengths (the *c* region). More extensive work on the emission lifetime and the effects of temperature and pressure on the *a* and *b* region bands is required however, to allow a more detailed description of these complexes.

CHAPTER VII

THE MERCURY PHOTOSENSITIZATION OF PARAFFINS; SUMMARY AND CONCLUSIONS

The Hg° and Hg* sensitization reactions of propane have been examined in detail. Both these atoms decompose propane producing *n*-propyl and isopropyl radicals:

$$Hg^* + C_3H_8 \longrightarrow (HgC_3H_8)^* \qquad [25]$$

$$(HgC_3H_8)^* \longrightarrow i\text{-Pr} + H + Hg \qquad [26]$$

$$\longrightarrow n\text{-Pr} + H + Hg \qquad [27]$$

$$Hg^\circ + C_3H_8 \longrightarrow (HgC_3H_8)^\circ \qquad [30]$$

$$(HgC_3H_8)^\circ \longrightarrow i\text{-Pr} + H + Hg \qquad [31]$$

$$\longrightarrow n\text{-Pr} + H + Hg \qquad [32]$$

The following rate constant ratios have been determined in the 0° to 200°C range:

$$k_{27}/k_{26} = 0.89 \exp(-1.25\text{x}10^3/RT)$$

and

$$k_{32}/k_{31} = 0.78 \exp(-1.90\text{x}10^3/RT)$$

At room temperature the relative *n*-propyl to isopropyl yields are about 1:31 for the Hg° atom reaction and 1:9 for the Hg* reaction. A value of 1:1 has been reported for the $Hg6(^1P_1)$ reaction with propane (117). These results substantiate the suggestion that the enthalpy change of the reaction is the main criterion of reactivity

of excited mercury atoms towards various C-H bonds (76,117). The temperature dependence of the *n*-propyl to isopropyl ratio indicates that a potential barrier exists along the reaction path, the height of which will depend upon the polarizability and the C-H bond strength of the paraffin as well as the electronic energy of the excited mercury atom.

Large values of H/D kinetic isotope effects have been observed for the H-atom transfer reactions of alkyl radicals (121). These reactions are considered to proceed through a three centre transition state

$$RH + R' \longrightarrow R\cdots\cdot H\cdots\cdot R' \longrightarrow R + HR'$$

in which the formation of the new bond compensates for the breaking of the old bond. An empirical bond-energy-bond-order (BEBO) method developed by Johnston (120) predicts activation energies and kinetic isotope effects for these reactions in agreement with experiment. For example, the predicted potential energies of activation of 9 and 10 kcal/mole for the reactions [50] and [51]

$$CH_3 + C_3H_8 \longrightarrow i\text{-Pr} + CH \qquad [50]$$

$$\longrightarrow n\text{-Pr} + CH_4 \qquad [51]$$

are in reasonable agreement with the experimental values of 10.2 and 11.6 kcal/mole, respectively (120).

The observed cross sections for the quenching of Hg* atoms by hydrogen and olefins are much larger than those of the paraffins (76). However, H/D kinetic isotope effects are larger for the latter than the former. These differences in behaviour have been explained

in terms of the primary interaction site of the Hg* with the substrate. The interaction of Hg* with the π electrons of ethylene and the σ electrons of hydrogen leads to a large quenching cross section value (102,124,151) but excited mercury atoms appear to react with paraffins through a transition state analogous to abstraction reactions,

$$R\cdots H\cdot\,.\,.\,\cdot Hg^*$$

resulting in small quenching cross sections and large H/D isotope values (76).

We have applied the BEBO method to the mercury photosensitized decomposition of paraffins assuming that the electronically excited atoms behave analogously to alkyl radicals. A similar approach has been successfully used to predict the activation energies of ground state triplet and excited singlet oxygen atom reactions with hydrocarbons (149). In order to apply the BEBO method, the paraffins are considered as diatoms, R-H, and the excited metal atom as the abstracting species with a final bond energy of the metal hydride equal to the electronic excitation energy plus the heat of formation of the M-H bond. Potential energies of activation have been calculated for the reactions of the triplet and singlet excited levels of mercury, cadmium, and zinc with the various C-H bonds in paraffins. The details of the computations are given in Appendix D and the results are listed in Tables XXVI and XXVII. Since there are no experimental quantities available with which to compare these values, the absolute numbers must be viewed with caution. Only the differences between the values are meaningful and can be compared

with the present experimental results. The calculations predict the experimentally observed trends in the Hg° and Hg* sensitization of propane. The potential energy of activation for the production of *n*-propyl radicals is predicted to be larger than that for the isopropyl radical by about 1.05 kcal/mole for the Hg° atom reaction, 0.90 for the Hg* atom reaction, and only 0.35 for the Hg' reaction. In addition, these values should be considered as lower limits since the triplet repulsion term has been neglected in the computations.

Various other theoretical approaches have been advanced to explain the experimental results of the energy transfer in mercury photosensitization. Yang (16,100) explained the difference in reactivity between Hg* and Hg° atoms with hydrogen and paraffins in terms of symmetry arguments. He approximated hydrocarbons as diatoms, and considered the total angular momentum quantum number to represent the mercury atom. The products of the reactions were taken to be HgH and H or R depending upon the substrate used. By assigning C_s symmetry to the (R-H-Hg)* complex, he came to the conclusion that the quenching of metastable atoms to the ground state is allowed if R has p character; in the quenching by H_2, H can only be in the s state, and consequently this transition is forbidden. The quenching of Hg* is allowed, regardless of the state of R. The recently observed Hg° quenching cross sections (127) together with the present experimental results create serious doubts about this explanation, however.

Vikis and Moser (119) investigated the quenching of excited mercury atoms by alkanes using the RRKM theory of unimolecular

reactions. The theoretical model was based on the formation of a relatively long lived complex (RH-Hg)* on a potential energy surface leading to the quenching of excited Hg atoms primarily by C-HHg bond rupture. In order to obtain quantitative predictions, the authors were forced to make numerous assumptions about the nature of the complex. The same surface, correlating with $Hg^{+}H^{-} + R$, was assumed to be common to all the excited mercury states. The minimum of this surface was assumed to be about 85 kcal/mole above the ground state. The agreement of the quenching cross sections with experiment (58) appears to be fortuitous however, since the proposal that both the Hg° and Hg* levels combine to form a single complex with the paraffin is not compatible with the present observations. If crossover to the decomposition surfaces occurred from a single surface for both Hg° and Hg* + C_3H_8 reactions, no difference would be expected between the activation energies for the production of *n*-propyl and isopropyl radicals, ΔE° and ΔE*. Since ΔE° = 1.90 and ΔE* = 1.25 kcal/mole, the reaction surfaces must remain separate up to the point where decomposition crossover occurred.

Band fluorescence has been observed experimentally during the mercury photosensitization of every paraffin studied. These bands have been assigned to transitions from a weakly bonding van der Waals molecule formed between an excited mercury atom and a paraffin molecule. Lennard-Jones force constants calculated from the polarizabilities and ionization potentials of the species involved, predict the trends observed in the band fluorescence of the mercury-paraffin complexes. A much deeper potential well is

expected for the excited state than the ground state (Table XXIV): for example, the interaction energy of the $(HgC_3H_8)^*$ complex was calculated to be between 2.5 and 5 kcal/mole depending upon the internuclear distance assumed.

If we make the reasonable assumption that the mercury-propane complex observed in the band fluorescence measurements is the same as that involved in the photosensitized decomposition studies, we can combine both these studies together with the theoretical calculations to develop a detailed description of the nature of the mercury photosensitization of paraffins. The excited mercury-propane potential energy surface will be described in detail because of its relation to the present work.

The various processes occurring in the mercury photosensitization of propane are compatible with the potential energy diagram given in Figure 51. The excited mercury atom, Hg*, approaches the propane molecule on an attractive surface with a binding energy ε^* proportional to the polarizability of the two species. The Hg* level splits into two separate states, designated as $\Omega = 0$ and $\Omega = \pm 1$, under the perturbing influence of the paraffin (93) considered as an atom. At closer approaches the system can cross to a decomposition surface giving either isopropyl or *n*-propyl radicals. The difference between these two crossing points, ΔE^*, is about 1.25 kcal/mole (Chapter IV). In addition, the $(HgC_3H_8)^*$ surface with $\Omega = \pm 1$ and the $(HgC_3H_8)^\circ$ surface collapse together allowing spin-orbit relaxation of the Hg* atom. The upper $(HgC_3H_8)^*$ surface with $\Omega = 0$ does not correlate with the $^3P_0$ level and

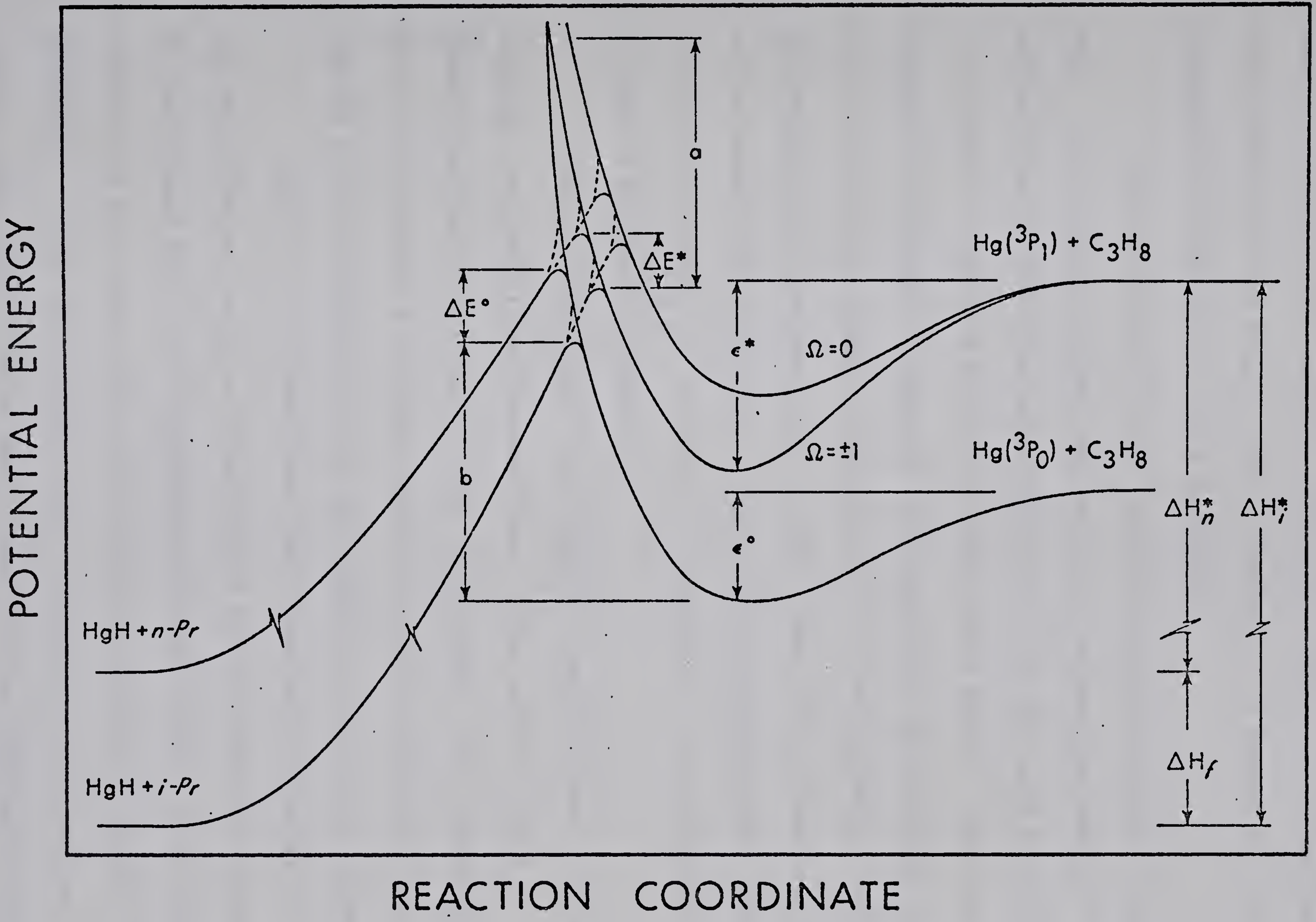
POTENTIAL ENERGY
REACTION COORDINATE
a
ΔE^*
ΔE°
b
$Hg(^3P_1) + C_3H_8$
ϵ^*
$\Omega=0$
$\Omega=\pm1$
$Hg(^3P_0) + C_3H_8$
ϵ°
ΔH_n^*
ΔH_i^*
ΔH_f
HgH + n-Pr
HgH + i-Pr

FIGURE 51: Potential energy diagram for excited mercury-propane system, considering propane as a single mass point with $J = 0$.

therefore spin-orbit relaxation cannot occur via this state (93). From the quantum yield studies, the energy difference between spin-orbit relaxation and decomposition crossing, *a* in Figure 51, is estimated to be between 3 and 6 kcal/mole.

The collision of an Hg° atom with propane follows a similar path. The initially formed complex has an interaction energy ε° smaller than ε^* since the polarizability of the Hg° atom is assumed to be smaller than that of the Hg* atom (Table XXIV). Upon closer approach, crossover to isopropyl or *n*-propyl and HgH surfaces occurs with an activation energy difference ΔE° of 1.90 kcal/mole. Since the decomposition quantum yield for Hg° atoms, Φ°, is less than unity and increases with temperature, the height of decomposition crossover above the $(HgC_3H_8)^\circ$ complex, *b* in Figure 51, is estimated to be about 6 kcal/mole (Chapter V).

Both the $(HgC_3H_8)^*$ and $(HgC_3H_8)^\circ$ complexes have a finite lifetime and transitions between these states and the (HgC_3H_8) ground state will give rise to band fluorescence. The intensity of the fluorescence will depend upon the optical selection rules and the rate of decomposition of the complex through other channels.

Use of the Lennard-Jones force constants (Appendix C) and the potential energies of activation for decomposition (Appendix D), calculated from the bond-energy-bond-order method, yield useful information about the interaction of excited mercury atoms with other paraffins. It can be predicted that the interaction of excited mercury atoms with isobutane would result in two important changes in the shape of the potential diagram, Figure 51. Both ε^* and ε°

would increase since the polarizability of isobutane is expected to be larger than that of propane and would give rise to a shift in the emission spectra observed with propane and isobutane. Since the bond energy of the tertiary C-H bond is 91 kcal/mole, and that of $(CH_3)_2CHCH_2$-H is 98 kcal/mole, the crossover to *t*-butyl radicals would occur at lower energies than the crossing to isopropyl radicals. Consequently, larger activation energy differences would be expected for the production of isobutyl compared to *t*-butyl radicals for both Hg° and Hg* reactions, $\Delta E^{\circ}_{i\text{-But}}$ and $\Delta E^{*}_{i\text{-But}}$, than those observed in the decomposition of propane. In addition, the difference $\Delta E^{\circ}_{i\text{-But}} - \Delta E^{*}_{i\text{-But}}$ is expected to be greater than that for propane, $\Delta E^{\circ}_{Pr} - \Delta E^{*}_{Pr}$.

The same rationale can also explain the less than unit quantum yield of decomposition observed in the mercury photosensitization of methane (110). Since the polarizability of methane is small and the H_3C-H bond energy is large, Φ^* will be small, and the crossing to decomposition will occur well above the level of separated Hg* + CH_4. The quenching cross section and decomposition quantum yield of methane should be low at room temperature and increase with temperature, which is consistent with experiment. The C-H bond energy in neopentane is 99 kcal/mole and the value of ε^* will be larger compared to CH_4. In this case the crossover to decomposition would occur at about the same energy as that of the separated Hg* + C_5H_{12} level. The depth of the excited complex would allow emission to compete with the decomposition reactions.

The large H/D kinetic isotope effects observed in the photosensitization of paraffins can also be interpreted in terms of

Figure 51. It is known that substituting a D-atom for the H-atom being abstracted by an alkyl radical increases the activation energy of the process (120). This increase has been explained by a difference in zero point energies rather than a change in the shape of the potential surface. For the Hg* interaction with R-D, the activation energy for decomposition will increase but the spin-orbit relaxation of the Hg* level will be unchanged because it does not directly involve a C-D bond. Therefore the amount of Hg° formation will increase relative to the decomposition reaction, and the overall quenching cross section of paraffins would decrease upon deuterium substitution. The activation energy of the Hg° + R-D reaction will also increase, resulting in a lower rate of reaction relative to its rate with light paraffins.

The lifetime of the excited complex is given by

$$\tau = (k_r + k_d + k_s + k_f)^{-1}$$

where k_r is the rate constant for dissociation back to Hg* + RH, k_d is the rate constant for decomposition of the paraffin, k_s is the rate constant for spin-orbit relaxation, and k_f is the rate constant for band fluorescence. A crude estimation of the lifetime of the $(HgC_3H_8)^*$ complex can be obtained from the simple Kassel equation (150)

$$k = A\left(\frac{E_T - E_a}{E_T}\right)^{S-1}$$

where A is the frequency factor $\sim 10^{13}$ $\sec^{-1}$. The activation energy of dissociation, E_a, is taken to be the interaction energy of the

complex, ε^*, about 5 kcal/mole for propane. The total energy of the complex, E_T, is E_a plus the thermal energy of propane which is about 2 kcal/mole at room temperature. Values ranging between 1/3 and 2/3 times the total number of oscillators have been used in the literature for the evaluation of the Kassel equation (150). With

$$s = 1/3\ (3N-6)$$

the rate constant of dissociation is

$$k \approx 10^{13}\left(\frac{7-5}{5}\right)^{9} \approx 10^{8}\ \mathrm{sec}^{-1}.$$

Thus the lifetime of the complex is about 1×10^{-8} sec.

BIBLIOGRAPHY

1. J. G. Calvert and J. N. Pitts, "*Photochemistry*", John Wiley and Sons, 1966, Ch. II.
2. R. J. Cvetanović, *Prog. in Rxn. Kin.*, 2, 39 (1964).
3. H. E. Gunning and O. P. Strausz, *Adv. in Photochem.*, 1, 209 (1963).
4. M. C. Bigeon, *J. Physique*, 28, 51 (1967).
5. J. V. Michael and C. Yeh, *J. Chem. Phys.*, 53, 59 (1970).
6. J. A. Aubrecht, B. M. Whitcom, R. A. Anderson and R. C. Pickett, *J. Opt. Soc. Amer.*, 58, 196 (1968).
7. A. Lurio, *Phys. Rev.*, 140, A1505 (1965).
8. A. J. Yarwood, O. P. Strausz and H. E. Gunning, *J. Chem. Phys.*, 41, 1705 (1964).
9. T. Holstein, *Phys. Rev.*, 72, 1212 (1947); 83, 1159 (1951).
10. A. C. G. Mitchell and M. W. Zemansky, "*Resonance Radiation and Excited Atoms*", The Macmillan Company, New York, 1934.
11. E. W. Samson, *Phys. Rev.*, 40, 940 (1932).
12. L. M. Biberman, *Zh. Eksperim. i Theor. Fiz.*, 17, 416 (1947).
13. M. W. Zemansky, *Phys. Rev.*, 36, 919 (1930).
14. K. Yang, *J. Am. Chem. Soc.*, 88, 4575 (1966).
15. K. Yang, *J. Am. Chem. Soc.*, 87, 5294 (1965).
16. K. Yang, *J. Am. Chem. Soc.*, 89, 5344 (1967).
17. B. V. Waddell and G. S. Hurst, *J. Chem. Phys.*, 53, 3892 (1970).
18. M. G. Bellas, Y. Rousseau, O. P. Strausz and H. E. Gunning, *J. Chem. Phys.*, 41, 768 (1964).
19. A. Kato and R. J. Cvetanović, *Can. J. Chem.*, 45, 1845 (1967).

20. R. Payette, M. Bertrand and Y. Rousseau, *J. Am. Chem. Soc.*, 90 5341 (1968).

21. P. Pringsheim, "*Fluorescence and Phosphorescence*", Interscience Publishers, Inc., New York (1949), p. 224.

22. S. Mrowski, *Rev. Modern Phys.*, 16, 153 (1944).

23. T. Holstein, D. Albert and A. O. McCoubrey, *Phys. Rev.*, 76, 1259 (1949).

24. J. A. Berberet and K. C. Clark, *Phys. Rev.*, 100, 506 (1955).

25. R. W. Wood, *Proc. Roy. Soc.*, A106, 679 (1924).

26. E. Galviola and R. W. Wood, *Phil. Mag.*, 6, 1191 (1928).

27. M. L. Pool, *Phys. Rev.*, 38, 955 (1931).

28. G. H. Kimbell and D. J. LeRoy, *Can. J. Chem.*, 40, 1229 (1962).

29. T. Asada, R. Ladenburg and W. Tictzo, *Zeits. Phys.*, 29, 549 (1928).

30. I. Asyrbichanu, I. Kukurezyanu, V. Vasiliu and I. Popesku, *Optics and Spectra*, 11, 155 (1961).

31. J. H. Couliette, *Phys. Rev.*, 32, 636 (1928).

32. B. deB. Darwent and F. G. Hurtubise, *J. Chem. Phys.*, 20, 1684 (1952).

33. M. D. Scheer and J. Fine, *J. Chem. Phys.*, 36, 1264 (1962).

34. V. K. Bykhovskii and E. E. Nikitin, *Opt. Spectry.*, 16, 111 (1964).

35. A. B. Callear and R. G. W. Norrish, *Proc. Roy. Soc.*, A259, 304 (1960).

36. N. Basco, A. B. Callear and R. G. W. Norrish, *Proc. Roy. Soc.*, A260, 459 (1961).

37. A. B. Callear and R. G. W. Norrish, *Proc. Roy. Soc.*, A266, 299 (1962).

38. A. B. Callear and G. J. Williams, *Trans. Faraday Soc.*, 60, 2158 (1964).

39. A. B. Callear, *Appl. Opt. Suppl.*, 2, 145 (1965).

40. S. Penzes, A. J. Yarwood, O. P. Strausz and H. E. Gunning, *J. Chem. Phys.*, 43, 4524 (1965).

41. A. B. Callear and R. E. M. Hedges, *Trans. Faraday Soc.*, 66, 605 (1970).

42. A. B. Callear and R. E. M. Hedges, *Nature*, 218, 163 (1968).

43. A. B. Callear and R. E. M. Hedges, *Trans. Faraday Soc.*, 66, 615 (1970).

44. A. B. Callear and J. McGurk, *Chem. Phys. Letters*, 7, 491 (1970)

45. A. B. Callear and J. C. McGurk, *Chem. Phys. Letters*, 6, 417 (1970).

46. A. B. Callear and J. C. McGurk, *Nature*, 266, 844 (1970).

47. A. C. Vikis, G. Torrie and D. J. LeRoy, *Can. J. Chem.*, 48, 3771 (1970).

48. H. Horiguchi and S. Tsuchiya, *Bul. Chem. Soc. Japan*, 44, 1213 (1971).

49. R. H. Newman, C. G. Freeman, M. J. McEwan, R. F. C. Claridge and L. F. Phillips, *Trans. Faraday Soc.*, 66, 2827 (1970).

50. C. G. Freeman, M. J. McEwan, R. F. C. Claridge and L. F. Phillips, *Trans. Faraday Soc.*, 66, 2974 (1970); 67, 2004 (1971).

51. G. London, A. C. Vikis and D. J. LeRoy, *Can. J. Chem.*, 48, 1420 (1970).

52. W. Opechowski, *Zeits. f. Physik.*, 109, 485 (1938).

53. M. C. Bigeon, *J. Phys. (Paris)*, 28, 157 (1967).

54. M. C. Bigeon and J. L. Cajan, *Compt. Rend.*, 260, 6565 (1965).

55. B. Stevens, "*Collisional Activation in Gases*", Pergamon Press Ltd., London, 1967.

56. D. R. Herschback, *Adv. Chem. Phys.*, 10, 319 (1966).

57. A. C. Vikis and H. C. Moser, *J. Chem. Phys.*, 53, 1491 (1970).

58. J. M. Campbell, S. Penzes, H. S. Sandhu and O. P. Strausz, *Int. J. Chem. Kin.*, 3, 175 (1971).

59. S. Penzes, H. S. Sandhu and O. P. Strausz, submitted to *Int. J. Chem. Kin.*, (1971).

60. S. Penzes, *Ph.D. Thesis*, University of Alberta, 1968.

61. T. Foerster, *Angew. Chem. Int. Ed. Engl.*, 1969, 333 (1969).

62. S. Ch'en and M. Takeo, *Rev. Mod. Phys.*, 29, 20 (1957).

63. A. Michels, H. Dekluiver and C. A. Ten Selden, *Physica*, 25, 1321 (1959).

64. H. Kuhn and O. Oldenberg, *Phys. Rev.*, 41, 72 (1932).

65. O. Oldenberg, *Z. Physik.*, 47, 184 (1927); 49, 609 (1928); 50, 580 (1928); 51, 40, 605 (1928); 55, 1 (1929).

66. G. Glockler and F. W. Martin, *J. Chem. Phys.*, 2, 46 (1934).

67. S. Penzes, O. P. Strausz and H. E. Gunning, *J. Chem. Phys.*, 45, 2322 (1966).

68. H. E. Gunning, S. Penzes, H. S. Sandhu and O. P. Strausz, *J. Am. Chem. Soc.*, 91, 7684 (1969).

69. C. G. Freeman, M. J. McEwan, R. F. C. Claridge and L. F. Phillips, *Chem. Phys. Letters*, 6, 482 (1970).

70. C. G. Freeman, M. J. McEwan, R. F. C. Claridge and L. F. Phillips, *Chem. Phys. Letters*, 5, 555 (1970).

71. C. G. Freeman, M. J. McEwan, R. F. C. Claridge and L. F. Phillips, *Chem. Phys. Letters*, 8, 266 (1971).

72. C. G. Freeman, M. J. McEwan, R. F. C. Claridge and L. F. Phillips, *Chem. Phys. Letters*, 9, 578 (1971).

73. J. Koskikallio, A. B. Callear and J. H. Connor, *Chem. Phys. Letters*, 8, 467 (1971).

74. C. G. Freeman, M. J. McEwan, R. F. C. Claridge and L. F. Phillips, *Trans. Faraday Soc.*, 67, 67 (1971).

75. R. H. Newman, C. G. Freeman, M. J. McEwan, R. F. C. Claridge and L. F. Phillips, *Trans. Faraday Soc.*, 67, 1360 (1971).

76. Y. Rousseau, O. P. Strausz and H. E. Gunning, *J. Chem. Phys.*, 39, 962 (1963).

77. A. O. McCoubrey, *Phys. Rev.*, 93, 1249 (1954).

78. C. G. Matland, *Phys. Rev.*, 92, 637 (1953).

79. R. C. Tolman, "*Statistical Mechanics with Application to Physics and Chemistry*", The Chemical Catalog Co. Inc., New York, 1927, p. 67.

80. J. E. McAlduff and D. J. LeRoy, *Can. J. Chem.*, 43, 2279 (1965).

81. J. E. M Alduff, D. D. Drysdale, D. J. LeRoy, *Can. J. Chem.*, 46 199 (1968).

82. S. Penzes, H. E. Gunning and O. P. Strausz, *J. Chem. Phys.*, 47, 4869 (1967).

83. G. Karl, P. Kruus and J. C. Polanyi, *J. Chem., Phys.*, 46, 224 (1967).

84. G. Karl, P. Kruus, J. C. Polanyi and W. M. Smith, *J. Chem. Phys.*, 46, 244 (1967).

85. A. Jones and F. P. Lossing, *Can. J. Chem.*, 45, 1685 (1967).

86. A. Bjerre and E. E. Nikitin, *Chem. Phys. Letters*, 1, 179 (1967).

87. W. M. Preston, *Phys. Rev.*, 51, 298 (1936).

88. A. Jablonski, *Z. Physik.*, 70, 723 (1931).

89. L. O. Olson, *Phys. Rev.*, 60, 739 (1941).

90. H. Kuhn, *Proc. Roy. Soc.*, A158, 212 (1937).

91. O. Jefimenko, *J. Chem. Phys.*, 39, 2457 (1963).

92. Y. Leycuras, *J. Quant. Spectrosc. Radiat. Transfer*, 6, 131 (1966).

93. J. Fiutak and M. Frackowiak, *Bull. Acad. Polon. Sci., Ser. Sci., Math., Astron., Phys.*, 11, 175 (1963).

94. J. Szudy, *Acta. Phys. Polon.*, 29, 605 (1966).

95. G. A. Vesnicheva and N. P. Penkin, *Opt. Spect.*, 23, 453 (1967).

96. M. L. Sosinskii and E. N. Morozov, *Opt. Spect.*, 23, 475 (1967).

97. G. I. Zav'yalov, A. Y. Zav'yalova, N. A. Prilezhaeva, M. P. Belyaev, M. V. Gileva and V. S. Grudanov, *Isz. Vyssh. Ucheb. Zavod., Fiz.*, 11, 156 (1968).

98. J. A. Butchard, R. F. C. Claridge and L. F. Phillips, *Chem. Phys. Letters*, 8, 139 (1971).

99. S. N. Vinogradov and H. E. Gunning, *J. Phys. Chem.*, 68, 1962 (1964).

100. K. Yang, J. D. Paden and C. L. Hassell, *J. Chem. Phys.*, 47, 3824 (1967).

101. J. C. Light, *J. Chem. Phys.*, 40, 3221 (1964).

102. T. Pollock, E. Jakubowski, H. E. Gunning and O. P. Strausz, *Can. J. Chem.*, 47, 3474 (1969).

103. B. deB. Darwent, *J. Chem. Phys.*, 18, 1532 (1950).

104. Y. Rousseau and H. E. Gunning, *Can. J. Chem.*, 41, 465 (1963).

105. Y. Rousseau, G. N. C. Woodall and H. E. Gunning, *J. Chem. Phys.*, 37, 2722 (1962).

106. G. N. C. Woodall and H. E. Gunning, *Bull. Soc. Chim. Belg.*, 71, 725 (1962).

107. L. Melander, "*Isotope Effects on Reactions Rates*", Ronald Press Co., New York, 1960.

108. E. A. Milne, *J. London Math. Soc.*, 1, 1 (1926).

109. F. S. Larkin, *Can. J. Chem.*, 46, 1005 (1968).

110. R. A. Back and D. van der Auwera, *Can. J. Chem.*, 40, 2339 (1962).

111. E. W. R. Steacie, "*Atomic and Free Radical Reactions, Volume II*", Macmillan Co., New York, 1964.

112. M. M. Papic and K. J. Laidler, *Can. J. Chem.*, 49, 535; 549 (1971).

113. R. A. Holroyd and G. W. Klein, *J. Phys. Chem.*, 67, 2273 (1963).

114. J. P. Chesick, *J. Am. Chem. Soc.*, 86, 3597 (1964).

115. E. Jakubowski, P. Kebarle, O. P. Strausz and H. E. Gunning, *Can. J. Chem.*, 45, 2287 (1967).

116. P. Kebarle and M. Avrahami, *J. Chem. Phys.*, 38, 700 (1963).

117. R. A. Holroyd and T. E. Pierce, *J. Phys. Chem.*, 68, 1392 (1964).

118. S. Takumuku and R. A. Back, *Can. J. Chem.*, 42, 1426 (1964).

119. A. C. Vikis and H. C. Moser, *J. Chem. Phys.*, 53, 2333 (1970).

120. H. S. Johnston, "*Gas Phase Reaction Rate Theory*", Ronald Press Co., New York, 1966, p. 176.

121. A. F. Trotman-Dickenson, *Adv. Free Rad. Chem.*, I, 1 (1966).

122. K. Yang, *J. Phys. Chem.*, 67, 562 (1963).

123. K. Yang, *J. Am. Chem. Soc.*, 84, 719 (1962).

124. L. E. Reid and D. J. LeRoy, *Can. J. Chem.*, 46, 3275 (1968).

125. R. E. Berkley, G. N. C. Woodall, O. P. Strausz and H. E. Gunning, *Can. J. Chem.*, 47, 3305 (1969).

126. J. G. Calvert and J. N. Pitts, "*Photochemistry*", John Wiley and Sons, 1966, p. 640.

127. W. A. Noyes, Jr. and P. A. Leighton, "*The Photochemistry of Gases*", Reinhold Publishing Corp., New York, 1941, pp. 200-202.

128. T. Pollock, *Ph.D. Thesis*, University of Alberta (1971).

129. R. A. Back, *Can. J. Chem.*, 37, 1834 (1959).

130. J. O. Terry and J. H. Futrell, *Can. J. Chem.*, 45, 2327 (1967).

131. J. P. Chesick, *J. Am. Chem. Soc.*, 84, 2448 (1962).

132. K. W. Watkins and L. A. O'Deen, *J. Phys. Chem.*, 73, 4094 (1969).

133. E. L. Metcalfe and A. F. Trotman-Dickenson, *J. Chem. Soc.*, 4620 (1962).

134. K. Yang, *J. Am. Chem. Soc.*, 86, 3941 (1964).

135. F. S. Sutton, *J. Chem. Phys.*, 36, 2923 (1962).

136. G. Dixon-Lewis, M. M. Sutton and A. W. Williams, *Disc. Faraday Soc.*, 33, 205 (1962).

137. M. J. Kurylo, N. C. Peterson and W. Braun, *J. Chem. Phys.*, 54, 4662 (1971).

138. J. A. Kerr and J. G. Calvert, *J. Am. Chem. Soc.*, 83, 3391 (1961).

139. R. M. Reim and K. O. Kutschke, *Can. J. Chem.*, 38, 2332 (1960).

140. P. Cadman, Y. Inel, A. F. Trotman-Dickenson, *J. Chem. Soc.*, A, 1207 (1970).

141. E. U. Condon, *Physic. Rev.*, 32, 858 (1928).

142. G. Herzberg, "*Molecular Spectra and Molecular Structure, I. Spectra of Diatomic Molecules*", D. Van Nostrand Co., Princeton, N.J., 1950, pp. 377-400.

143. J. O. Hirschfelder, C. F. Curtiss and R. B. Bird, "*Molecular Theory of Gases and Liquids*", John Wiley and Sons, Inc., New York, 1954, p. 963.

144. H. H. Landolt and R. Bornstein, "*Zahlenwerte und Functionen aus Physik Chemie, Astronomie, Geophysik und Technik*", Band II, Teil 2, Springer-Verlag, Berlin, 1950.

145. R. S. Mulliken, *Chem. Phys. Letters*, 7, 11 (1970).

146. R. S. Mulliken, *J. Chem. Phys.*, 55, 288 (1971).

147. R. S. Mulliken, *J. Chem. Phys.*, 55, 309 (1971).

148. J. Szudy, *Bul. Acad. Pol. Sci.*, 17, 315 (1969).

149. S. W. Mayer and L. Schieler, *J. Chem. Phys.*, 72, 2628 (1968).

150. K. J. Laidler, "*Chemical Kinetics*", McGraw-Hill Book Company, New York, 1965, p. 153.

151. J. A. Kerr and A. F. Trotman-Dickenson, *Prog. Rxn. Kin.*, I, 105 (1961).

152. R. A. Svehla, *NASA Technical Report*, R132 (1962).

153. "*Handbook of Chemistry and Physics*", 48th ed., Chemical Rubber Publishing Co., Cleveland, Ohio, 1967.

154. J. D. Allen and M. C. Flowers, *Trans. Faraday Soc.*, 64, 3300 (1968).

155. A. D. Buckingham and B. J. Orr, *Trans. Faraday Soc.*, 65, 673 (1969).

156. S. Stokes and A. B. K. Duncan, *J. Am. Chem. Soc.*, 77, 2609 (1955).

157. G. S. Schwarzenbach and K. Lutz, *Helv. Chim. Acta*, 23, 1139 (1940).

APPENDIX A

EXPERIMENTAL DETERMINATION OF THE $R_{(n)}/R_{(n+i)}$ RATIO

Total rates of production of *n*-propyl and isopropyl radicals were calculated from the hexane and pentane products assuming that they are formed via the following reactions:

$$2n\text{-Pr} \longrightarrow n\text{-hexane (Hx)} \qquad [16]$$

$$\longrightarrow C_3H_8 + C_3H_6 \qquad [17]$$

$$n\text{-Pr} + i\text{-Pr} \longrightarrow \text{2-methylpentane (MP)} \qquad [18]$$

$$\longrightarrow C_3H_8 + C_3H_6 \qquad [19]$$

$$2i\text{-Pr} \longrightarrow \text{2,3-dimethylbutane (DMB)} \qquad [20]$$

$$\longrightarrow C_3H_8 + C_3H_6 \qquad [21]$$

$$\text{Et} + n\text{-Pr} \longrightarrow n\text{-pentane (P)} \qquad [35]$$

$$\longrightarrow C_2H_4 + C_3H_8 \text{ or } C_2H_6 + C_3H_6 \qquad [36]$$

$$\text{Et} + i\text{-Pr} \longrightarrow \text{isopentane } (i\text{-P}) \qquad [37]$$

$$\longrightarrow C_2H_4 + C_3H_8 \text{ or } C_2H_6 + C_3H_6 \qquad [38]$$

Let us define $R_{(n)}$ as the rate of disappearance of *n*-propyl radicals and $R_{(n+i)}$ as the total rate of disappearance of both *n*-propyl and isopropyl radicals in the system:

$$R_{(n)} = (k_{10}+k_{17})[n\text{-Pr}]^2 + (k_{18}+k_{19})[i\text{-Pr}][n\text{-Pr}] + (k_{35}+k_{36})[n\text{-Pr}][\text{Et}]$$

$$R_{(n+i)} = (k_{16}+k_{17})[n\text{-Pr}]^2 + (k_{18}+k_{19})[n\text{-Pr}][i\text{-Pr}] + (k_{20}+k_{21})[i\text{-Pr}]^2$$

$$+ (k_{35}+k_{36})[n\text{-Pr}][\text{Et}] + (k_{37}+k_{38})[i\text{-Pr}][\text{Et}]$$

Since the rates of production of hexanes and pentanes are given by

$$R_{\text{Hx}} = k_{16}[n\text{-Pr}]^2$$

$$R_{\text{MP}} = k_{18}[n\text{-Pr}][i\text{-Pr}]$$

and so on, we have:

$$R_{(n)} = 2(1 + k_{17}/k_{16})R_{\text{Hx}} + (1 + k_{19}/k_{18})R_{\text{MP}} + (1 + k_{36}/k_{35})R_{\text{P}} \qquad [52]$$

$$R_{(n+i)} = 2(1 + k_{17}/k_{16})R_{\text{Hx}} + 2(1 + k_{19}/k_{18})R_{\text{MP}} + 2(1 + k_{21}/k_{20})R_{\text{DMB}} + (1 + k_{36}/k_{35})R_{\text{P}} + (1 + k_{38}/k_{37})R_{i\text{-P}} \qquad [53]$$

The right hand side of equations [52] and [53] have been computed for each experiment from the measured rates of production of the pentane and hexane products. The chromatographic peak of *n*-hexane was often too small to measure accurately and was calculated from the cross-combination ratio (121)

$$R_{\text{MP}}^2/(R_{\text{DMB}}R_{\text{Hx}}) = 4.0$$

Disproportionation to combination ratios of the radicals were taken as being independent of temperature (151) and the values used (130) are listed in Table XXII. The rates of production of *n*-pentane and isopentane, R_{P} and $R_{i\text{-P}}$, are assumed to be zero in the reactions without added ethylene.

TABLE XXII

Disproportionation to Combination Ratios of Radicals

Radicals			
A	B	k_d/k_c [a]	k_d/k_c [b]
Et	Et	0.134	
Et	*i*-Pr	0.181	0.306
i-Pr	Et	0.125	
Et	*n*-Pr	0.064	0.118
n-Pr	Et	0.053	
n-Pr	*n*-Pr	0.154	
n-Pr	*i*-Pr	0.408	
i-Pr	*i*-Pr	0.69	

a) For the disproportionation reaction leading to AH + B(-H), from reference (130).

b) For the disproportionation reaction leading to either AH + (B-H) or A(-H) + BH.

APPENDIX B

DERIVATION OF STEADY STATE EQUATIONS

1. Mercury Photosensitization of Hydrogen-Propane Mixture

The important reactions occurring in the mercury photosensitization of hydrogen in the presence of a small amount of propane are:

$$\mathrm{Hg} + h\nu(2537\,\mathring{\mathrm{A}}) \longrightarrow \mathrm{Hg}^* \qquad [\mathrm{I}]$$

$$\mathrm{Hg}^* + \mathrm{H}_2 \longrightarrow \mathrm{H} + \mathrm{HgH}(\mathrm{Hg} + \mathrm{H}) \qquad [15]$$

$$\mathrm{H} + \mathrm{C}_3\mathrm{H}_8 \rightleftarrows i\text{-Pr} + \mathrm{H}_2 \qquad [12]$$

$$\rightleftarrows n\text{-Pr} + \mathrm{H}_2 \qquad [13]$$

$$n\text{-Pr} + \mathrm{C}_3\mathrm{H}_8 \rightleftarrows i\text{-Pr} + \mathrm{C}_3\mathrm{H}_8 \qquad [14]$$

$$2n\text{-Pr} \longrightarrow n\text{-hexane (Hx)} \qquad [16]$$

$$\longrightarrow \mathrm{C}_3\mathrm{H}_8 + \mathrm{C}_3\mathrm{H}_6 \qquad [17]$$

$$n\text{-Pr} + i\text{-Pr} \longrightarrow \text{2-methylpentane (MP)} \qquad [18]$$

$$\longrightarrow \mathrm{C}_3\mathrm{H}_8 + \mathrm{C}_3\mathrm{H}_6 \qquad [19]$$

$$2i\text{-Pr} \longrightarrow \text{2,3-dimethylbutane (DMB)} \qquad [20]$$

$$\longrightarrow \mathrm{C}_3\mathrm{H}_6 + \mathrm{C}_3\mathrm{H}_8 \qquad [21]$$

The steady state equations for [n-Pr] and [i-Pr] are:

$$\frac{d[n\text{-Pr}]}{dt} = k_{13}[\mathrm{H}][\mathrm{C}_3\mathrm{H}_8] - k_{13}[n\text{-Pr}][\mathrm{H}_2] - [\mathrm{C}_3\mathrm{H}_8]\{k_{14}[n\text{-Pr}] - k_{-14}[i\text{-Pr}]\}$$

$$- (k_{16}+k_{17})[n\text{-Pr}]^2 - (k_{18}+k_{19})[n\text{-Pr}][i\text{-Pr}]$$

$$= 0$$

$$\frac{d[i\text{-Pr}]}{dt} = k_{12}[H][C_3H_8] - k_{-12}[i\text{-Pr}][H_2] + [C_3H_8]\{k_{14}[n\text{-Pr}] - k_{-14}[i\text{-Pr}]\}$$
$$- (k_{18}+k_{19})[i\text{-Pr}][n\text{-Pr}] - (k_{20}+k_{21})[i\text{-Pr}]^2$$
$$= 0$$

Since $R_{(n)}$ and $R_{(n+i)}$ are given by

$$R_{(n)} = (k_{10}+k_{17})[n\text{-Pr}]^2 + (k_{18}+k_{19})[n\text{-Pr}][i\text{-Pr}]$$

$$R_{(n+i)} = (k_{16}+k_{17})[n\text{-Pr}]^2 + (k_{18}+k_{19})[n\text{-Pr}][i\text{-Pr}] + (k_{20}+k_{21})[i\text{-Pr}]^2$$

therefore

$$R_{(n)} = k_{13}[H][C_3H_8] - k_{-13}[n\text{-Pr}][H_2] - [C_3H_8]\{k_{14}[n\text{-Pr}] - k_{-14}[i\text{-Pr}]\}$$

$$R_{(n+i)} = (k_{12}+k_{13})[H][C_3H_8] - \{k_{-12}[i\text{-Pr}] + k_{-13}[n\text{-Pr}]\}[H_2].$$

Division of $R_{(n)}$ by $R_{(n+i)}$ gives,

$$R_{(n)}/R_{(n+i)} = Q_1 + Q_2 + Q_3 \qquad [22]$$

$$Q_1 = \frac{k_{13}[H][C_3H_8]}{(k_{12}+k_{13})[H][C_3H_8] - \{k_{-12}[i\text{-Pr}] + k_{-13}[n\text{-Pr}]\}[H_2]}$$

$$Q_2 = -k_{-13}[H_2][n\text{-Pr}]/R_{(n+i)}$$

$$Q_3 = [C_3H_8]\{k_{14}[n\text{-Pr}] - k_{-14}[i\text{-Pr}]\}/R_{(n+i)}$$

2. Photosensitization of Propane and Propane-Nitrogen Mixtures

The important reactions occurring in this system are:

$$\mathrm{Hg} + h\nu(2537\,\mathrm{\mathring{A}}) \longrightarrow \mathrm{Hg}^* \qquad [\mathrm{I}]$$

$$\mathrm{Hg}^* + \mathrm{C_3H_8} \longrightarrow (\mathrm{HgC_3H_8})^* \qquad [25]$$

$$(\mathrm{HgC_3H_8})^* \longrightarrow i\text{-Pr} + \mathrm{H} + \mathrm{Hg} \qquad [26]$$

$$\longrightarrow n\text{-Pr} + \mathrm{H} + \mathrm{Hg} \qquad [27]$$

$$\longrightarrow \mathrm{C_3H_8} + \mathrm{Hg}^\circ \qquad [28]$$

$$\longrightarrow \mathrm{C_3H_8} + \mathrm{Hg} + h\nu' \qquad [29]$$

$$\mathrm{Hg}^\circ + \mathrm{C_3H_8} \longrightarrow (\mathrm{HgC_3H_8})^\circ \qquad [30]$$

$$(\mathrm{HgC_3H_8})^\circ \longrightarrow i\text{-Pr} + \mathrm{H} + \mathrm{Hg} \qquad [31]$$

$$\longrightarrow n\text{-Pr} + \mathrm{H} + \mathrm{Hg} \qquad [32]$$

$$\longrightarrow \mathrm{C_3H_8} + \mathrm{Hg} + h\nu'' \qquad [33]$$

$$\mathrm{Hg}^* + \mathrm{N_2} \rightleftarrows \mathrm{Hg}^\circ + \mathrm{N_2} \qquad [44]$$

$$\mathrm{Hg}^\circ + \mathrm{Hg} + \mathrm{A} \longrightarrow \mathrm{Hg}_2^* + \mathrm{A} \qquad [10]$$

$$\mathrm{H} + \mathrm{C_3H_8} \longrightarrow i\text{-Pr} + \mathrm{H_2} \qquad [12]$$

$$\longrightarrow n\text{-Pr} + \mathrm{H_2} \qquad [13]$$

$$n\text{-Pr} + \mathrm{C_3H_8} \rightleftarrows i\text{-Pr} + \mathrm{C_3H_8} \qquad [14]$$

$$2n\text{-Pr} \longrightarrow n\text{-Hexane} \qquad [16]$$

$$\longrightarrow \mathrm{C_3H_6} + \mathrm{C_3H_8} \qquad [17]$$

$$n\text{-Pr} + i\text{-Pr} \longrightarrow \text{2-methylpentane} \qquad [18]$$

$$\longrightarrow \mathrm{C_3H_6} + \mathrm{C_3H_8} \qquad [19]$$

$$2i\text{-Pr} \longrightarrow \text{2,3-dimethylbutane} \qquad [20]$$

$$\longrightarrow C_3H_6 + C_3H_8 \qquad [21]$$

a. Derivation of the Expressions for F and Φ_T.

The steady state equations for $[(HgC_3H_8)^*]$, $[Hg°]$, and $[(HgC_3H_8)°]$ are:

$$\frac{d[(HgC_3H_8)^*]}{dt} = k_{25}[Hg^*][C_3H_8] - (k_{26}+k_{27}+k_{28}+k_{29})[(HgC_3H_8)^*]$$

$$= 0 \qquad [54]$$

$$\frac{d[Hg°]}{dt} = k_{28}[(HgC_3H_8)^*] + k_{44}[Hg^*][N_2] - k_{-44}[Hg°][N_2]$$

$$- k_{10}[Hg°][Hg][A] - k_{30}[Hg°][C_3H_8] \qquad [55]$$

$$= 0$$

$$\frac{d[(HgC_3H_8)°]}{dt} = k_{30}[Hg°][C_3H_8] - (k_{31}+k_{32}+k_{33})[(HgC_3H_8)°]$$

$$= 0 \qquad [56]$$

Substituting the expression for $[(HgC_3H_8)^*]$ from equation [54] into [55] and solving for $[Hg^*]/[Hg°]$ yields

$$\frac{[Hg^*]}{[Hg°]} = \frac{k_{-44}[N_2] + k_{10}[Hg][A] + k_{30}[C_3H_8]}{k_{25}\Phi'[C_3H_8] + k_{44}[N_2]}$$

$$= \frac{K_{44}^{-1} + \dfrac{k_{30}[C_3H_8]}{k_{44}[N_2]} + \dfrac{k_{10}[Hg][A]}{k_{44}[N_2]}}{\dfrac{k_{25}\Phi'[C_3H_8]}{k_{44}[N_2]} + 1}$$

where

$$\Phi' = k_{28}/(k_{26}+k_{27}+k_{28}+k_{29})$$

$$K_{44}^{-1} = k_{-44}/k_{44}.$$

Multiplying the expression for [Hg*]/[Hg°] by $(\sigma^{2*}/\sigma^{2°})_{C_3H_8}$ (= k_{25}/k_{30}) gives

$$F = (\sigma^{2*}/\sigma^{2°})_{C_3H_8}[Hg^*]/[Hg°]$$

$$= \frac{(\sigma^{2*}/\sigma^{2°})_{C_3H_8} K_{44}^{-1} + \frac{k_{25}[C_3H_8]}{k_{44}[N_2]} + \left(\frac{\sigma^{2*}}{\sigma^{2°}}\right)_{C_3H_8} \frac{k_{10}[Hg][A]}{k_{44}[N_2]}}{1 + \Phi' \frac{k_{25}[C_3H_8]}{k_{44}[N_2]}} \qquad [57]$$

When $[N_2] = 0$ this reduces to $F = 1/\Phi'$.

The overall quantum yield of propyl radicals is given by their rate of production divided by all the possible modes of deactivation of excited mercury quanta according to

$$\Phi_T = \frac{R_{26+27} + R_{31+32}}{R_{-I} + (1-\Phi')R_{25} + R_{30} + R_{10}}$$

where $R_{26+27} = (k_{26}+k_{27})[(HgC_3H_8)^*]$ etc. Division by R_{25} and expansion gives

$$\Phi_T = \frac{\Phi^* + \Phi° k_{30}[Hg°]/k_{25}[Hg^*]}{\frac{k_{-I}}{k_{25}[C_3H_8]} + (1-\Phi') + \frac{k_{30}[Hg°]}{k_{25}[Hg^*]} + \frac{k_{10}[Hg°][Hg][A]}{k_{25}[Hg^*][C_3H_8]}}$$

where

$$\Phi^* = (k_{26}+k_{27})/(k_{26}+k_{27}+k_{28}+k_{29})$$

$$\Phi° = (k_{31}+k_{32})/(k_{31}+k_{32}+k_{33}).$$

Thus from the expression for F ([57])

$$\Phi_T\left\{1 + \left(\frac{\sigma^{2*}}{\sigma^{2\circ}}\right)_{C_3H_8} \frac{k_{10}[Hg][A]}{k_{25}[C_3H_8]} + F\left(1-\Phi' + \frac{k_{-I}}{k_{25}[C_3H_8]}\right)\right\} = \Phi^*F + \Phi^\circ \qquad [49]$$

b. Derivation of k_{27}/k_{26} and k_{32}/k_{31} Ratios for Propane and Propane-Nitrogen Mixtures

The steady state equations for [*n*-Pr], [*i*-Pr] and [H] in this system are given by:

$$\frac{d[n\text{-Pr}]}{dt} = k_{27}[(HgC_3H_8)^*] + k_{32}[(HgC_3H_8)^\circ] + k_{13}[H][C_3H_8]$$

$$-\{k_{14}[n\text{-Pr}] - k_{-14}[i\text{-Pr}]\}[C_3H_8] - (k_{16}+k_{17})[n\text{-Pr}]^2$$

$$- (k_{18}+k_{19})[n\text{-Pr}][i\text{-Pr}]$$

$$= 0$$

$$\frac{d[i\text{-Pr}]}{dt} = 0 = k_{26}[(HgC_3H_8)^*] + k_{31}[(HgC_3H_8)^\circ] + k_{12}[H][C_3H_8]$$

$$+ \{k_{14}[n\text{-Pr}] - k_{-14}[i\text{-Pr}]\}[C_3H_8] - (k_{18}+k_{19})[n\text{-Pr}][i\text{-Pr}]$$

$$- (k_{20}+k_{21})[i\text{-Pr}]^2.$$

$$\frac{d[H]}{dt} = 0 = (k_{26}+k_{27})[(HgC_3H_8)^*] + (k_{31}+k_{32})[(HgC_3H_8)^\circ]$$

$$- (k_{12}+k_{13})[H][C_3H_8].$$

These are related to the experimental quantities, $R_{(n)}$ and $R_{(n+i)}$, by

$$R_{(n)} = (k_{16}+k_{17})[n\text{-Pr}]^2 + (k_{18}+k_{19})[n\text{-Pr}][i\text{-Pr}]$$

$$R_{(n)} = k_{27}[(HgC_3H_8)^*] + k_{32}[(HgC_3H_8)^\circ] + k_{13}[H][C_3H_8]$$

$$- \{k_{14}[n\text{-Pr}] - k_{-14}[i\text{-Pr}]\}[C_3H_8]$$

$$R_{(n+i)} = (k_{16}+k_{17})[n\text{-Pr}]^2 + (k_{18}+k_{19})[n\text{-Pr}][i\text{-Pr}] + (k_{20}+k_{21})[i\text{-Pr}]^2$$

$$= (k_{26}+k_{27})[(HgC_3H_8)^*] + (k_{31}+k_{32})[(HgC_3H_8)^\circ]$$

$$+ (k_{12}+k_{13})[H][C_3H_8].$$

From d[H]/dt,

$$R_{(n+i)} = 2(k_{26}+k_{27})[(HgC_3H_8)^*] + 2(k_{31}+k_{32})[(HgC_3H_8)^\circ]$$

or

$$R_{(n+i)} = 2(k_{12}+k_{13})[H][C_3H_8]$$

Division of $R_{(n)}$ by $R_{(n+i)}$ including the contribution from the non-uniform absorption of light gives:

$$\frac{2R_{(n)}}{R_{(n+i)}} = Q_4 + k_{13}/(k_{12}+k_{13}) - \delta Q_3$$

where

$$\delta = \frac{2\{1 - \exp(-\ \varepsilon[Hg]L/2)\}}{\{\varepsilon[Hg](1 - \exp(-\ \varepsilon[Hg]L))\}}$$

$$Q_3 = \{k_{14}[n\text{-Pr}] - k_{-14}[i\text{-Pr}]\}[C_3H_8]/R_{(n+i)}$$

$$= \frac{R_{DMB}^{1/2}}{R_{(n+i)}}\left(\frac{R_{MP}}{R_{DMB}} - 2\ \ K_{14}^{-1}\right)\frac{k_{14}}{k_{20}^{1/2}}\ [C_3H_8]$$

and

$$Q_4 = \frac{k_{27}[(HgC_3H_8)^*] + k_{32}[(HgC_3H_8)^\circ]}{(k_{26}+k_{27})[(HgC_3H_8)^*] + (k_{31}+k_{32})[(HgC_3H_8)^\circ]}$$

From equations [54] and [56], Q_4 is given by

$$Q_4 = \frac{\dfrac{k_{27}k_{25}[Hg^*]}{(k_{26}+k_{27}+k_{28}+k_{29})} + \dfrac{k_{32}k_{30}[Hg^\circ]}{(k_{31}+k_{32}+k_{33})}}{\dfrac{(k_{26}+k_{27})k_{25}[Hg^*]}{(k_{20}+k_{27}+k_{28}+k_{29})} + \dfrac{(k_{31}+k_{32})k_{30}[Hg^\circ]}{(k_{31}+k_{32}+k_{33})}}$$

Dividing the numerator and denominator by $k_{30}[Hg^\circ]$ and substitution of F, Φ^*, and Φ° yields

$$Q_4 = (F\Phi^* + \Phi^\circ)^{-1} \left\{ \frac{k_{27}F}{(k_{26}+k_{27}+k_{28}+k_{29})} + \frac{k_{32}}{(k_{31}+k_{32}+k_{33})} \right\}$$

$$= \Phi^*F(F\Phi^* + \Phi^\circ)^{-1} \frac{k_{27}}{k_{26}+k_{27}} + \Phi^\circ(F\Phi^* + \Phi^\circ)^{-1} \frac{k_{32}}{k_{31}+k_{32}}$$

$$= \frac{k_{27}}{k_{26}+k_{27}} \beta + \frac{k_{32}}{k_{31}+k_{32}} (1-\beta)$$

where

$$\beta = \Phi^*F/(F\Phi^* + \Phi^\circ).$$

APPENDIX C

CALCULATION OF LENNARD-JONES FORCE CONSTANTS FOR VARIOUS COLLISION PAIRS

The empirical Lennard-Jones (6-12) potential function has been extensively used to describe the interaction of two spherically symmetric colliding species:

$$V_{(r)} = 4\varepsilon\left[\left(\frac{\sigma}{r}\right)^{12} - \left(\frac{\sigma}{r}\right)^{6}\right] + \frac{1}{2}\mu\frac{g^2b^2}{r^2}$$

The quantity σ is the finite internuclear distance where the potential function is zero and ε is the value of the depth of the potential well. The last term represents the centrifugal contribution where μ is the reduced mass, g is the initial radial velocity, and b is the impact parameter. The present calculations have been carried out assuming $b = 0$.

The Lennard-Jones force constants for the interaction of ground state mercury with various substrates have been computed employing the mixture rules

$$\varepsilon_{mix} = (\varepsilon_1 \times \varepsilon_2)^{\frac{1}{2}}$$

$$\sigma_{mix} = (\sigma_1 + \sigma_2)/2$$

and are summarized in Table XXIII. The ε_{mix} values vary from about 0.5 to 1.0 kcal/mole for the interactions of paraffins with the ground state mercury atom.

To calculate ε for the collision of Hg* and Hg° atoms

with hydrocarbon molecules, London's relationship (143) for the attractive part of the potential was used,

$$V_{(r)} = -\frac{3}{2}\frac{\alpha_1\alpha_2}{r^6}\frac{I_1 I_2}{(I_1+I_2)}$$

where α_1 and α_2 are the polarizabilities and I_1 and I_2 are the ionization potentials of the molecules in question. By equating this with the attractive term in the Lennard-Jones potential function, we have

$$\frac{-4\varepsilon\sigma^6}{r^6} = -\frac{3}{2}\frac{\alpha_1\alpha_2}{r^6}\frac{I_1 I_2}{(I_1+I_2)}$$

and

$$4\varepsilon\sigma^6 = -\frac{3}{2}\alpha_1\alpha_2 I_1 I_2/(I_1+I_2)$$

Since σ values for the Hg*-HR and Hg°-HR collision are not available, we have assumed these to be either the same as or 10% less than σ_{mix} for the Hg-HR collision. A correction term has been established for computing the ε values for the interaction of the paraffin with ground state mercury by London's relation. The ε values for the interaction of the excited state atom were then multiplied by this factor $\varepsilon_{mix}/\varepsilon_{London}$. The values of polarizabilities and ionization potentials used, are taken from Table XXIII. Computed values of for the Hg*-HR and Hg°-HR collisions are listed in Table XXIV.

TABLE XXIII

Lennard-Jones Force Constants Calculated for the Collision of Ground State Mercury with Different Molecules

Collision Pair		L-J Constants for B_2 Dimer[a]						
		σ	ε	α_B^b	I_B	σ_{mix}	ε_{mix}	ε_{London}
A	B	Å	kcal/mole	$Å^3$	ev	Å	kcal/mole	kcal/mole
Hg	H_2	2.827	0.119	0.79	15.42	2.862	0.449	0.394
Hg	CH_4	3.758	0.295	2.60	12.95	3.328	0.706	0.487
Hg	C_2H_6	4.443	0.428	4.47	11.76	3.670	0.851	0.445
Hg	C_3H_8	5.118	0.471	6.29	11.21	4.008	0.892	0.361
Hg	*i*-C_4H_{10}	5.278	0.656		10.80			
Hg	$C(CH_3)_4$	6.464	0.384		10.29			
Hg	Hg	2.898	1.690	5.1	10.43			

[a] From reference (152).

[b] From reference (143) p. 950.

[c] From reference (144) p. 360.

TABLE XXIV

Lennard-Jones Force Constants Calculated for Collision of Excited Mercury Atoms with Different Molecules

Collision Pair		$Hg(^1S_0)$		$\varepsilon x K^c$; kcal/mole			
				$Hg(^3P_0)^a$		$Hg(^3P_1)^b$	
A	B	σ_{mix} Å	ε_{mix} kcal/mole	$\sigma=\sigma_{mix}$	$\sigma=0.9\sigma_{mix}$	$\sigma=\sigma_{mix}$	$\sigma=0.9\sigma_{mix}$
Hg	H_2	2.862	0.449	0.600	1.128	1.166	2.195
Hg	CH_4	3.328	0.706	0.966	1.817	1.881	3.540
Hg	C_2H_6	3.670	0.851	1.179	2.218	2.298	4.324
Hg	C_3H_8	4.008	0.892	1.244	2.341	2.426	4.565

[a] $\alpha(Hg°) = 10.\ Å^3$ and $I(Hg°) = 5.85$ ev (68).

[b] $\alpha(Hg^*) = 20.0Å^3$ and $I(Hg^*) = 5.63$ ev (10) p. 178.

[c] $K = \varepsilon_{mix}/\varepsilon_{London}$ for the ground state mercury substrate surface.

APPENDIX D

COMPUTATION OF POTENTIAL ENERGIES OF ACTIVATION FOR THE ATOM PHOTOSENSITIZED DECOMPOSITION OF PARAFFINS

The empirical Bond-Energy-Bond-Order method of calculating potential energies of activation or radical abstraction reactions has been described in detail by Johnston (120). For the general H-atom abstraction reaction

$$AH + B \longrightarrow \underset{r_1}{A\cdots} \underset{r_2}{H\cdots} B \longrightarrow A + BH$$

it is assumed that the potential energy of activation is given by the maximum of the potential function

$$V = D_e(A\text{-}H) - E_{AH} - E_{HB} + E_{AB}$$

computed for a path of total bond order of unity ($n_1 + n_2 = 1$). The quantity D_e is the single bond energy (including zero point energy), E_{AH} and E_{BH} are the AH and BH bond energies at a given n_1, and E_{AB} is the triplet repulsion energy between A and B. This can be written in terms of one bond order n ($n = n_1 = 1 - n_2$) and an empirical bond energy index for each bond:

$$V = E_{AH}(1 - n^{p_1}) - E_{BH}(1-n)^{p_2} + E_{AB}$$

The bond energy index is given by

$$p = \frac{0.26 \ln(D_e/\varepsilon_x)}{r_x - r_e}$$

where ε_x and r_x are the potential depth and the equilibrium internuclear distance of the Lennard-Jones diatomic noble gas cluster.

We have modified this method to calculate the relative potential energies of activation for the atomic photosensitized decomposition of paraffins assuming the following model:

$$\mathrm{R{-}H} + \mathrm{Hg}^* \longrightarrow \underset{r_1\quad r_2}{\mathrm{R}\cdots\mathrm{H}\cdots\mathrm{Hg}^*} \longrightarrow \mathrm{R} + \mathrm{H{-}Hg}$$

The paraffin is approximated as a diatom, R-H, and the excited mercury is taken to behave as a radical. It is further assumed that Hg-H is the final product having a bond energy equal to the sum of the electronic energy of the excited mercury atom plus the heat of formation of Hg-H of 10.6 kcal/mole, including the zero point energy. The bond energy index of HgH is calculated using the Lennard-Jones force constants (Table XXV) of Hg-He as the zero order bond. This is necessary since Lennard-Jones force constants are not available for Rn, the noble gas analog of mercury. It is difficult to assess the contribution due to triplet repulsion at this stage, and it has been neglected in the present computations. Potential energies of activation have been computed for the mercury, cadmium, and zinc sensitized decomposition of various paraffins by this method and the results are displayed in Tables XXVI and XXVII.

This method predicts that the activation energy for hydrogen abstraction reactions by an electronically excited metal atom will increase with increasing bond energy of the paraffin and decrease with increasing excitation energy of the metal atom. Because of the approximate nature of the model considered, these potential energies of activation are meaningful only in relative terms. In addition,

since the contribution due to the triplet term is always symmetrical in bond order, the predicted values for $\Delta E'$, ΔE^*, and ΔE° for the various C–H bonds are then lower limits.

TABLE XXV

Lennard-Jones Force Constants for Different Collision Pairs

Collision Pair	ε(kcal/mole)	σ(Å)	Reference
Hg-Hg	1.691	2.898	143
Cd-Cd	2.438	2.606	152
Zn-Zn	2.768	2.284	152
He-He	0.0204	2.556	143
Xe-He	0.0946	3.75[a]	120
Kr-He	0.0832	3.46[a]	120

[a] Equilibrium internuclear distance R_x.

TABLE XXVI

Calculated Potential Energies of Activation for Excited Mercury-Paraffin Systems Using Attractive Term Only[a,b]

		$Hg(^3P_0)$	$Hg(^3P_1)$	$Hg(^1P_1)$
Hg*-H Bond Energy Assumed[c]		117.8	122.8	164.5
Paraffin Bond	D_e(R-H)			
CH_3-H	108.2	9.70	8.46	3.11
C_2H_5-H	102.1	7.56	6.57	2.40
$(CH_3)_2CH$-H	98.7	6.51	5.67	2.05
$(CH_3)_3C$-H	95.1	5.54	4.81	1.74
$(CH_3)CCH_2$-H	103.2	7.92	6.89	2.51

[a] In kcal/mole

[b] Hg-H Bond Energy Index equal to 1.279 and R-H Bond Energy Index equal to 1.089.

[c] Excitation energy plus D_e(Hg-H) = 10.59 kcal/mole.

TABLE XXVII

Calculated Potential Energies of Activation for Excited Cadmium- and Zinc-Paraffin Systems Using Attractive Terms Only[a]

		Cd($^3P_1$)	Cd($^1P_1$)	Zn($^3P_1$)	Zn($^1P_1$)
M*-H Bond Energy Assumed[b]		104.9	142.0	114.5	155.4
M*-H Bond Energy Index[c]		1.4097	1.4097	1.4323	1.4323
Molecule	D_e(R-H)				
CH_3-H	108.2	17.8	8.9	15.3	7.8
C_2H_5-H	102.1	14.8	7.4	12.7	6.5
$(CH_3)_2$CH-H	98.7	13.2	6.6	11.4	5.8
$(CH_3)_3$C-H	95.1	11.7	5.8	10.2	5.2
$(CH_3)_3CCH_2$-H	103.2	15.3	7.6	13.2	6.7

[a] In kcal/mole

[b] Excitation energy plus D_e(Cd-H) = 17.6 kcal/mole or D_e(Zn-H) = 22.0 kcal/mole

[c] Calculated with (M*-H) Bond Energy of the $^3P_1$ level and R(Cd-H) = 1.7617 or R(Zn-H) = 1.5945 from reference (142), p. 538.

B30019